5-2004

Compatibilizing Polymer Blends Using Reactive Telechelic Oligomers and Copolymers

Charles Paul O'Brien
University of Tennessee - Knoxville

To the Graduate Council:

I am submitting herewith a dissertation written by Charles Paul O'Brien entitled "Compatibilizing Polymer Blends Using Reactive Telechelic Oligomers and Copolymers." I have examined the final electronic copy of this dissertation for form and content and recommend that it be accepted in partial fulfillment of the requirements for the degree of Doctor of Philosophy, with a major in Chemistry.

Mark D. Dadmun, Major Professor

We have read this dissertation and recommend its acceptance:

Jeffrey D. Kovac, John F. Turner, Kevin M. Kit

Accepted for the Council:

Carolyn R. Hodges

Vice Provost and Dean of the Graduate School

(Original signatures are on file with official student records.)

To the Graduate Council:

I am submitting herewith a dissertation written by Charles Paul O'Brien entitled "Compatiblizing Polymer Blends Using Reactive Telechelic Oligomers and Copolymers." I have examined the final paper copy of this dissertation for form and content and recommend that it be accepted in partial fulfillment of the requirements for the degree of Doctor of Philosophy, with a major in Chemistry.

Mark D. Dadmun, Major Professor

We have read this dissertation and recommend its acceptance:

Dr. Jeffrey D. Kovac

Dr. John F. C. Turner

Dr. Kevin M. Kit

Accepted for the Council:

Vice Chancellor and Dean of Graduate Studies

COMPATIBILIZING POLYMER BLENDS USING REACTIVE TELECHELIC OLIGOMERS AND COMPOLYMERS

A Dissertation
Presented for the
Doctor of Philosophy
Degree
The University of Tennessee, Knoxville

Charles Paul O'Brien
May 2004

Acknowledgments

I would like to thank Dr. Mark Dadmun for his work as research advisor and teacher as well as all the members of the Dadmun research group for their insight and suggestions over the years. I would also like to thank Dr. John Turner, Dr. Jeffrey Kovac, and Dr. Kevin Kitt for their work on my thesis committee.

In addition, thanks to my parents Joe and Patty as well as my sisters Rose and Stephanie and my brother Patrick for constant support and encouragement. A special thanks to my wife Jennifer for her patience and love both before and during my pursuit of a graduate degree.

Abstract

The compatibilization of polymer blends via reactive compatibilization and block copolymers was studied. The results presented in this thesis suggest that the process of reactive compatibilization provides a mechanism by which blocky copolymeric compatibilizers can be formed during processing, as demonstrated by the changes in the mechanical and optical properties of the phase separated polymer blends. The results also show, however, that the presence of unreacted smaller oligomers can act as a plasticizer in the blend and can thus detrimentally affect the mechanical properties of the blend if any remains after processing. Careful control of the mixing conditions or post processing thermal annealing is required to minimize this potentially deleterious effect. However, the data presented here suggest that this optimization is possible. In addition, the compatibilization of polymer blends with blocky, random, and alternating copolymer was studied. Depth profiling of polymer samples containing copolymers as compatibilizers was achieved with FRES (forward recoil spectroscopy) and neutron reflectivity and the results were compared with fracture toughness data that was previously reported. The results show that molecular weight of the alternating copolymer as well as the molecular weight of block segments in block copolymers are important parameters for copolymers to act as compatibilizers.

Table of Contents

List of Tables

List of Figure

Chapter 1

Compatibilization of Polymer Blends

1.1 Introduction

The following chapter contains a summary of polymer blend compatibilization where the difference between polymer blend miscibility and compatibilization is explained. In addition, several methods that have been used to compatibilize polymer blends are reviewed including the use of crosslinking agents, hydrogen bonding, copolymer additives, and reactive processing.

Experimental techniques that are used to study polymer blends after compatibilization are also analyzed, including depth profiling techniques such as forward recoil spectrometry, neutron reflectivity, and secondary ion mass spectrometry. These techniques allow the study of how a compatibilizer accesses and modifies a polymer blend biphasic interface. Studies of blend morphology, and ultimately mechanical properties are investigated to illustrate how blend compatibilizers alter the physical and mechanical properties of a polymer blend.

1.2 Background

In 1991, polymer blends accounted for roughly 2 billion pounds of material per year or 3% of all polymer production.[3] Recent reports show that polymer blends represent 30% by weight of the polymer market and have had a growth rate of 9%. [4,5] The use of polymer blends continues to grow because blends are an alternative to

designing new monomers and/or polymers to satisfy new markets and obtain properties that are industrially useful. The development of new molecules is an expensive investment in both time and money and the ability to tailor polymeric materials for a specific application through blending is a promising alternative as properties of two existing polymers can be combined to meet a variety of needs.

The ability to blend polymers successfully also is of great significance for recycling and conservation of natural resources because recycling polymer products provides a means to create new products without using new chemicals. In addition, products that would normally take up space in a landfill can be turned into new usable products. Unfortunately, polymers must be separated into distinct chemical composition, such as polystyrene (PS) and poly (ethylene terephthalate) (PET) before they can be recycled or a heterogeneous blend with poor properties will result. Separation of different types of plastic is both time consuming and labor intensive which adds another hurdle to recycling the materials. Thus, the ability to compatibilize two different homopolymers to create useful new and recycled products without separation of the individual plastic components is important for the conservation of natural resources and reduction of landfill waste.

The focus of this dissertation is to study the use of difunctional (telechelic) oligomers and copolymers as compatibilizers in polymer/polymer blends. Compatibilization is important for most polymer blend systems since most polymer pairs are immiscible and will phase separate leading to poor mechanical properties. Compatibilizers, however, can be used to maintain specific morphologies in immiscible

polymer blends.[6-9] The ability to control a polymer/polymer blend morphology also allows for tailored and improved mechanical properties.

1.3 Polymer Miscibility

As stated above, most polymers are immiscible, which leads to phase separation of the blend and poor mechanical properties. Miscibility is described as thermodynamic solubility where the free energy of mixing two components is negative ($\Delta G_{mix} \leq 0$). The free energy of mixing depends on both molecular interactions (enthalpy) and entropy of the mixing process. In the case of small molecule mixtures, the increased entropy of the system upon mixing often overcomes unfavorable interactions between molecules.

In polymers, the free energy of mixing is approximated by the Flory-Huggins theory, which states:

$$\Delta G_{mix}/VRT=(\phi_1/\nu_1 N_1)\ln\phi_1+(\phi_2/\nu_2 N_2)\ln\phi_2+\phi_1\phi_2(\chi/\nu)$$

In this equation, V is the volume of sample, T is absolute temperature, R is the gas constant, ϕ_x is the volume fraction of component x (1 or 2), ν_x is the molar volume of its reference repeat units, N_x is the degree of polymerization, ν is a reference volume and χ is the Flory interaction parameter. As illustrated in the Flory-Huggins equation, miscibility of polymers is dependent not only on the chemical structure of the polymer, but also thermodynamic variables such as blend composition and temperature. The first two terms in this equation represent the entropy of mixing and the last term represents enthalpy. As can be seen in the Flory-Huggins equation, the entropy terms contain the degree of polymerization in their denominator. Since polymers in general have a high

degree of polymerization there is relatively low entropy of mixing when compared with the configurational entropy of a polymer chain. The enthalpy of mixing term does not contain the degree of polymerization and thus the enthalpy of mixing does not rely considerably on the molecular weight of the polymer. For most mixtures the enthalpy of mixing is determined by χ and is usually positive. Thus, with a negligible entropy term and a positive enthalpy term, ΔG_{mix} will be greater than zero and the polymer mixture will phase separate with little entanglements at the polymer/polymer biphasic interface leading to poor properties.[10-12]

1.4 Polymer Compatibility

The weak interface and its lack of entanglement are the weakest point in an immiscible blend. Therefore if this interface can be strengthened, the blend may become strong enough to be useful. Immiscible blends, therefore, can be compatibilized to increase interfacial adhesion, prevent droplet coalescence, improve phase dispersion, and increase the overall property of the blend by the addition of an interfacial modifier to the blend.[6,7,9,13-23] Compatibility is a relative term that is often defined based on the application of the polymer blend. For example, a blend can be considered compatible relative to another blend based on improvements in mechanical properties. These mechanical properties, however, depend on the specific morphological properties of the blend such as domain size and dispersion.

Thus, the ability of a compatibilizer to improve the properties of the blend will depend on the location of the compatibilizer in the blend, the effect of the

compatibilizer on the morphology and growth of phase domains in the blend, and the resulting physical properties of the blend. In the special case of reactive compatibilization a compatibilizer is formed at the polymer-polymer interface in the phase separated blend during processing. Thus, it is especially important to know to what extent the compatibilizer has formed and the location of the reactive components that will form the compatibilizer within the blend system.[24] Several methods for compatibilizing immiscible polymers such as addition of copolymer, or the introduction of specific interactions (i.e. hydrogen bonding), have been studied as processes that can be used by industry to improve the final properties of phase separated polymer blends.[13-16]

1.5 Crosslinking Agents

The term crosslinking refers to joining multiple polymer chains. Crosslinking can be facilitated through many agents such as oxidizing agents or generators of free radicals. The amount of crosslinking can be controlled and varied to meet specific requirements; for instance, the process of vulcanization introduces small amounts of crosslinking into rubber polymers to impart improved elastic properties. Conversely, phenol-formaldehyde resins have a high degree of crosslinking to increase the rigidity, heat and stress stability.[10] Crosslinking as a means to compatibilize various polymer blends has also been studied.[25-29]

Sanchez et al. examined a poly (methyl acrylate) (PMA)/poly (methyl methacrylate) (PMMA) interpenetrating network (IPN) fabricated by polymerizing

methyl acrylate (MA) using benzoin as a photoinitiator. Varying concentrations of ethylene glycol dimethacrylate, a crosslinking agent, were polymerized along with the MA. The resulting PMA was placed in a solution of methyl methacrylate (MMA), photoinitator, and crosslinking agent and the MMA is then polymerized to form a network of PMMA within the crosslinked network of PMA. When an interpenetrating network is formed using PMA/PMMA, the system is not compatible and phase separates at low crosslink densities.

Sample IPNs of PMA/PMMA containing increasing concentrations of crosslink density were analyzed using dynamic mechanical analysis (DMA). In the DMA experiments, the two characteristic relaxations of PMA and PMMA converged into one relaxation when crosslink density increased from 0.1 to 10 percent. This merger of relaxations indicates that a sample is homogeneous.

Studies were also performed where the percent of crosslinking agent was varied (0.1, 0.5, and 10%) for the PMA component of the IPN, while the PMMA was polymerized with a constant 10% of the crosslinking agent. Similarly, the percent of crosslink agent was held steady at 10% for the PMA while the PMMA was polymerized with varying percentages of crosslink agent. It was found that the crosslink density of the network polymerized first (PMA) had the greatest effect on the compatibility of the IPN. Thus, increasing the crosslink density of the individual components of the IPN, especially the first component, leads to a forced compatibilization of the blend and a homogeneous network. [29]

1.6 Hydrogen Bonding

Non-bonding interactions between two polymers can be introduced by chemically modifying one or both components in a polymer blend to improve the properties of the blend. Such interactions can include van der Waals interactions, dipole-dipole interactions and hydrogen bonding. The ability of these interactions to effect the compatibility of a polymer/polymer blend depends on both the strength and number of interactions between each polymer chain.[16,30,31]

Radmard and Dadmun used FTIR to study the effect of spacing of a functional group capable of hydrogen bonding along the backbone of an amorphous polymer, Poly (styrene-co-4-vinylphenol) (PS-co-VPh), with a series of increasingly rigid polyethers. Spacing of the functional group (-OH) was accomplished by varying the amount of vinylphenol in the PS-co-VPh; the amount of VPh used was 10, 20, or 100 percent. As the percent of VPh in the blend increased, the spacing between functional groups along the polymer backbone decreased. Each of the three polymers containing different percentages of VPh were blended with three different polyethers and then solvent cast onto KBr plates for IR analysis. In IR analysis, the OH functional group in the PVPh has a stretching vibration at 3525cm^{-1} for non-bonded –OH, while –OH groups that are hydrogen bonded to other –OH groups have a stretching vibration at 3370cm^{-1}. In contrast, -OH groups that have hydrogen bonded to the oxygen in the polyethers form stronger hydrogen bonds. Thus, the corresponding O-H bond associated with hydrogen bonding to the ether oxygen (intermolecular hydrogen bonding) is weaker than the O-H bond associated with hydrogen bonding to another OH group (intramolecular hydrogen

bonding). Therefore, the stretching of the O-H bond associated with hydrogen bonding to an ether oxygen will occur at lower IR frequencies.

The IR data obtained in this study showed a shift in the IR of the blend versus the IR of the pure PS-co-VPh. The difference in these stretching frequencies was defined as $\Delta\nu$. As $\Delta\nu$ increases, the amount of intermolecular hydrogen bonding increases. It was found that $\Delta\nu$ increased as the percent of VPh decreased in the blend from 100 to 20 to 10 percent. Their results coincided with previous studies to show that increased distance between functional groups increased the frequency of hydrogen bonding in the polymers.

The data from IR also yielded information about hydrogen bonding and the rigidity of the ether polymer. As the rigidity of the polyether increased, the $\Delta\nu$ decreased for any given percentage of PVPh in the PS-co-VPh. Thus, if the number of hydrogen bonding sites is held constant, intermolecular hydrogen bonding will increase with increasing flexibility in the polyether chain. However, when only 10 percent VPh is incorporated into the PS-co-VPh, the effect of the polyether rigidity is much less when compared to samples containing 20 and 100 percent VPh. The spacing between –OH groups in the 10 percent sample allows flexibility for the –OH groups to arrange to form hydrogen bonds with even the most rigid of polyethers. Thus, increasing the spacing of hydrogen bonding groups along an amorphous polymer chain yields a method for rigid polymers to effectively participate in hydrogen bonding with an amorphous polymer. [30]

Viswanathan and Dadmun used FTIR to study the extent of hydrogen bonding between an amorphous polymer, PS-co-VPh, with a rigid, liquid crystalline polyurethane (LCPU), 4,4'-bis(6-hydroxyhexoxy) biphenyl. The amount of VPh was varied between 5-100 percent of the PS-co-VPh to vary the number of hydrogen bonding sites along the copolymer chain. As the amount of VPh increased from 5 to 20 percent, data from IR showed that intermolecular hydrogen bonding increased. However, increasing the amount of VPh over 20 percent in the PS-co-VPh showed little increase in the amount of intermolecular hydrogen bonding. Therefore, only 20-mol% of the vinylphenol functional group was needed in the amorphous polymer to obtain the largest degree of hydrogen bonding.

In addition, DSC and optical microscopy were used to study the miscibility of the LCPU/PS-co-VPh blend over various blend compositions. The VPh content of the PS-co-VPh copolymer was varied between 10, 20, and 30 percent and DSC curves showed a single Tg for the LCPU/PS-co-VPh (20) at blend compositions of greater than 60wt% copolymer. Single Tgs for the blend were also reported for the other blends at compositions greater than 80wt% copolymer. Optical microscopy data confirmed that the blend containing PS-co-VPh (20) had a wider window of miscibility than the other two blends.[31]

1.7 Copolymer Addition

Experimentally it has been determined that the addition of a copolymer that is made from the same monomers as the blend components will improve the mechanical

properties of a phase separated blend.[7,17] The enhancement of mechanical properties of the blend upon addition of the copolymer is attributed to the migration of the copolymer to the biphasic interface where it acts to lower the interfacial tension, increase interfacial adhesion by acting as a molecular stitch across the interface, and to inhibit droplet coalescence.[6,9,18,32-39] The effectiveness of the copolymer additive as an interfacial modifier has been studied as a function of a number of variables including the amount of copolymer added, copolymer architecture, and monomer sequence of the copolymer.[9,19-21,23,40-48]

Especially of interest to this project is that the sequence distribution of the copolymer has been shown to influence the ability of a copolymer to compatibilize immiscible polymer blends.[21,22] In particular, Dadmun has examined the ability of copolymers with different microstructures to act as an interfacial modifier in homopolymer blends using Monte Carlo simulation. Copolymers that had block, alternating, and random structures and composed of monomer A and monomer B were studied as compatibilizers to an A/B polymer mixture. All three copolymers were capable of migrating to the A/B interface, but the arrangement of the copolymers at the interface was influenced by the copolymer architecture. Expansion of a copolymer at the biphasic interface increases entanglements of that copolymer with each homopolymer and enhances the ability of the copolymer to serve as an interfacial modifier. Block copolymers tended to expand across the interface while alternating copolymers were equally expanded along the interface. However, random copolymers expanded the least both across and along the interface. Thus, random copolymers were

interpreted to be the least effective as interfacial modifiers, while both alternating and block copolymer were expanded at the interface to allow for entanglements and interfacial modification. The results suggest that a diblock or an alternating copolymer will reinforce the interface the most effectively and would thus be the best compatibilizers.

Copolymers that were designed to be a hybrid between alternating and random and a hybrid with architecture between random and blocky were also studied. In the case of the alternating/random hybrid, the expansion of the copolymer at the interface was less than that of the random copolymer resulting in a minimum number of entanglements. However, the block/random hybrid expanded across the interface better than all other structures except the pure block copolymer and the block/random hybrid also expanded along the interface better than all other structures except the pure alternating copolymer. The analysis suggests that a copolymer with a structure between a random and a block copolymer (a blocky copolymer) would be the most effective compatibilizer as it expands isotropically at the biphasic interface and does not form microphases or micelles easily.[23]

Eastwood and Dadmun completed experiments that demonstrate that block copolymer architecture and block length played important roles in defining the ability of a copolymer to modify a blend system. Styrene/methyl methacrylate block copolymers and a random copolymer consisting of styrene and methyl methacrylate were examined to determine the influence of copolymer architecture on its ability to compatibilize a PS/PMMA interface. Fracture toughness (G_c), of a PS/PMMA interface compatibilized

with a diblock, triblock, pentablock, and heptablock copolymer were measured using the asymmetric double cantilever beam (ADCB) test. In this study, each block size was held constant as the number of blocks in the copolymer was increased. Increasing the number of blocks in the copolymer coincided with an increase of the fracture toughness of the blend. In the second investigation, the number of blocks in the copolymer was held constant and the size of the individual blocks was increased from 21 to 30 to 50 thousand M_w. As the block size increased, the number of entanglements between the copolymer and surrounding homopolymer increased yielding an increase in fracture toughness. Thus, the lengths of each block in the copolymer must be long enough to enter into and entangle with each homopolymer at the biphasic interface in order to increase fracture toughness. If block lengths are long enough to entangle into each homopolymer, then increasing the number of blocks in the copolymer modifier will improve the fracture toughness of the blend.[1]

1.8 Reactive Processing

Reactive processing of polymer blends refers to any processing technique where chemical reactions occur. The chemical reactions that occur during processing can be grouped into several major categories including formation of graft copolymer, controlled degradation, functionalization, polymerization, and coupling reactions.[49] Of particular interest to our studies is the coupling reaction of oligomers/polymers to form copolymers at an interface of a polymer/polymer blend.[8,50-58]

Theoretical simulations of reactive processing have recently been undertaken.[54,55,59] O'Shaughnessy et al. developed a theory to study the formation of diblock copolymers via coupling of two end-reactive polymers at a polymer/polymer blend biphasic interface. The reaction kinetics of the system depend on the relative reactivity of the functional groups, entanglement at the interface of the polymer blend system, and crowding of the interface by the reactive molecules. O'Shaughnessy et al. theorized that reactions at the biphasic interface were effectively switched off when a critical coverage of the reactive oligomers reached the biphasic interface. This critical coverage did not form sufficient diblock copolymer to significantly reduce the surface tension of the polymer blend. Although it was theorized that reduced surface tension could not be achieved, it was possible that reactions at the biphasic interface produced enough copolymer to prevent droplet coalescence.[54]

Schulze et al. have experimentally studied the migration of oligomers with a single functional endgroup (amine terminated) to a polymer-polymer interface using two sample geometries as illustrated in figure 1.1. In geometry I, PMMA that is terminated with an anhydride group (PMMA-anh) (M_n 35,000) is spun cast onto a surface. A second film of PS (M_n 230,000) containing deuterated PS which are terminated with amine endgroups (dPS-NH_2) is formed via spin casting onto a glass slide and then floated onto the PMMA layer. Sample II is formed by spin coating the PMMA-anh onto a surface and PS is then spun cast onto a glass slide and floated onto

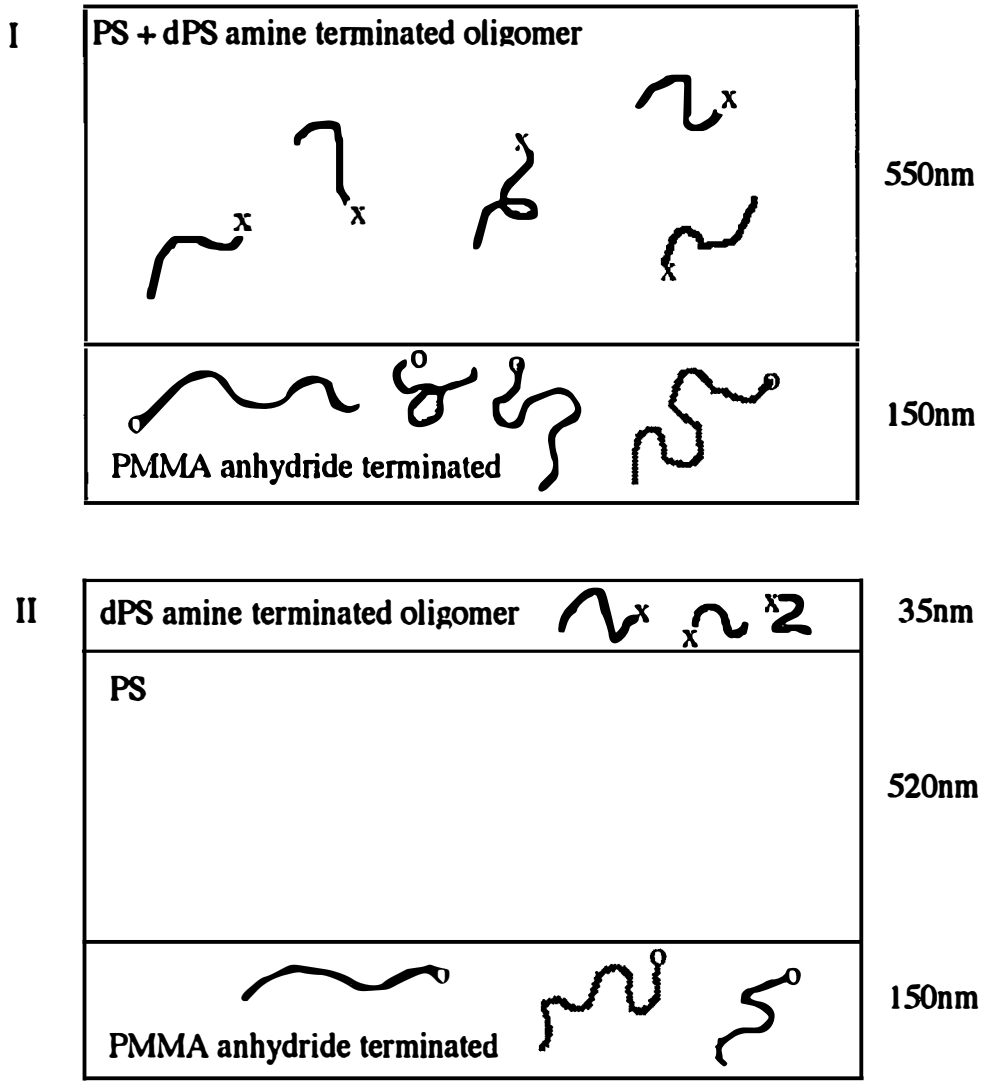

Figure 1.1 Sample geometries used by Schulze et al to study the formation of diblock copolymers at a biphasic interface of PS/PMMA-anh. In this representation X and O are reactive sites on the PS oligomers and PMMA respectively that can react to form P(S-b-MMA) copolymers.

the PMMA-anh. Finally, the dPS-NH_2 is spun cast onto a glass slide and floated onto the PS layer. The Mn of the dPS-NH_2 was allowed to vary for each sample geometry (32,000; 37,000; 92,000). For each geometry, the samples are annealed at 174°C under vacuum for various times. During both experiments, the dPS-NH_2 diffuses through the polystyrene homopolymer to the biphasic interface that is saturated with anhydride functional groups. In this system, the reactive group from the amine- terminated dPS can react with the anhydride group of the PMMA and form a diblock copolymer at the interface.

Depth profiling data acquired using FRES (forward recoil spectrometry) showed that it could take up to 24h for significant reaction to occur. However, for each molecular weight of dPS-NH_2, it should take less than 1h to diffuse 550nm through the PS. This suggests that the limiting factor for the formation of diblock copolymer to take place is the diffusion and reaction of the two functional groups *at* the interface and is not dependent on the rate of diffusion of the dPS-NH_2 through the bulk to the interface.[60]

Yin et al. have also calculated the rate of reaction of functional endgroups attached to polymers at 180°C. In this system, a cup and rotor mixer was used to mix blends consisting of 75 wt% PS and 25% PMMA. The PS phase contained 24wt% low molecular weight PS-NH2 and 76-wt% high molecular weight PS-NH2. The PMMA phase contained 40 wt% anhydride terminated anthracene-labeled PMMA and 60 wt% nonreactive PMMA. The conversion of reactive polymer to diblock copolymer was followed using size exclusion chromatography (SEC).

Two different molecular weights (M_n 26,000 and 72,000) of PS-NH_2 were used, and both molecular weights of PS-NH_2 reacted with the PMMA-anh within the first two minutes of mixing. After the first two minutes of mixing, the conversion of the PS-NH_2 to copolymer sharply decreases. In addition, the average particle diameter of the PS phase decreased sharply within the first two minutes of mixing followed by almost no change at longer time intervals. The leveling off of particle diameter size and the decrease in reaction rate was a direct result of copolymer formation at the interface and agrees with O'Shaughnessy that reaction at the interface will switch off once a critical coverage of copolymer is reached at the interface. As copolymer forms at the interface, the remaining reactive chains cannot access the interfacial region where reaction can occur.

As mixing time increased to 20 minutes, the percent conversion of the higher molecular weight PS-NH_2 was negligible. However, during the same 20 minutes, the lower molecular weight PS-NH_2 was able to reach the interface and react to convert nearly 5% more than in the initial 2 minutes. Thus, the initial phase of the reactive compatibilization process does not depend on the molecular weight of the reactive polymers, but its second phase is molecular weight dependent as the reactive polymers must diffuse through the diblock region to reach mutually reactive sites. The higher molecular weight PS-NH_2 diffuses slowly through this region, which reduces their reaction rate, while the lower molecular weight PS-NH2 diffuses through this region and continues to react at longer, mixing time. [52]

1.9 Compatibilization Analysis

Choosing a compatibilization technique for a polymer/polymer blend is merely the first step in creating a well-compatibilized blend. To insure effective compatibilization a number of important processes must be understood. For instance, in the special case of reactive compatibilization the diffusion of the reactive entities to the interface is a critical step in the process. Following that a reaction must occur once the reactive species reach the polymer/polymer interface. To understand this process the diffusion of the reactive component can be monitored using depth-profiling techniques, and the extent of reaction can be studied.

The effect of the compatibilizer on the blend's morphology and mechanical properties can also be used as a mechanism to monitor the reactive processing scheme. The morphology of the blend can be used to resolve how well a blend has been compatibilized as effective compatibilization leads to smaller phase domains. Alternatively, as the main goal of the reactive compatibilization process is to create a useful polymer blend, the mechanical properties of the compatibilized blend can be monitored to evaluate the success of the compatibilization process.

1.10 Depth Profiling

Depth profiling is a technique that allows the characterization of a polymer system throughout the depth of the sample. Depth profiling of polymer samples has been used to study diffusion of both polymers and small molecules within polymers, surface segregation, and polymer interfaces.[51,60-66] Thus, this technique is well suited to

studying the diffusion of compatibilizers to a biphasic interface in a polymer system as well as the interfacial broadening observed when a copolymer is placed at the biphasic interface of a polymer/polymer blend. Several analytical techniques used to study the depth profile of polymers include forward recoil spectrometry (FRES), neutron reflectivity, and secondary ion mass spectrometry (SIMS).

1.11 Forward Recoil Spectrometry

Forward Recoil Spectrometry (FRES), also known as elastic recoil detection, is a method used to measure the concentration of hydrogen or deuterium in solids as a function of depth. In this experiment, the sample is exposed to a beam of alpha particles ($^4He^{2+}$) at an incident angle from the normal (figure 1.2). Hydrogen and/or deuterium are then scattered in a forward direction from a depth determined by the incident angle. A detector placed at an angle relative to the incident ion beam measures the relative amount of hydrogen and deuterium while other numerous scattered incident ions are filtered from the detector. The particles that are recoiled and the incident ion beam both experience a loss of energy that can then be converted into a depth profile of the sample. This technique is mainly a surface technique where the maximum depth that can be profiled is 700nm with a surface resolution of 80nm and is limited by the incident angle. [61] FRES is well suited to the study of polymer thin film systems and has been used for nearly two decades. [51,60,61] Major disadvantages associated with this

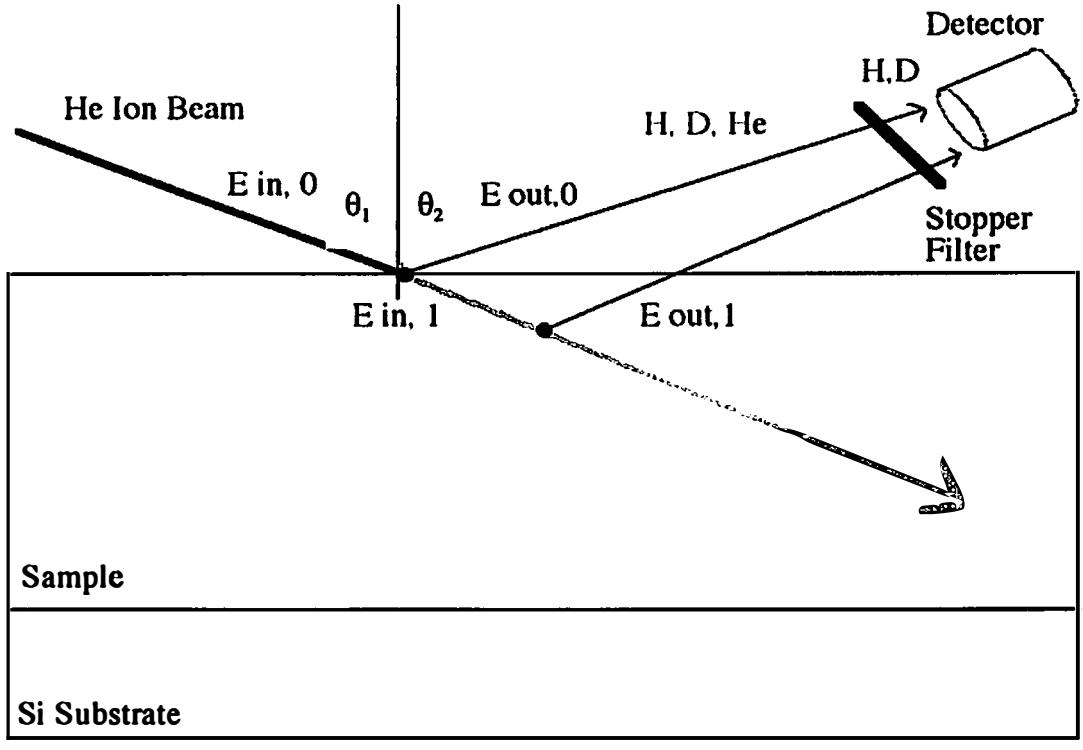

Figure 1.2 A representation of a forward recoil spectrometry (FRES) experiment. An $^4He^+$ ion with E_{in} strikes the sample at an angle θ_1. ^1H and ^2H are recoiled along with $^4He^+$ at an angle θ_2 and energy E_{out} towards the detector.

technique include poor surface depth resolution and the need to deuterium label part of the sample for contrast.

Schulze et al. used FRES to study the formation of diblock copolymers at a PS/PMMA interface. The incident angle was 15° and the detector was 30° from the incident beam; a reported 700nm was depth profiled with a resolution of 90 nm using this configuration. The experiments monitored the formation of copolymer at the interface over several hours. However, calculated diffusion times for the reactive oligomers to cross 550nm of polystyrene were much less than the time needed for substantial reaction to occur. This was interpreted to indicate that the formation of block copolymer at the interface is not limited by bulk diffusion to the interface, but diffusion and reaction at the interfacial zone are critical in the reaction process.[60]

1.12 Neutron Reflectivity

Neutron reflectivity has been used extensively in for depth profiling.[62-68] Neutron reflectivity is a non-destructive technique that allows the same sample to be continually depth profiled over a range of temperatures or for the sample to be used in additional experiments after depth profiling. Another major benefit of neutron reflectivity is the superior depth resolution (10Å) that can be achieved compared to other depth profiling techniques. To perform a depth profile of materials such as polymers that are mostly hydrocarbon some of the material must be deuterated. Deuterated materials will contrast with hydrogenated material because the difference between the scattering length of deuterium and hydrogen is large.[63] Figure 1.3 shows a typical

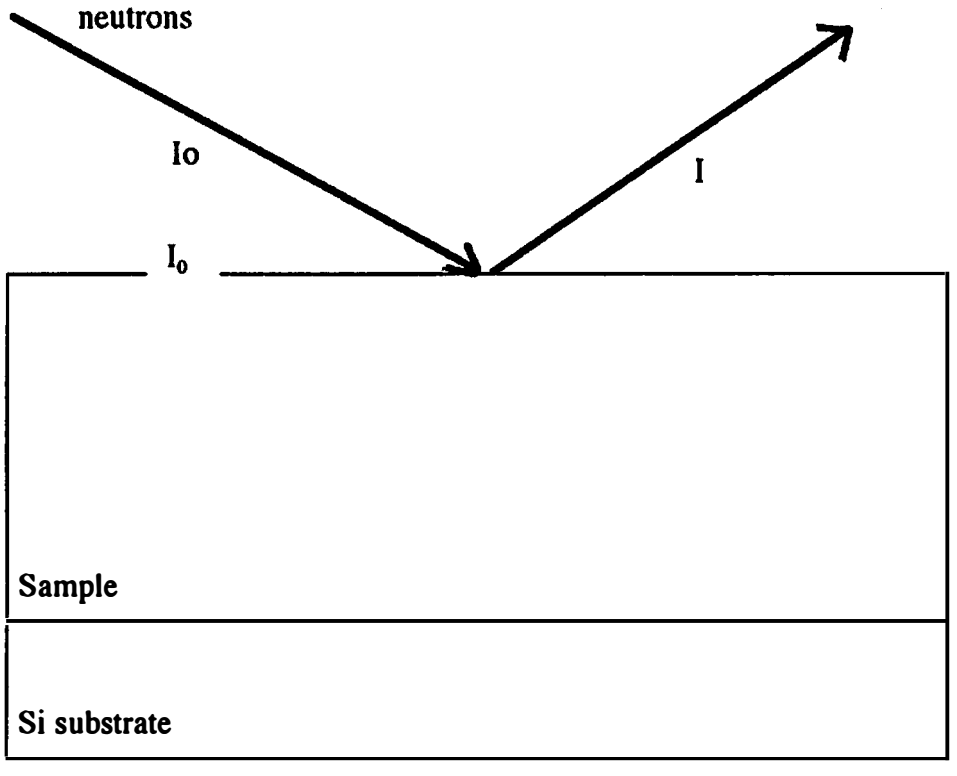

Figure 1.3 Illustration of neutron reflectivity depth profiling experiment. A neutron beam with initial intensity I_0 strikes the sample and an angle θ and is reflected with an intensity I at angle θ.

experimental setup where I represents the reflected neutron intensity while I_0 represents the initial neutron intensity.

Kulasekere et al. used neutron reflectivity to study the interface of a polystyrene (PS)-poly (methyl methacrylate)(PMMA) blend with a random copolymer of PS-PMMA as an interfacial modifier. Samples for neutron reflectivity were prepared by spin casting an 800Å layer of PMMA onto a silicon substrate. Next, a P (S-r-MMA) copolymer film with a thickness of 150Å was spin cast onto a glass slide and floated onto the PMMA layer. Finally, a PS film (800Å) was spun cast onto a glass slide and floated onto the copolymer layer and the entire sample was then annealed at 170°C for 12 hours.

Neutron reflectivity profiles of the system were performed with neutrons having a wavelength of 2.35Å. Depth profiles showed that random copolymers with a styrene fraction of 0.68 were able to equally penetrate the PS and PMMA homopolymers. Although this same composition of random copolymer is immiscible in both PS and PMMA, a symmetric broadening of the interface did occur. [19] Schnell et al. studied the fracture toughness between PS and different styrene based polymers, poly (p-methylstyrene) and copolymers of poly (bromostyrene-styrene), using ADCB. In addition, the width of the interfaces of these polymer systems was determined using neutron reflectivity. Neutron reflectivity samples were prepared as above using spin casting and floating techniques. The experiments were performed using neutrons with a wavelength of 4.3nm; the incident angle was varied and depth profiles were determined

to monitor interfacial width of the samples. This interfacial width was then compared to the fracture toughness of polymer samples with identical composition. The study showed that at low interfacial widths (<6nm) the fracture toughness was very low. At intermediate interfacial widths (6-11nm) the fracture toughness increases dramatically with increased interfacial width. Finally, at large interfacial widths (>11nm) the fracture toughness approaches the bulk toughness.[63]

1.13 Secondary Ion Mass Spectrometry

Secondary Ion Mass Spectrometry (SIMS) is a depth profiling technique characterized by a primary ion source, sample, secondary ions, and a detector. Figure 1.4 is a simple schematic of a SIMS experiment. A beam of primary ions hits the sample causing atoms and molecules on the surface of the sample to be ejected or sputtered. Some of the sputtered atoms are ionized and then selected by energy by an electrostatic analyzer and by mass in the magnetic sector. The ions are then directed into the counting system using another electrostatic analyzer; ions are counted using a faraday cup or an electron multiplier. The resulting mass spectra can be assessed as a function of time. Since the energy put into the sample over time is known along with the energy required to burn through a standard sample, mass spectra can also be determined as a function of depth.

SIMS has been used for many years as a depth-profiling tool for inorganic compounds. SIMS spectra are obtained by hitting the sample with a primary atomic ion beam, which is traditionally an atomic ion such as Ar^+, He^+, and Ge^+. As the

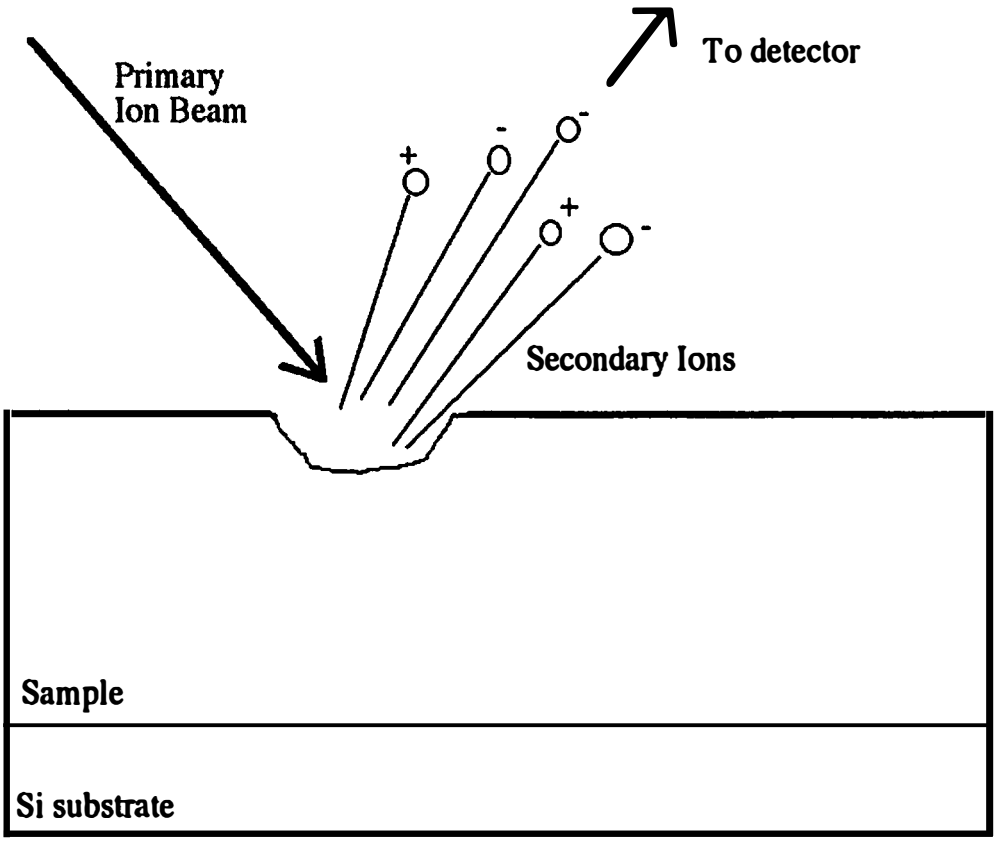

Figure 1.4 Representation of a secondary ion mass spectrometry (SIMS) depth profile experiment. A primary ion beam strikes the sample causing ionization. These ions are then sputtered towards a detector.

beam penetrates the sample, molecules from the sample are ionized, and these secondary ions are then funneled into a detector. The intensity of the primary ion beam is known and can be converted into depth. The silicon industry uses SIMS routinely to depth profile samples to look for trace elements within silicon crystals. These elements are usually only in the ppm to ppb range; the sensitivity of SIMS allows detection of these elements even at these low levels.

SIMS has also been used to study polymers.[69-74] Yokoyama et al. used SIMS to study the diffusion of deuterated polystyrene-b-2-vinylpyridine (dPS-PVP) within a well-ordered polystyrene-b-2-vinyl pyridine (PS-PVP) film. Samples for SIMS were made by spin casting PS-PVP onto silicon. Next, dPS-PVP (20nm) was spun cast onto a glass slide and floated onto the PS-PVP surface, and the samples were then annealed at 178°C. A sacrificial layer of PS was then floated onto the dPS-PVP so steady state sputtering conditions during SIMS could be reached before the bilayer sample was analyzed. The primary ion beam consisted of a 2keV, 20nA Ar^+ beam at a 30° angle from the sample surface.

A study of the PS-PVP block copolymer was performed to determine the order of the spherical domains of the PVP block within the PS. The PVP domains were determined by monitoring the CN^- signal during depth profiling. The rough data showed a global maximum of the PVP occurring close to the Si substrate, which illustrates that the PVP blocks preferred the Si substrate. In addition, the PVP signal oscillated in a periodic fashion as a function of depth. The rough data was then fit to a model where the PVP anchors the diblocks at the Si surface follow by a bcc structure of

PVP spheres, (110) planes parallel to the Si, within the PS. A dPS-PVP block copolymer was then placed on top of the PS-PVP ordered structure using the same spin coating and floating technique. After annealing at 178°C for 300s, the dPS segments of the block copolymers surrounded the first layer of PVP sphere domains at 45nm. After the sample was annealed for 41,700s, much of the dPS-PVP is still located at 45nm. However, some dPS-PVP had diffused to a depth of 80nm into the sample. This depth corresponds to the second layer of PVP spheres within the bcc structure. In order to achieve the hopping of the dPS-PVP from one PVP layer to another, the dPS-PVP has to overcome a thermodynamic barrier with a probability proportional to exp ($-\alpha\chi N_{core}$). In this case, α is a constant, χ is the Flory-Huggins interaction parameter, and N_{core} is the number of segments of the PVP block in the spherical domains. [72]

Although previously used to depth profile some polymers, it has been shown that the effects of ion damage prevent traditional SIMS from being used to depth profile most organic solids as is done for inorganic materials.[73,74] The primary ion beam used in most SIMS experiments causes charring of the sample that leads to signal decay in organic molecular solids such as polymers. Polyatomic primary ions have been shown to confine the damage done to organic samples as well as increasing the number of secondary ions. [73,74] The combination of these two factors is promising for the depth profiling of organic molecular solids.

Gillen et al has created a SIMS instrument that uses molecular ($SF5^+$) primary ions instead of the traditional atomic ions.[73,74] Samples of PMMA and other organic materials were depth profiled using both an atomic primary ion (Ar^+) and a molecular

primary ion (SF_5^+). Figure 1.5 illustrates how the secondary ion intensity varies for a sample of PMMA when depth profiled with atomic primary ions (squares) and molecular primary ions (triangles). The intensity of the secondary ions dramatically drops off when using atomic primary ions. In contrast, the intensity of secondary ions of PMMA remains constant throughout the experiment using molecular ions.

The decrease in signal associated with the use of a primary atomic beam is caused by the energy and depth of penetration of an atomic primary ion on the sample. Figure 1.6 illustrates the depth an atomic ion can penetrate the sample relative to that of a polyatomic ion. The polyatomic ion travels approximately 4.5nm into the sample while the atomic ion can penetrate over 12nm into the sample. Only the top layer of the sample is accessible to sputtering and can thus be efficiently ejected. Those atoms below the sputter layer are damaged by the primary atomic ion beam and cannot be removed via sputtering due to their depth in the sample. Molecular primary ions only penetrate the sample 4.5nm that allows ionized and damaged molecules to be sputtered from the sample. In contrast, the atomic primary ion beam ionizes and damages the sample for a depth of greater than 12nm, the damaged material is below the sputtering layer, and is therefore not removed. As the profile progresses, only damaged material will be sputtered from the sample since the atomic primary ion is continually damaging the sample below the sputter layer.

In addition, the polyatomic ion fragments into atoms when it hits the sample.

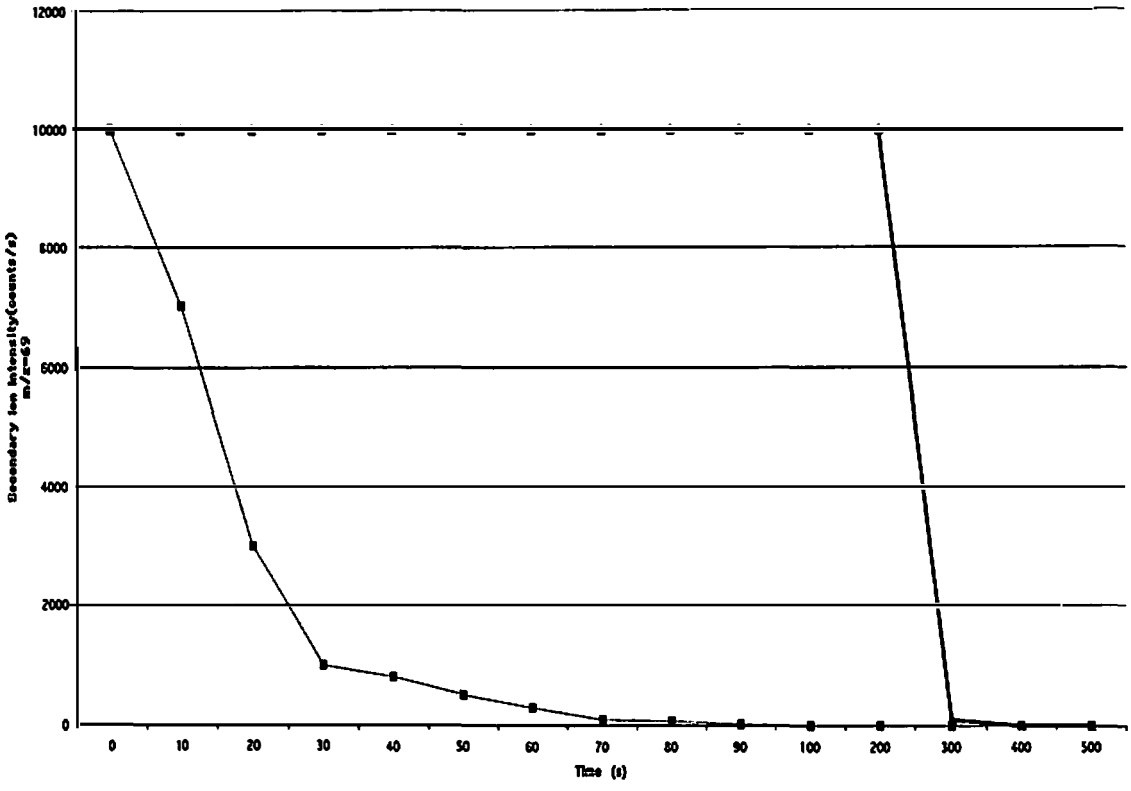

Figure 1.5 Illustration of signal decay for a SIMS depth profile experiment when atomic primary ions (squares) are used versus molecular primary ions (triangles). Typical signal decay of the m/z 69 fragment for PMMA is illustrated. [74]

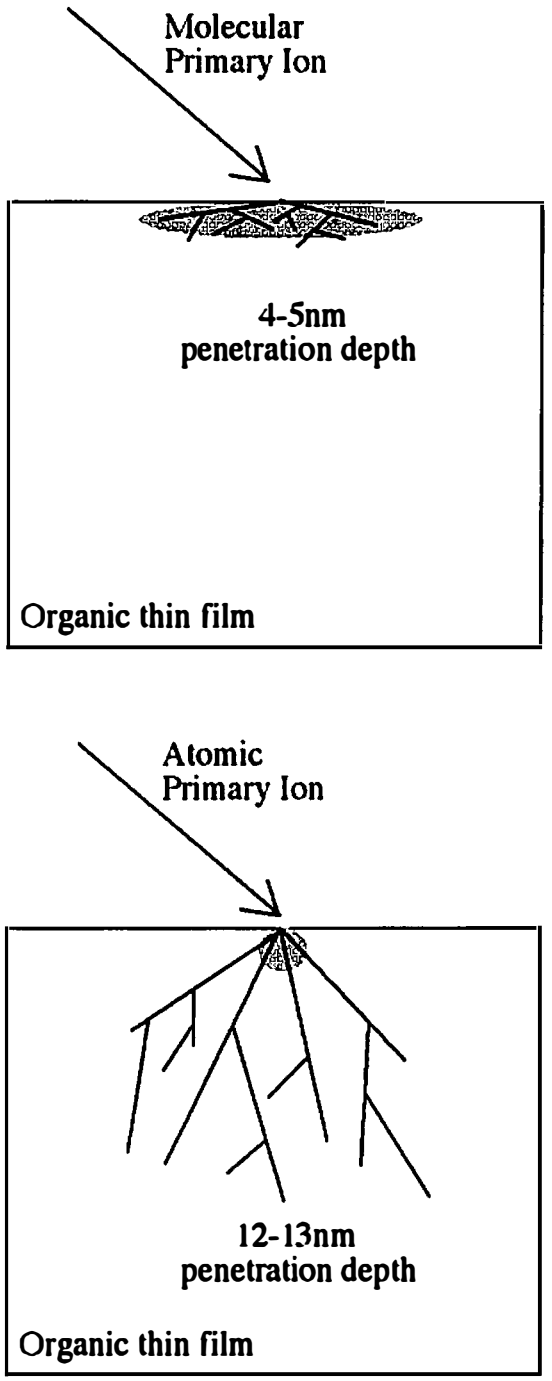

Figure 1.6 Comparative primary ion beam induced damage to an organic sample during a secondary ion mass spectrometry experiment. [74] Atomic primary ions penetrate deeper into the sample with more energy causing damage that can not be sputtered.

For the polyatomic ion, each individual atom contains a fraction of the initial ion beam energy given by the equation:

$$E_c=E_o\,(M_c/M_t)$$

In this equation, E_c is the energy of a particular atom after collision with the sample, E_o is the initial energy of the polyatomic ion, M_c is the mass of an individual atom, and M_t is the mass of the molecular ion. On the other hand, the Ar^+ ion of a primary atomic ion beam preserves its full impact energy. The increased energy and penetration depth of the atomic ion can cause intramolecular bond breakage, which damages the sample. As discussed above, this damage is below the sputter layer and accumulates as the experiment continues. The buildup of damaged material below the sputter layer causes the decrease in ion intensity as illustrated in figure 1.5.[73,74]

1.14 Blend Morphology

Polymer blends can exhibit an array of morphologies that can be manipulated by the composition of the blend, forced quenching from a high temperature, and the degree of compatibilization. Domain type, dispersion and size within a polymer blend are a major focus point for many compatibilization studies. Large phase domains and a high interfacial tension resulting in a coarse morphology usually define incompatible blends. High interfacial tension also results in poor interfacial adhesion that decreases the mechanical properties of the blend as discussed in section 1.15. Compatibilizers occupy the interface, lower interfacial tension, and prevent droplet coalescence. Thus, a good

compatibilizer will result in smaller phase domains and increased interfacial adhesion.[75-80]

Huang et al studied the compatibilization of poly (ethylene-2, 6-naphthalate) (PEN) with PS using styrene-glycidyl methacrylate (SG) copolymers. The SG copolymers react with PEN to form graft copolymer compatibilizers, SG-g-PEN, at the PEN/PS interface. The glycidyl methacrylate (GMA) portion of the SG copolymer varied between 2(SG2), 5(SG5), and 10(SG10) percent. Polymers were blended in a 30mm co-rotating twin-screw extruder at 260°C-290°C.

Blends were cryogenically fractured and scanning electron microscopy (SEM) was used to study the morphology of the sample perpendicular to the plane of flow. SEM micrographs of PS/PEN blends showed large domains of PS within the PEN when no compatibilizer was used. As the amount of SG5 was increased from 2 to 10 percent, the domains of PS grew smaller until the PS domains were indistinguishable in the SEM at 10 percent SG5. The authors theorized that as the compatibilizer levels increased, interfacial tension decreased and it became more difficult for the PS droplets to merge together.

In addition, SEM micrographs of blends that had an addition of ethyltriphenylphosphonium bromide (ETPB) to catalyze the in situ reaction of PEN and SG were also studied. The phase domains of PS in PEN grew smaller with the addition of catalyst for the blends containing only 2 percent SG5. However, the phase size of PS actually increased for the blends with 5 and 10 percent SG5 added. Similarly, SEM micrographs of blends with SG2, SG5, and SG10 were compared. The phase domain

size of the PS decreased when the compatibilizer was modified from SG2 to SG5. No decrease in PS domains was obtained when the compatibilizer was changed from SG5 to SG10.

The addition of catalyst and an increase in the GMA content of the SG created a higher degree of grafting in the copolymer and may even lead to crosslinking. The higher degree of grafting in the copolymer formed may result in styrene segments that are too short to entangle into the PS phase. The copolymer is no longer an effective compatibilizer and the domain sizes of the PS in the catalyzed blends for 5 and 10 percent SG5 are larger than those in the uncompatibilized blends. Thus, the degree of grafting and ultimately the length of graft copolymer segments in the in situ formed copolymer is important in determining the effectiveness of a compatibilizer.[75]

Charoensirisomboon et al also studied the morphology of a polymer/polymer blend system when a block or graft copolymer was generated by reactive processing.[8] In this system polysulfone(PSU) was blended with polyamide(PA). The polysulfone was also functionalized in several experiments with maleic anhydride, epoxy, or phthalic anhydride and designed to react with the PA to form graft or block PSU-PA copolymers. The samples were mixed at 260°C for 6 minutes and then quenched at –40°C and microtomed to 60nm. Ruthenium tetroxide (RuO_4) was used to stain the PSU and transmission electron microscopy was used to study morphology. The PSU-PA blend that did not contain a functionalized PSU had domain sizes in the 1.3 μm range; when the PSU was functionalized, the domain sizes in the PSU-PA blend decreased to the nm range with a minimum of 70nm. The authors believed that the system with

functionalized PSU formed copolymers which acted as emulsifiers and prevented droplet coalescence.[8]

1.15 Mechanical Properties

Improved or targeted material performance is the primary objective when blending polymers. The mechanical properties of a blend can vary greatly depending on the blends miscibility or level of compatibilization. An effective compatibilizer will lower interfacial tension, decrease droplet coalescence, and increase interfacial adhesion. The interfacial adhesion between polymer blend components directly affects the mechanical properties of the blend. A low interfacial adhesion at the polymer/polymer blend interface will allow failure to occur at the polymer biphasic interface. Many experiments in this field center on fracture toughness, interfacial adhesion, elongation, stress, and total energy at break.[81-87]

Creton et al. investigated a system of PS sheets and poly (2-vinylpyridine) (PVP) sheets compatibilized with poly (styrene-b-2-vinylpyridine) (PS-b-PVP). The copolymer was spun cast onto the PVP sheet and the PS sheet was placed on top yielding a sandwich structure of PS/PS-b-PVP/PVP that was annealed under slight pressure at 160°C. The fracture toughness of the sample was then tested using an asymmetric double cantilever beam (ADCB). ADCB tests use a razor to start a crack at the interface of the two homopolymer layers. The razor blade is pushed along the interface at a constant rate and the crack length from the razor blade to the crack tip is

measured over time. The crack length from the razor blade can then be converted into the critical crack extension force (G_c)

In the first study, the length of the PVP block in the PS-PVP copolymers was allowed to vary. After propagating a crack in the sample at the interface, the sample was examined using scanning electron microscopy. For PVP block lengths less than the entanglement molecular weight, the PVP chains were pulled out of the bulk PVP as the crack was propagated leaving samples with little plastic deformation. As the PVP block in the copolymer was increased above the entanglement molecular weight, the failure mechanism became dependent on the areal density of copolymer chains at the interface. For low interfacial density of copolymer, no plastic deformation occurs at the crack tip and copolymer chains break at their midpoint. When the interfacial density is increased, crazing begins to occur and failure takes place at the interface through the breakdown of the craze. During this process, copolymer scission occurs near the joint of the two blocks of copolymer. When the copolymer density is increased sufficiently, the craze formed can achieve widths up to several microns. For these higher areal densities, the G_c of the samples scales as the square of the areal density of the block copolymers and the G_c approaches the fracture toughness of the homopolymers.[17]

Brown studied a system where a diblock copolymer poly (styrene-b-methyl methacrylate) (PS-b-PMMA) was used to compatibilize a PS/PMMA interface. The samples were made by combining the PS and PMMA sheets in a press at 150°C for 2h. Samples containing compatibilizer were made by spin casting a layer of copolymer

directly onto the PMMA layer before pressing. The resulting samples contained a PS-b-PMMA copolymer sandwiched between the PS and PMMA layers.

The interfacial toughness (G_c) was then studied as a function of the copolymer molecular weight and thickness. Mechanical testing and an asymmetric double cantilever beam (ADCB) were used to determine G_c. The addition of the block copolymer was shown to increase the toughness of the interface by a factor of fifty over the uncompatibilized sample. This increase in interfacial toughness was achieved by even a small amount of copolymer (20 nm film). The interfacial toughness continued to increase with elevated copolymer layer thickness (t) until a width is reached where the interface of the PS/PMMA was completely saturated with copolymer (t_m). When $t > t_m$, the toughness reached a plateau and may have began to decrease due to copolymers saturating the interface and forming micelles that do not increase the interfacial adhesion between the PS and PMMA. The interfacial toughness also increased with increasing molecular weight as $M^{0.5}$. [7]

1.16 Synopsis

Compatibilization of immiscible polymer blends using block copolymers has been studied as discussed previously. The work reported in this dissertation examines the feasibility of a proposed reactive processing scheme to create blocky copolymers in-situ at the polymer/polymer interface. The model system is shown schematically in figure 1.7. In this scheme, telechelic oligomers that are composed of the same

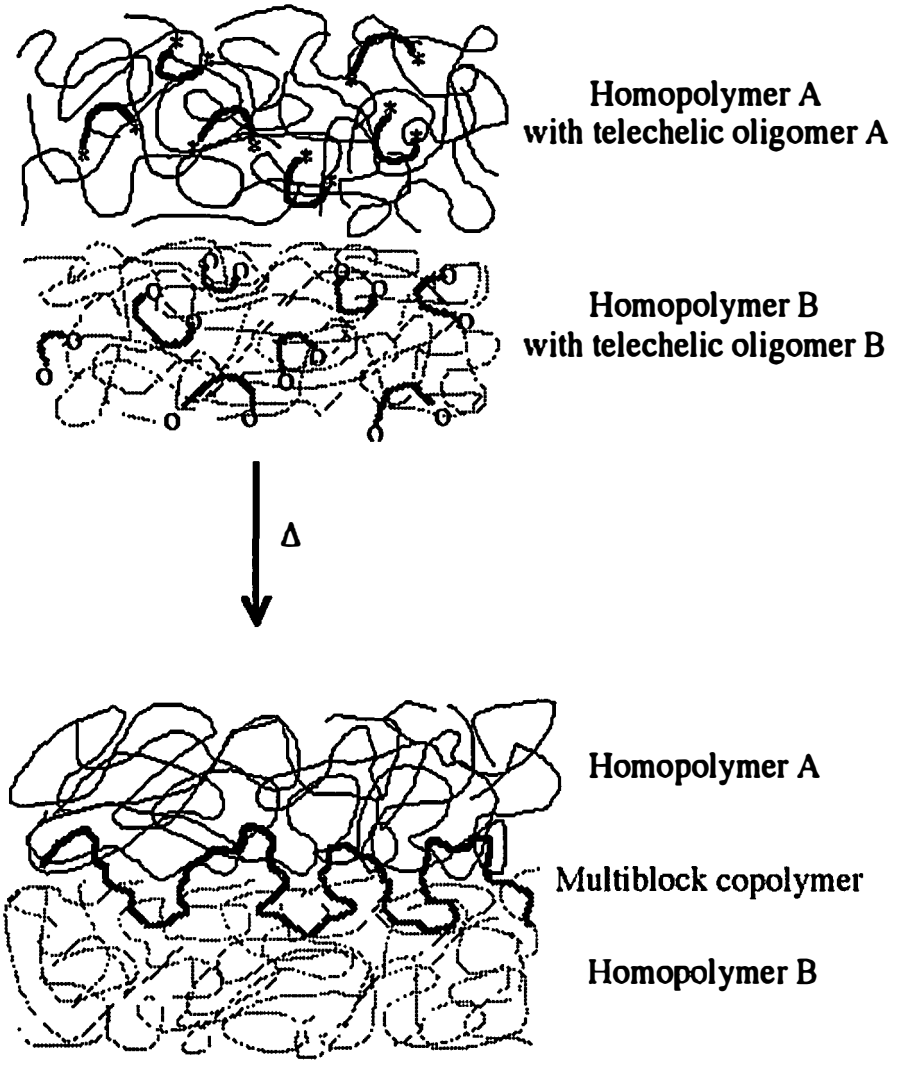

Figure 1.7 Illustration of reactive processing using telechelic oligomers to form a multi-block copolymer at a biphasic interface. In this illustration stars and circles are reactive endgroups on oligomers.

monomers as the two homopolymers are added to a blend. In this figure, the homopolymers are denoted by the solid (homopolymer A) and dotted (homopolymer B) long chain molecules, while the telechelic oligomers are denoted as shorter chains with reactive end groups (stars and circles). The oligomers are designed so that the stars and circles are mutually reactive, i.e. epoxide and carboxylic acid or anhydride and amine. As these four components are added to the processing equipment it is expected that the solid-line oligomers will dissolve in the homopolymer A phase while the dotted oligomers will dissolve in the homopolymer B phase. During mixing, the stars and circles will only encounter each other at the biphasic interface and will react to form a copolymer chain with two reactive end groups. Thus, this condensation polymerization of the oligomers can continue to occur during processing and a long chain blocky copolymer will be created at the interface to act as a compatibilizer. The small size of the oligomers will allow them to diffuse to the interface more quickly than long chain molecules and may alleviate the excess time needed in the blending process for the diffusion of a long chain copolymer additive to the interface. A model system containing poly (ethylene oxide) (PEO), poly (bisphenol-A-co-epichlorohydrin) (PBAE), and reactive telechelic oligomers of PEO and PBAE was examined using mechanical testing, optical microscopy, differential scanning calorimetry, and optical transparency. Since PBAE is a glassy polymer and PEO is an elastomer, their mechanical properties vary greatly and the compatibilization of a PEO/PBAE blend could lead to a blend with interesting properties. At the time of this study both PEO and PBAE also had commercially available telechelic oligomer counterparts.

The reactive compatibilization of polymer blends was also studied using the depth profiling technique of FRES. Samples containing PMMA-COOH, PS, and diepoxy terminated deuterated PS were used to study the migration of a difunctional reactive oligomers to a polymer/polymer interface. The PS/PMMA-COOH system was chosen for several reasons. First, the acid/epoxy reaction is a relatively fast reaction, second only to the amine/anhydride reaction for functional polymers as reported by Orr.[88] The PMMA-COOH was commercially available and the deuterated telechelic PS could be synthesized. In addition PS/PMMA is a well-defined immiscible system and the stopping powers of PS on $^{4}He^{+}$, ^{1}H, and ^{2}H are all known and necessary for FRES analysis.

Finally, the compatibilization of blends was studied using depth profiling and different compatibilizer chain architecture. A system composed of a copolymer layer (PS-b-PMMA) sandwiched between PS and PMMA homopolymers was studied using FRES and neutron reflectivity. Analysis of the thickness of the blocky copolymer layers was compared with ADCB results previously reported by Eastwood et al as discussed in section1.7.[1] Samples containing layers of alternating copolymer P (S-alt-MMA) sandwiched between two PS and PMMA homopolymer layers were also investigated using FRES. These results are compared with ADCB data as well as neutron reflectivity depth profiles of the same systems previously studied by Michael Arlen and explained in detail in Chapter 4. As stated above, the stopping powers of PS on He, H, and H are known and are needed to evaluate the FRES raw data. Therefore, both systems contained PS as the top layer of the sample. PMMA is immiscible with PS and

P (MMA/S) copolymers are readily available which makes PMMA the top candidate to study with PS.

Chapter 2

Experimental

2.1 Commercially Available Chemicals

It is not practical to synthesize all chemicals needed and polymers and solvents were purchased when possible. The poly (bisphenol-A-co-epichlorohydrin) (PBAE) (M_w = 40,000) and the corresponding diepoxy terminated oligomer (M_{an} = 4,000) were purchased from Aldrich chemical. Poly (ethylene oxide) (PEO) (M_w = 100,000) and the corresponding diamine terminated oligomer (M_w = 4,000) were purchased from Scientific Polymer Products Inc. All materials were placed in a Napco vacuum oven at 100 °C for 1 hour before use to remove residual moisture.

Methanol, sulfuric acid, hexane, toluene, and sodium sulfate were purchased from Fisher Chemical Company. Methanol and hexane were purified as described below when used in anionic synthesis, while sulfuric acid, toluene, and sodium sulfate were used as purchased. Benzene, n-butyl lithium(2.5M solution in hexane), calcium hydride, styrene, and dibutyl magnesium(1M solution in heptane) were obtained from Aldrich Chemical Company. Benzene and styrene were purified as described below, while n-butyl lithium(2.5M solution in hexane), calcium hydride, and dibutyl magnesium (1M solution in heptane) were used as purchased.

Deuterated styrene, carboxy terminated poly(methyl methacrylate) (PMMA-COOH) (Mw=15,400 PDI=1.14), deuterated poly(methyl methacrylate) (d-PMMA) (Mw=230000 PDI=1.07), and all alternating copolymers of PS/PMMA were obtained

from Polymer Source Inc. Deuterated styrene was purified as described below, while PMMA-COOH, dPMMA, and all alternating copolymers were used as purchased.

2.2 Synthesized Chemicals

There are several methods used to polymerize a material including condensation, free radical, and anionic techniques. Of these techniques, anionic polymerization offers the best method of synthesizing polymers with low polydispersity, well-defined architectures, and specific end groups. One of the main limitations of this technique includes working in an atmosphere free from water and oxygen that can terminate the living anionic ends of the growing polymer chain. To meet the stringent atmosphere requirements, an anionic high vacuum line able to maintain $1x10^{-5}$ torr was constructed based on plans acquired from Dr. Jimmy Mays. Figure 2.1 shows a representation of the vacuum line constructed. As can be seen, both a mechanical roughing pump and a mercury diffusion pump created the vacuum. The traps were filled with liquid nitrogen to insure contaminants did not reach the mechanical pump. The configuration showed in figure 2.1 also allows several different reaction processes to occur at the same time since three separate sections of the vacuum line can be isolated when necessary.

Polystyrene was synthesized using standard anionic methods.[89] A standard procedure for the synthesis is as follows:

Purification of Styrene: Styrene and calcium hydride were placed in a one neck round bottom flask with a magnetic stir bar. The styrene was stirred using a Corning

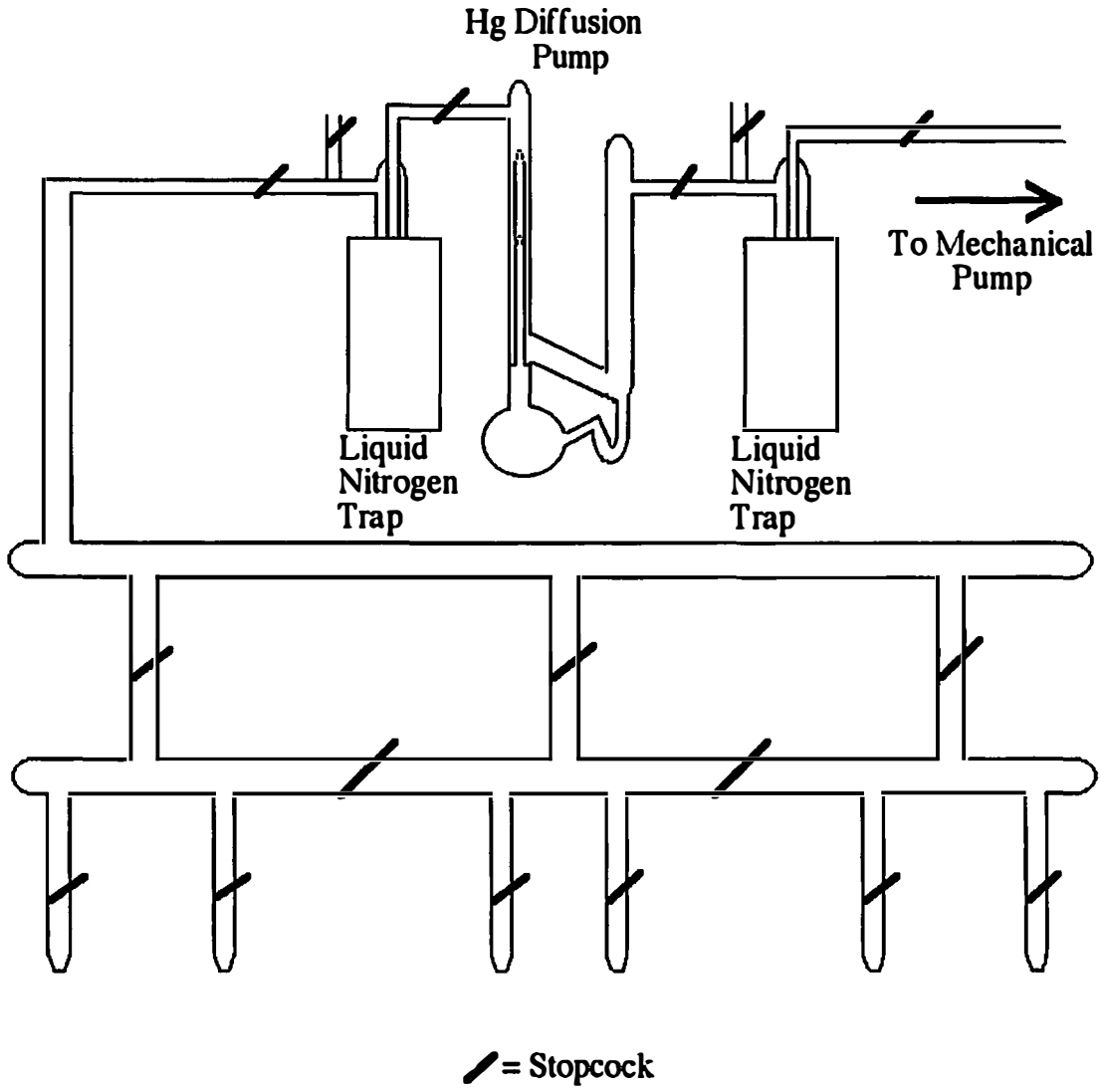

Figure 2.1 Representation of vacuum line used for anionic polymerization. Three sections that can be isolated allowed for multiple reactions and distillations.

stirrer/hot plate over the calcium hydride overnight at room temperature. Another single necked round bottom flask equipped with a stir bar was injected with 2ml of dibutyl magnesium and placed on the vacuum line. The flask was evacuated overnight to remove solvent. After stirring overnight, the styrene/calcium hydride flask was placed on the vacuum line and degassed three times using a freeze/thaw technique. The section of vacuum line containing both flasks was isolated from the main line by closing the stopcocks. Styrene was distilled to the flask containing dibutyl magnesium by placing liquid nitrogen under the dibutyl magnesium flask and a room temperature water bath under the styrene/calcium hydride flask. The styrene/dibutyl magnesium was allowed to stir for 2 hours. Finally, the purified styrene is distilled to precalibrated break seal ampoules by placing a room temperature bath under the styrene/dibutyl magnesium flask and wrapping a towel strip soaked in liquid nitrogen around an individual ampoule until full. The ampoules were then flame sealed from the anionic line and placed in a freezer until needed.

Purification of Benzene: Benzene was purified to be used as a solvent for polymerization. Benzene and sulfuric acid were placed in a single necked round bottom flask equipped with a magnetic stir bar. The mixture was allowed to stir one week at room temperature. Benzene was separated from the sulfuric acid using a separatory funnel. The resulting benzene was placed along with calcium hydride in a single necked round bottom flask equipped with a stir bar. The benzene was stirred over thecalcium hydride at room temperature for 24h. A cylindrical flask containing n-butyl lithium and styrene was placed on the vacuum line and allowed to evacuate. The

benzene mixture was then placed on the vacuum line and degassed using the freeze/thaw method. The benzene was then distilled using a room temperature to liquid nitrogen bath into the cylindrical flask containing n-butyl lithium and styrene that was already attached to the line. As the benzene thawed in the cylindrical flask, the solution became red/orange due to the presence of living styrene anions and ensured that the benzene was pure.

Dilution of Initiator: David Uhrig synthesized secondary butyl lithium in Dr. Jimmy Mays' lab at the University of Alabama at Birmingham. Initially, an individual vial of secondary butyl lithium held 1.53×10^{-3} moles of initiator. This concentration had to be adjusted in order to synthesize specific molecular weights of polymer. A special glassware system was used to dilute the secondary butyl lithium and is shown in figure 2.2. The break seal vial containing the secondary butyl lithium was attached at point A, while individual precalibrated break seal ampoules were attached along the bottom of the apparatus. This apparatus was then placed on the vacuum line and evacuated overnight and a Tesla coil was used to check for pinhole leaks. Hexane, used to dilute the initiator, was purified by placing the hexane with calcium hydroxide in a one necked round bottom flask equipped with a stir bar. The hexane was stirred over the calcium hydride overnight at room temperature using a Corning stirrer/hotplate. The next day, 2ml of n-butyl lithium was injected into a single necked round bottom flask equipped with a stir bar, and the flask was placed on the vacuum line and evacuated. The single neck round bottomed flask containing styrene/calcium hydride was then placed on the vacuum line and degassed using the freeze/thaw method. The hexane was distilled

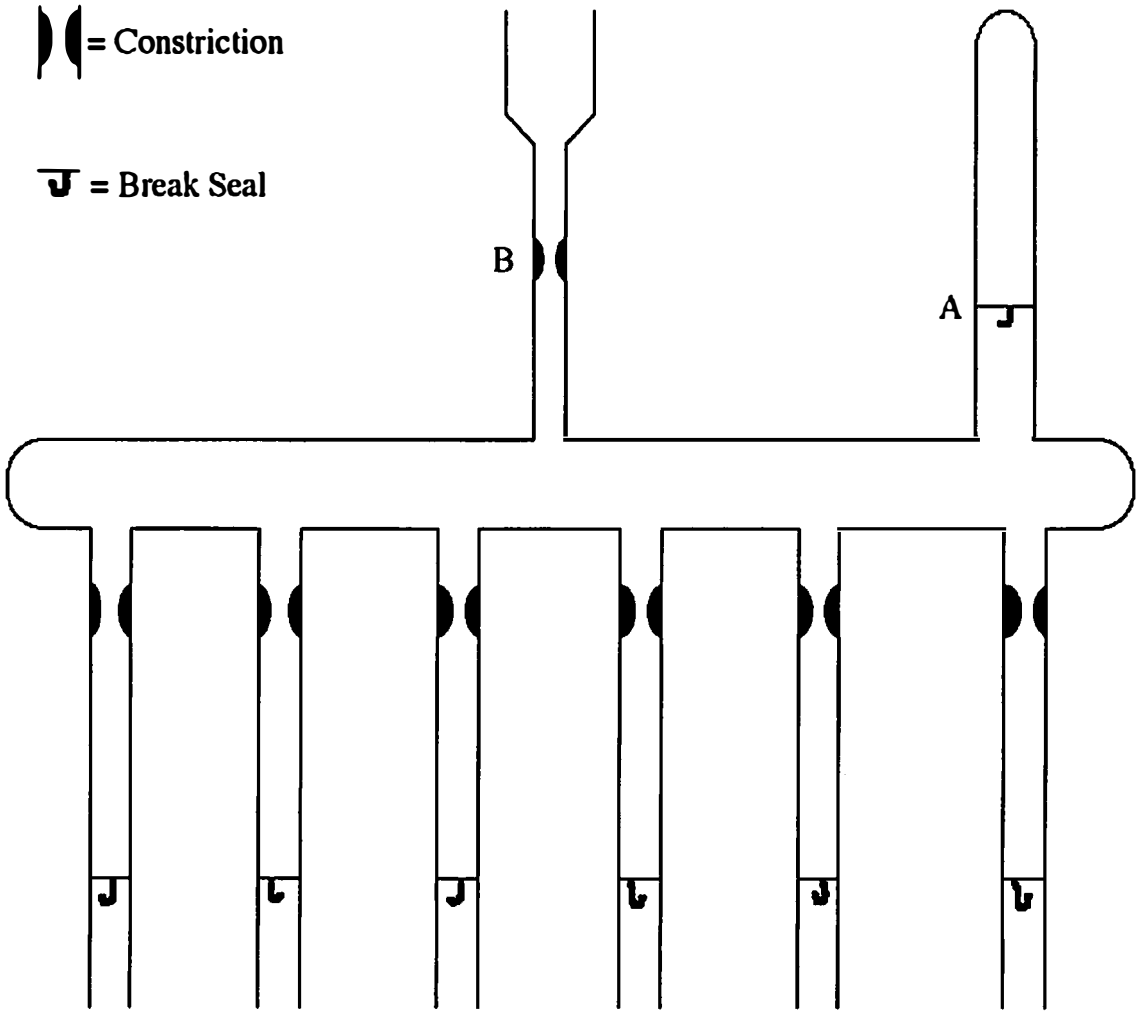

Figure 2.2 Dilution apparatus used for anionic polymerization techniques. A magnet sealed in glass tubing was used to break the seal at A to allow purified agent into the apparatus.

from the calcium hydride flask to the flask containing n-butyl lithium by placing a room temperature bath under the hexane/calcium hydride flask and liquid nitrogen under the n-butyl lithium flask. The hexane was stirred using a Corning stirrer/hotplate overnight at room temperature. The hexane was then distilled into the dilution apparatus by placing a room temperature bath under the hexane/n-butyl lithium flask and wrapping a liquid nitrogen soaked towel around the vials of the dilution apparatus. The dilution glassware was heat sealed from the vacuum line at point B. After cooling, the break seal to the initiator was broken and the secondary butyl lithium was mixed with the hexane and distributed to the individual break seal ampoules. Each ampoule was heat sealed from the apparatus and placed in a freezer until needed.

Purification of Terminator (Methanol): Methanol and sodium sulfate were placed in a single necked round bottom flask equipped with a magnetic stirrer. The flask was placed on the vacuum line and degassed using a freeze/thaw method. The methanol is then stirred over the sodium sulfate while preparing the ampoule glassware. An apparatus similar to that shown in Figure 2.2 was constructed except for a closed glass tube at point A. Precalibrated 1ml break seal ampoules where arranged on the bottom of the apparatus. The apparatus was placed on the vacuum line and evacuated and a Tesla coil was used to check for pinhole leaks. The system was isolated from the main vacuum line and methanol was distilled from the single necked flask to the ampoule apparatus. Placing a room temperature bath under the single neck flask and placing a towel soaked in liquid nitrogen around an individual ampoule facilitated distilling.

Individual ampoules were heat sealed from the apparatus after 1ml of methanol was obtained. The break seal ampoules were then placed in a freezer until needed.

Polymerization: Anionic polymerizations were carried out using the glassware illustrated in figure 2.3. In order to obtain polystyrene with 100,000 MW, the side ampoules contained styrene (5g), methanol (1ml), and secbutyl lithium ($5x10^{-5}$ mol) in hexane. The apparatus was placed on the vacuum line and evacuated. The entire apparatus was checked for pinhole leaks using a Tesla coil and then taken off the line. A 5ml portion of n-butyl lithium in hexane was injected into the apparatus and the apparatus was quickly put back on the line and evacuated. The residual hexane was evaporated leaving dry n-butyl lithium in the bottom of the apparatus. Purified benzene (100ml) was distilled from a cylindrical flask on the vacuum line into the polymerization apparatus using a room temperature/liquid nitrogen bath as described above.

The apparatus was then heat sealed from the vacuum line at point A. The entire apparatus was rinsed with the n-butyl lithium/benzene mixture to ensure no reactive material was present on the interior glass surface. Benzene and n-butyl lithium were collected back into the rinsing section at flask C, which was placed in a 50°C water bath for 2h and benzene was allowed to reflux and rinse the interior glass walls of any residual n-butyl lithium left behind after the initial rinsing. The entire apparatus is then tilted so the benzene is collected in flask B. Flask B is placed in a room temperature bath and flask D is placed in an ice water bath so that benzene could be distilled into the polymerization section of the apparatus without any contaminants. After the benzene

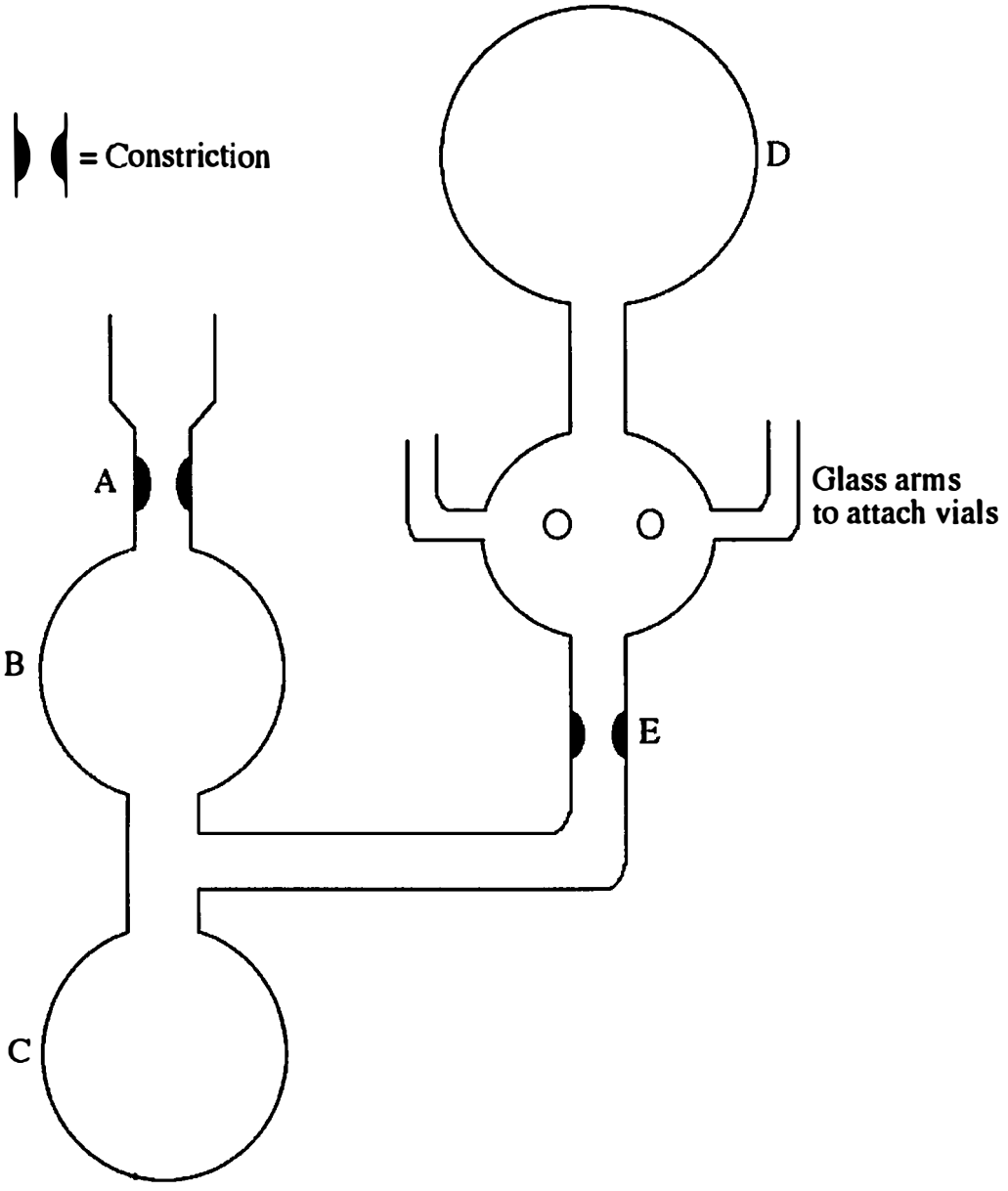

Figure 2.3 Polymerization apparatus used for anionic polymer synthesis. Polymerization occurred in section D and vials of monomer, initiator, and terminator were attached at the glass arms.

was completely distilled into flask D, the rinse section was separated from the polymerization section at point E. Break seals on vials attached at one of four points on the polymerization section were then broken. First, the break seal to the styrene was broken and the styrene was mixed with the benzene. Next, the break seal to the sec-butyl lithium initiator was broken and the contents mixed with the styrene and benzene in flask D. The mixture turned yellow as the living chain ends began to propagate. The polymerization was allowed to continue for one week at room temperature to ensure all monomer had reacted. After one week, the break seal for the methanol was broken and the yellow solution became clear as the anionic chains were terminated. The polymerization apparatus was cracked open by scoring the glass and touching the score with a molten glass tip, and the polystyrene was precipitated by pouring the mixture into cold methanol. The resulting polymer was dried and analyzed by GPC yielding 4.3g of 100,000 MW polystyrene with a PDI of 1.04 Deuterated styrene was purified as described above for styrene, and deuterated polystyrene was synthesized according to the same procedure.

Blocky copolymers of poly (methyl methacrylate) and poly (styrene) were synthesized by Eastwood as described in previous publications.[90,91] dPS-diepoxy (Mn=10,600) was synthesized via anionic methods in Dr. Jimmy Mays' lab.

2.3 Material Mixing

Physically blending a polymer system can be achieved by many methods. The use of twin screw extruders, single screw extruders, and melt mixers are all well known

methods to mix polymers on a large scale. Blends described in the initial part of this study were primarily composed of 70% PBAE and 30% PEO by weight with varying percentages of reactive oligomer. Each reactive oligomer was the same chemical composition as one of the homopolymers. Diepoxy terminated PBAE (Mn=4,00) and diamine terminated PEO (Mw=4,000) were mixed with the above homopolymers and made up 10 percent by weight of the sample. In addition, some samples were created with nonreactive oligomers that were the same molecular weight and structure as the oligomers mentioned above without reactive end groups. Subsequent samples were also made containing 70% PEO and 30% PBAE. The samples contained five percent by weight of the reactive oligomers mentioned above. For all samples, the reactive oligomers were always present in a 1:1 molar ratio. Polymers and oligomers were blended using an ATLAS mini mixer and molder at 150 °C for 15 minutes, and extruded into a bar mold that conformed to ASTM Test Method D 1708-96. The rotor speed can be adjusted to increase mixing, and the rotor/plunger is manually plunged in and out of the sample to increase mixing efficiency. The sample well of the heating cup can hold up to 2g of sample. When the sample is sufficiently mixed, the rotor/plunger is manually pushed to the bottom of the sample well to inject the sample into the mold. After molding, the bars are removed and quenched in liquid nitrogen.

2.4 Material Testing

There are many ways to test the mechanical properties of a blend including asymmetric double cantilever beam (ADCB), impact resistance tests, and tensile

tests.[1,10-12,17,41] In this set of experiments, tensile tests were performed, which refers to the act of stretching the material. Tensile stress (σ) is the force that is applied to the material, while tensile strain (ε) is defined as the resulting change in sample length that occurs. In an elastic deformation tensile stress (σ) is related to tensile strain (ε) by the following equation:

$$\sigma = E\varepsilon$$

The constant, E, is known as Young's modulus and is a specific characteristic to a given polymer system; the larger Young's modulus, the more rigid the polymer.[10-12] In this set of experiments, the polymer blend's elongation was monitored and Young's modulus was determined for each sample.

Tensile measurements were performed on an Instron series IX automated materials tester and evaluated using Instron series IX version 7.27.00 software. The measurements were taken using a crosshead speed of 10 mm/min and conformed to ASTM Test Method D 1708-96. At least five samples were tested for each data point. Polymer blends consisting of PBAE/PEO (70/30 wt%) with ten percent weight reactive telechelic oligomers as described above were tested as a function of time after mixing. In addition, polymer blends of PBAE/PEO (70/30 wt%) with ten percent nonreactive oligomer were also tested and compared with the reactive samples. Additional experiments used blends with a PEO/PBAE (30/70 wt%) composition and contained five percent by weight of reactive oligomers.

2.5 Optical Transparency Measurements

Polymers appear transparent or opaque depending on the refractive index properties of a specific material. Poly (methyl methacrylate) is a transparent material that has been used for the manufacturing of hard contact lenses, whereas most crystalline polymers appear cloudy or opaque. The crystalline domains of these polymers have different refractive indexes than the amorphous regions leading to the scattering of visible light that causes their opaque appearance. Similarly, polymer blends often appear opaque as the domain sizes of the individual polymers grow and reach a length scale that they scatter visible light.[10,11]

Optical transparency measurements were obtained using a Uniphase helium-neon laser (632.8 nm) and a Newport photodiode detector. Figure 2.4 shows the experimental setup of the laser, sample, and detector. The initial intensity of light (i) is transmitted through the sample (s) and hits the photodiode detector. A signal from the photo diode is then sent to the chart Recorder to monitor the intensity of light that passes through the sample. The data was recorded using a Yokogawa pen recorder over a 28-hour period using a speed of 2 cm/h. The samples run in this experiment all consisted of a PBAE/PEO (770/30 wt%) blend. The amount of reactive oligomer in the three samples varied from zero to ten weight percent reactive oligomer.

2.6 Phase Data

In most instances, polymer mixtures are not miscible. However, polymer mixtures can vary between miscible and non-miscible states depending on the specific

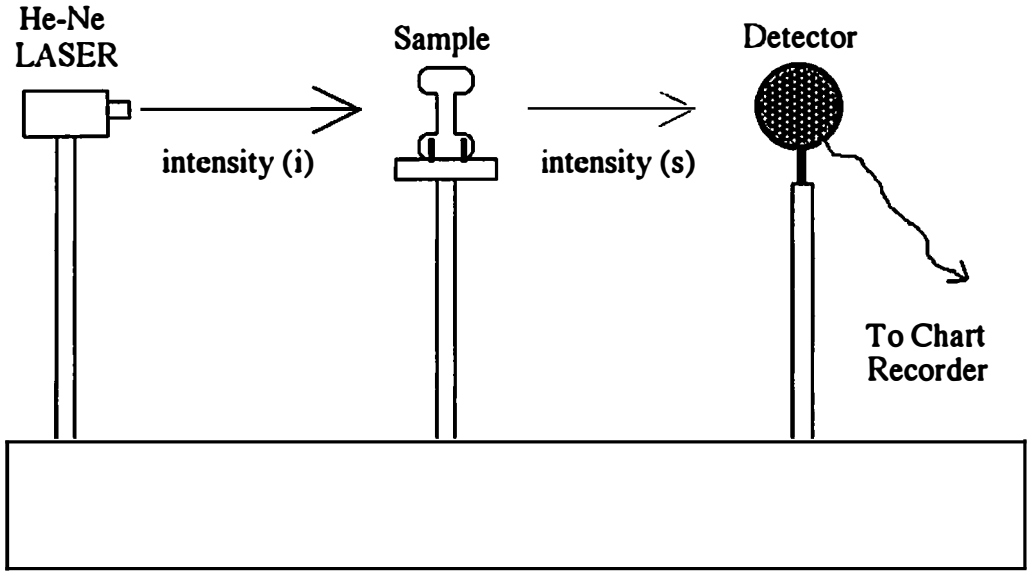

Figure 2.4 Illustration of an optical transparency apparatus. The initial intensity of light (i) passes through the sample. The intensity of light (s) that is transmitted through the sample passes into the detector and a signal is sent to a chart recorder.

composition of the blend, interactions, and the temperature. It is therefore important to understand the complete phase diagram of two polymers.[10]

Phase behavior data were obtained by preparing 3 wt% solutions of the PBAE/PEO blend in toluene and spotting them on a microscope slide. The composition of the blend varied from ten to seventy weight percent PBAE and each data point that was obtained is for a specific blend composition. After evaporation of the solvent, an Olympus B061 optical microscope equipped with a Mettler FP82HT hot stage controlled by a Mettler FP90 central processor was used to view the blend over a range of temperatures using phase contrast optics. At some temperatures, the blend had two distinct phases and droplets of PEO were clearly visible within the PBAE matrix. As the temperature of the system was increased the droplets of PEO became smaller and at high temperatures were indistinguishable from the PBAE matrix until only 1 phase region could be determined. The phase behavior was reproducible when the sample was cooled and heated again. The temperature where the PEO phase became indistinguishable from the PBAE was defined as the phase boundary for this composition. This procedure was completed for a range of compositions of this blend.

2.7 Thermal Analysis

The glass transition temperature (T_g) of a polymer is defined as the temperature at which long range (or segmental) motions stop. The melting temperature (T_m) of a polymer system is defined as the temperature where both translational and rotational energies become zero. Along with the temperature requirements, the polymer must also

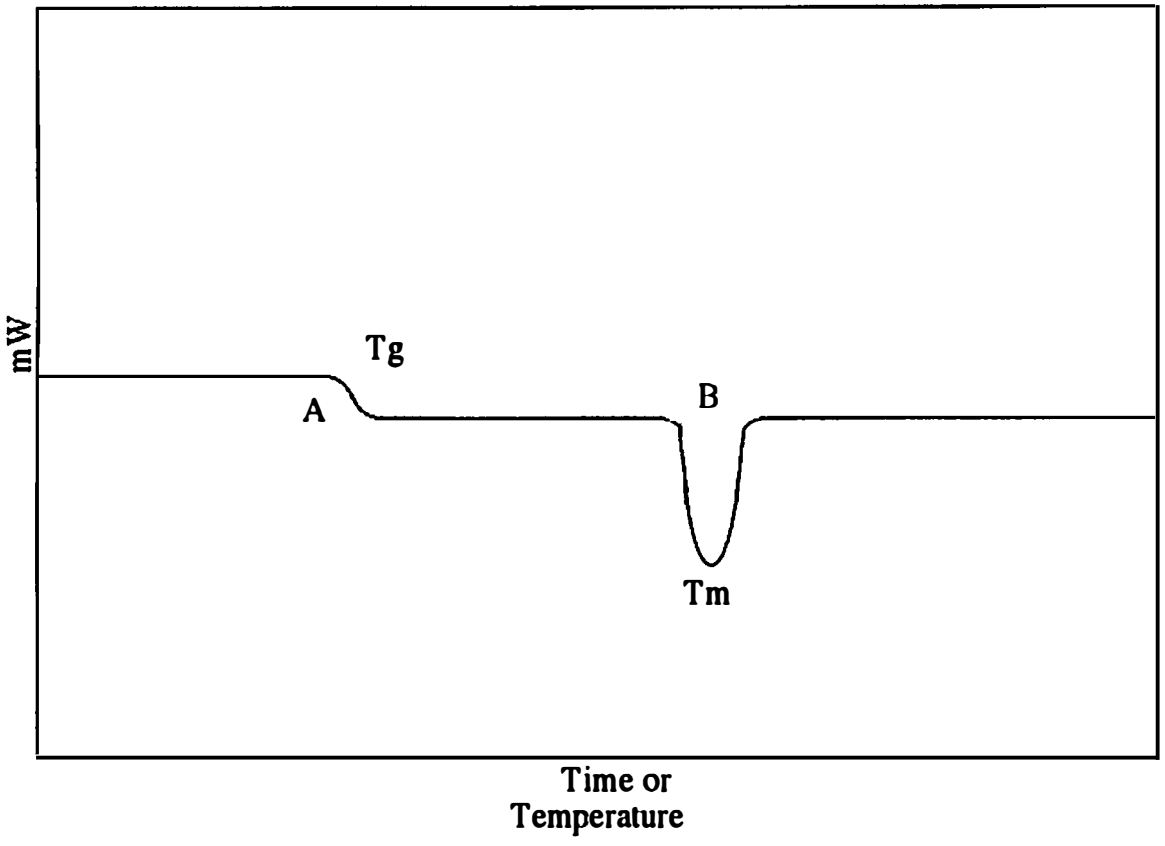

Figure 2.5 An illustrated DSC curve showing the characteristic change in slope at point A for a T_g and the valley at point B for a T_m.

have a symmetry that allows packing of molecules into an ordered lattice for a T_m to be observed. The T_m is a first-order transition characterized by a discontinuity in specific volume. Thus, a polymer system that is completely amorphous will only exhibit a T_g while a crystalline polymer exhibits both a T_g and a T_m.[10,12]

The most common method used to evaluate both T_g and T_m in polymer systems is differential scanning calorimetry (DSC). In DSC, the polymer sample is placed in a metal container while a reference sample is placed in another metal container. Both samples are heated at the same rate and time and sensors under each pan maintain an identical temperature between the two pans. When a temperature is reached where the polymer sample undergoes a thermal transition, a different amount of heat will be needed to maintain the same temperature as the reference pan. The change in electric current between the two pans can then be plotted, and the area under such a curve is a measure of the heat of transition.[3,10,11] Figure 2.5 illustrates a typical DSC of a polymer that has both a T_g and a T_m. Point A shows the slope change associated with the T_g while point B illustrates the valley associated with a T_m. The degree of crystallinity of the PEO in the blends was monitored by Differential Scanning Calorimetry using a Mettler-Toledo (Model DSC821e) calibrated with Indium at a scan rate of 5 °C/min. Since the T_g of PEO is below room temperature, a separate DSC equipped with a liquid nitrogen cooling system was used to monitor the T_g of the blend. The Advanced Thermal Analysis System (ATHAS) facilities were used for DSC samples that needed to be characterized below room temperature. Samples were run on a similar Mettler-

Toledo DSC equipped with a liquid nitrogen cooling system. The T_g reported for all samples is the midpoint T_g as determined by DSC. The Tg of the samples reported in this dissertation are from PBAE/PEO (70/30 wt%) blends with ten percent reactive oligomer as described in section 2.3.

Percent crystallinity for the PBAE/PEO (70/30 wt%) system was calculated from the T_m peak of the DSC curve. The area under the peak is equal to the heat of melting of the PEO(ΔH_m). The ΔH_m of PEO obtained from the DSC was then divided by the heat of melting a hundred percent crystalline sample obtained from the Polymer Handbook[92] and then multiplied by 100 to yield percent crystallinity. The percent crystallinity of a blend consisting of PBAE/PEO(70/30 wt%) and ten weight percent reactive oligomers was calculated as a function of time after mixing. In addition, percent crystallinity of a blend consisting of PBAE/PEO(70/30 wt%) with ten weight percent nonreactive oligomers was determined as a function of time and compared with the reactive oligomer samples.

2.8 Gel Permeation Chromatography (GPC)

Physical properties are directly related to molecular weight in a given polymer system. Low molecular weight molecules or oligomers within a polymer are known to decrease the T_g of the system. The low molecular weight molecules or plasticizers lower the Tg by effectively lowering the average molecular weight and increasing the relative free volume.[10,11]

Molecular weight measurements are classified as absolute or secondary methods. Absolute methods are a direct means of determining molecular weight and include the use of osmotic pressure, light scattering, and ultracentrifugation. Secondary methods provide a method of determining relative molecular weights using techniques that must be calibrated to a standard. These techniques include the use of intrinsic viscosity and gel permeation chromatography. Gel permeation chromatography (GPC), which is also known under the more illustrative name of size exclusion chromatography (SEC) is the method used in this project. In this technique, a given polymer sample is separated by size using a column of porous material. Figure 2.6 illustrates a polymer sample passing through a GPC column. As the sample enters the column, it encounters porous material; the smaller components of the sample enter into these porous regions while the larger material flows by the porous material. As the polymer sample continues to flow through the column, the larger molecules in the sample will exit faster as the smaller molecules continue to pass through the small pores. Therefore, the large molecules will elute first and the smaller molecules will elute last. Well-characterized, narrow molecular weight PS standard samples were passed through the GPC column to calibrate the column. Molecular weight and molecular weight distributions were ascertained by comparing elution times of the standard with a sample.[11] GPC analysis was performed on a Waters 590 using a Polymer Laboratory Plgel 5μm column and a Waters differential refractometer detector. Tetrahydrofuran was used as the solvent. Data was analyzed using GPC for Windows software.

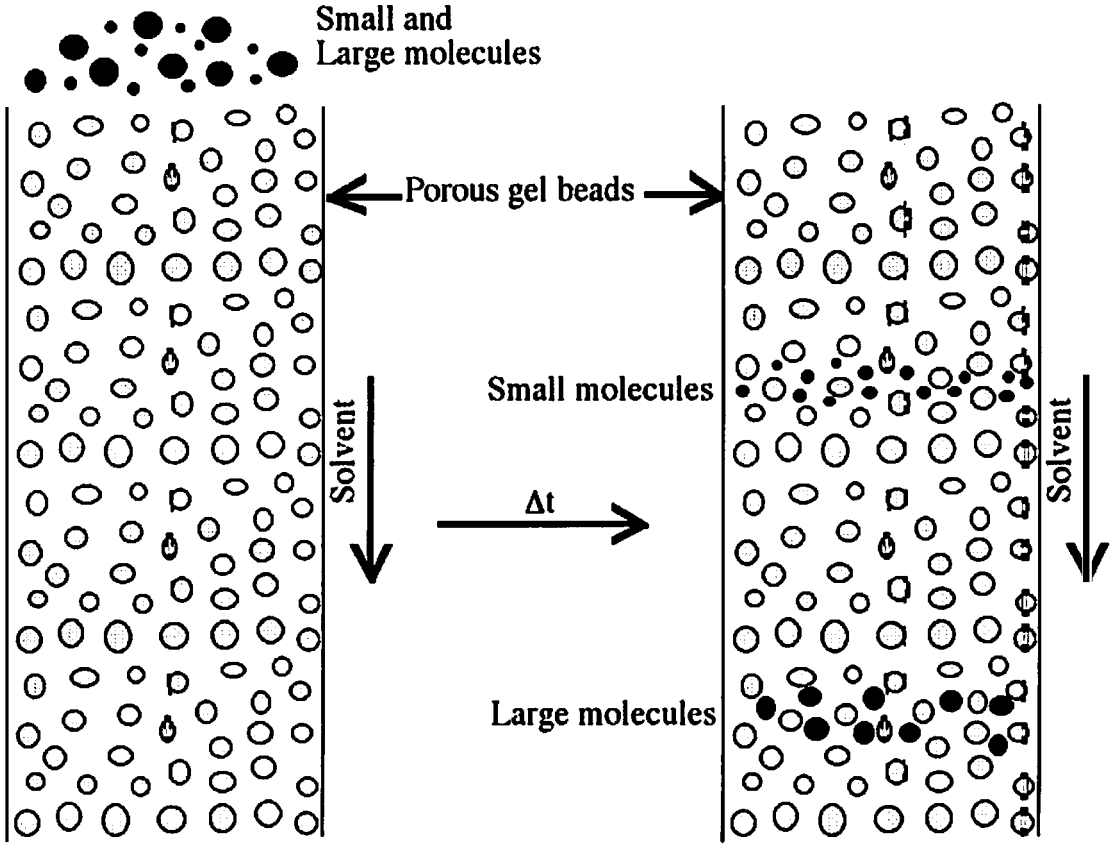

Figure 2.6 Illustration of separation obtained between small and large molecules in a column during gel permeation chromatography. Smaller molecules enter into the pores within the gel beads increasing their effective path length to the larger molecules.

2.9 Spin Coating

Resolution and reproducibility are important parameters to consider when depth profiling. It is essential in depth profiling experiments to have the sample as uniform as possible, since each layer must be as smooth as possible with a uniform thickness. Without uniform thickness, there is no reproducibility in data across a sample and resolution is usually limited by the roughness of the sample surface.

One method of creating a uniform, smooth polymer thin film is spin coating. In spin coating, a substrate such as a Si wafer is placed on a chuck and held there by a vacuum. A solution consisting of the sample in an appropriate solvent is used to coat the Si wafer. The chuck is then accelerated and spun for several seconds until all solvent is removed. The resulting polymer film thickness is a function of solution concentration, chuck speed, and solvent volatility.[93,94]

Polymer solutions consisting of the desired polymer and toluene were made and then filtered and coated onto a Si wafer. A Headway Research Inc. (model PWM32) spin coater was used to create a thin polymer film on the Si substrate. The acceleration and final speed of the chuck were varied along with solution concentrations to achieve desired film thicknesses.

2.10 Ellipsometry

Ellipsometry is a nondestructive technique that is used to determine the thickness of a sample based on the refractive index of the sample. Polymers were first spun coat onto Si wafers as described above and then analyzed by a DRE-Dr. Riss

Ellipsometerbau GmbH (model EL X-02C) ellipsometer. A class IIIA laser at 632.8nm was used for the incident radiation and a 70° angle was maintained for all measurements.

2.11 Forward Recoil Spectroscopy (FRES)

The ability to determine the chemical makeup of a sample throughout the samples depth is important for determining a compatibilizer's effectiveness. Both the diffusion of the compatibilizer to the interface as well as the width of the compatibilizer/homopolymer interface can be studied. A brief description of the FRES technique and applications can be found in Chapter I. For the experiments described in this dissertation, FRES data was collected at The University of Minnesota on at the Ion Beam Analysis Facility. A $^4He^+$ incident beam with energy of 3.0015 keV was used. The recoiling scattering angle was held at 30°. A current of 15-20 amps was placed on the sample until 20μC of charge was accumulated. Total time for data collection from one sample took 20 minutes. A 12μm Mylar stopping foil was placed between the sample and detector to filter off He ions. The geometry of the FRES experiment is shown in figure 1.2. A $^4He^+$ ion beam hits the partially deuterated sample (to provide contrast) causing ^1H, ^2H and $^4He^+$ to be recoiled from the sample. All species are directed towards the Mylar film where $^4He^+$ is stopped and the smaller ^1H and ^2H species pass through to the detector.

Each channel in the detector correlates to a specific energy. Each ^2H is recoiled with more energy than an ^1H resulting in two peaks in the raw data of detector counts vs channel as illustrated in figure 2.7. The peak on the left, centered on channel 250,

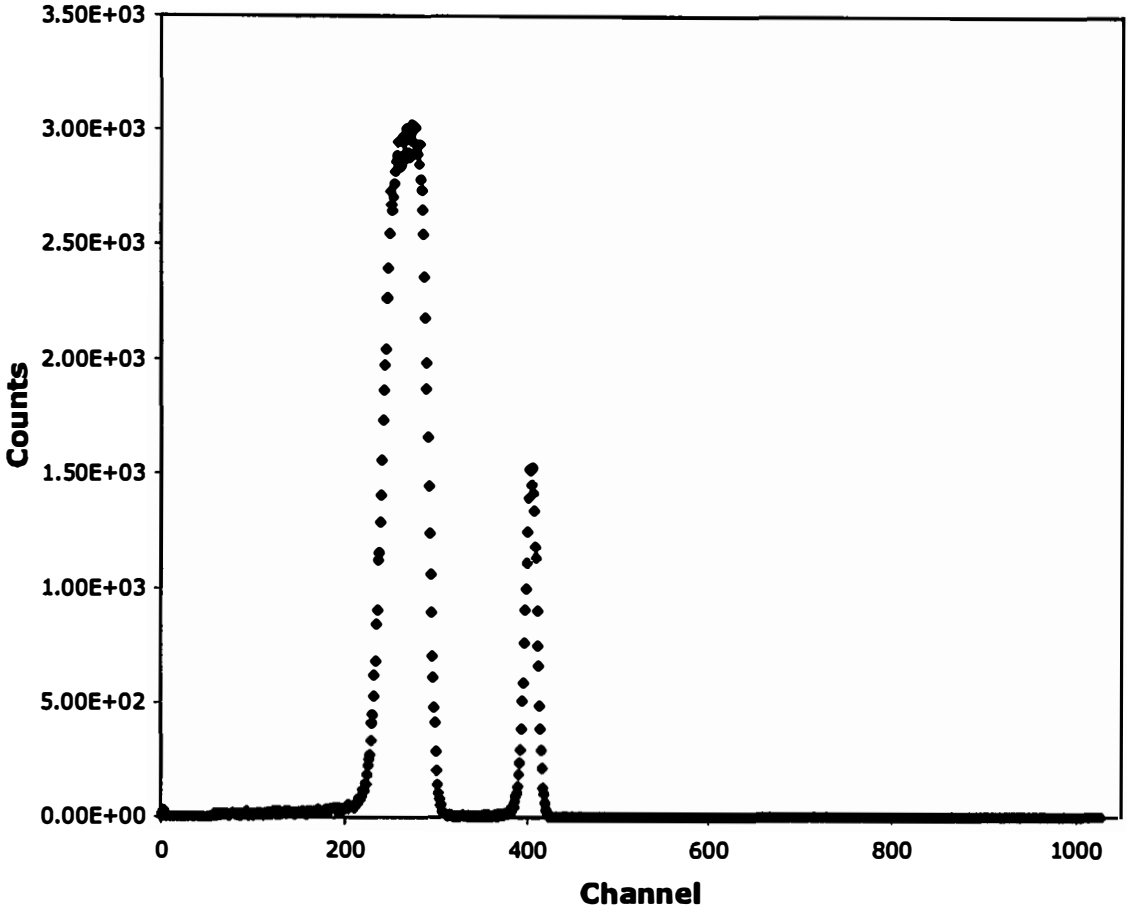

Figure 2.7 Data obtained from a typical FRES experiment as counts versus channel. The left hand peak is ^{1}H while the right hand is from ^{2}H. The right hand sides of each peak represent the highest energy species and are created by the ^{1}H or ^{2}H closest to the top of the sample.

corresponds to ^{1}H while the peak centered at channel 400 corresponds to ^{2}H. Consequently, the right hand side of each peak corresponds to those particles recoiled with the highest energy and thus are closest to the surface of the sample. The resulting counts versus channel spectra were processed into volume fraction versus depth using the Standard.for and Convert7.for programs written by Jonathon Schulze at The University of Minnesota.

These programs written by Schulze treat the sample as consisting of multiple horizontal slabs. The slabs are thin enough that the stopping powers within each slab can be considered a constant. The program first converts channel (energy) to depth. This correlation is determined by measuring the energy needed for the primary beam to reach a given ^{1}H or ^{2}H at a given depth, the energy loss of the ^{1}H and ^{2}H traveling through the bulk material (a function of depth), and the energy loss of the ^{1}H or ^{2}H traveling through the air and filter foil. In order to quantify this, the stopping powers of the bulk, air, and foil must be known along with the energy of each channel in the detector and the energy of channel zero of the detector and are tabulated.

Next, the yield or counts for each channel can be converted into volume fraction using both the Standard.for and Convert7.for programs. To do this, a standard sample consisting of a mixture of ^{1}H and ^{2}H with a known composition is examined by FRES. The Standard.for program then converts channel to depth as described above and corrects the yield for changes in stopping power with depth. The ratio of the average peak height of the ^{1}H yield to the ^{2}H yield (figure 2.8) is then used to determine the cross section ratio (f) via the following equation

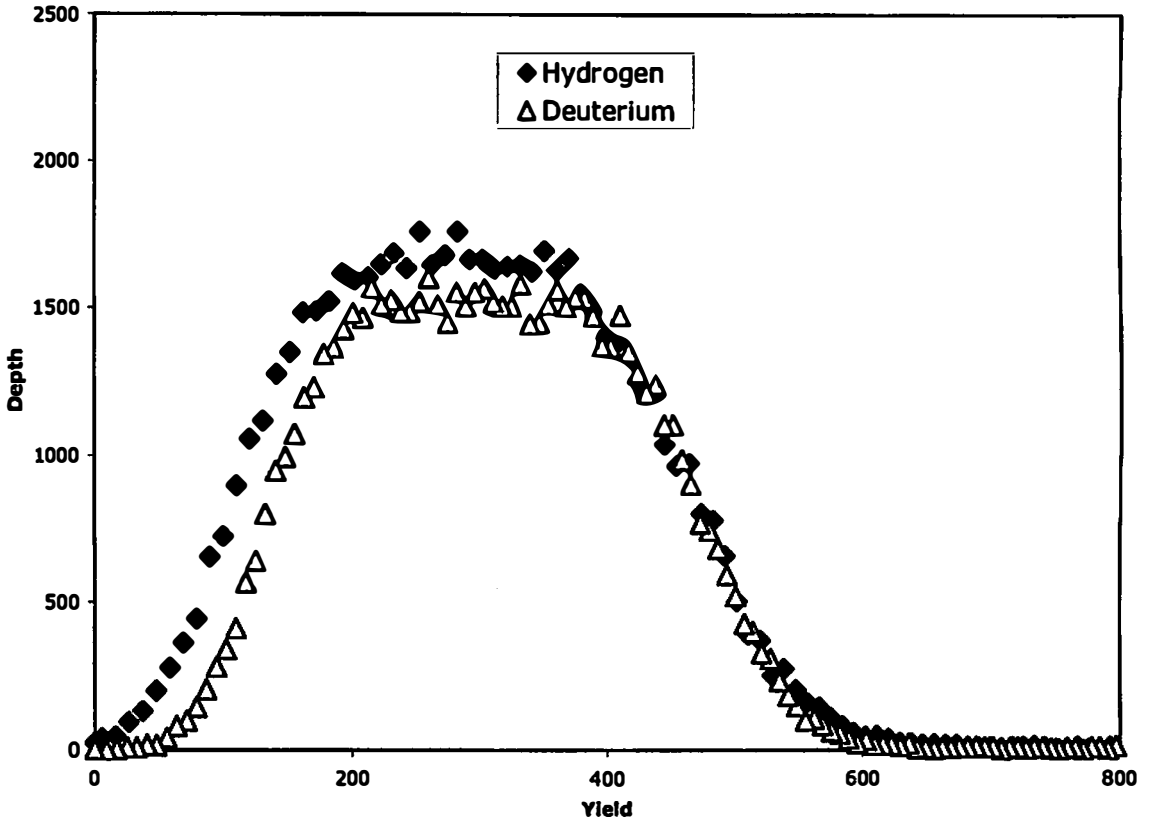

Figure 2.8 FRES data showing the hydrogen and deuterium peak from a dPS/PS standard sample. The ratio of the two peaks can be used to calculate the scattering cross section ratio.

$$f=(\phi^2H/\phi^1H)*(Y^1H/Y^2H)$$

where ϕ^2H and ϕ^1H are the volume fractions of the dPS and PS in the standard sample and Y^1H and Y^2H are the corresponding average peak values from the known composition sample. The Convert7.for program then uses this cross section ratio to convert yield to volume fraction for experimental samples. A typical depth profile curve for ^2H in anexperimental sample after conversion to volume fraction versus depth is shown in figure 2.9.

Two distinct sample geometries were used to examine reactive compatibilization of polymer blends and are illustrated in figures 4.1 and 4.2. The first sample geometry (figure 4.1) consists of a PMMA-COOH layer that is directly spin coated onto a Si wafer. Next, a PS film was spin coated onto a glass slide and then the PS film was floated onto deionized water and placed on top of the PMMA-COOH. Finally, the dPS-diepoxy was spin coated onto a glass slide and floated on top of the PS layer to create a trilayer sample. The second sample geometry (figure 4.2) is prepared by spin coating a PMMA-COOH layer directly onto a Si wafer followed by spin coating a blend of PS and dPS-diepoxy (8.4% by weight) directly onto a glass slide and floating them onto the PMMA-COOH layer. For each sample geometry, one sample was made and then cut into small pieces. The small samples were placed in a vacuum oven at 170°C for times spanning from 2 minutes to 120 hours. In addition to the bilayer and trilayer samples, a standard sample was made consisting of a 50/50 wt/wt mixture of PS and dPS which was spin coated onto a Si wafer which was used to calibrate the ^1H and ^2H signal from FRES.

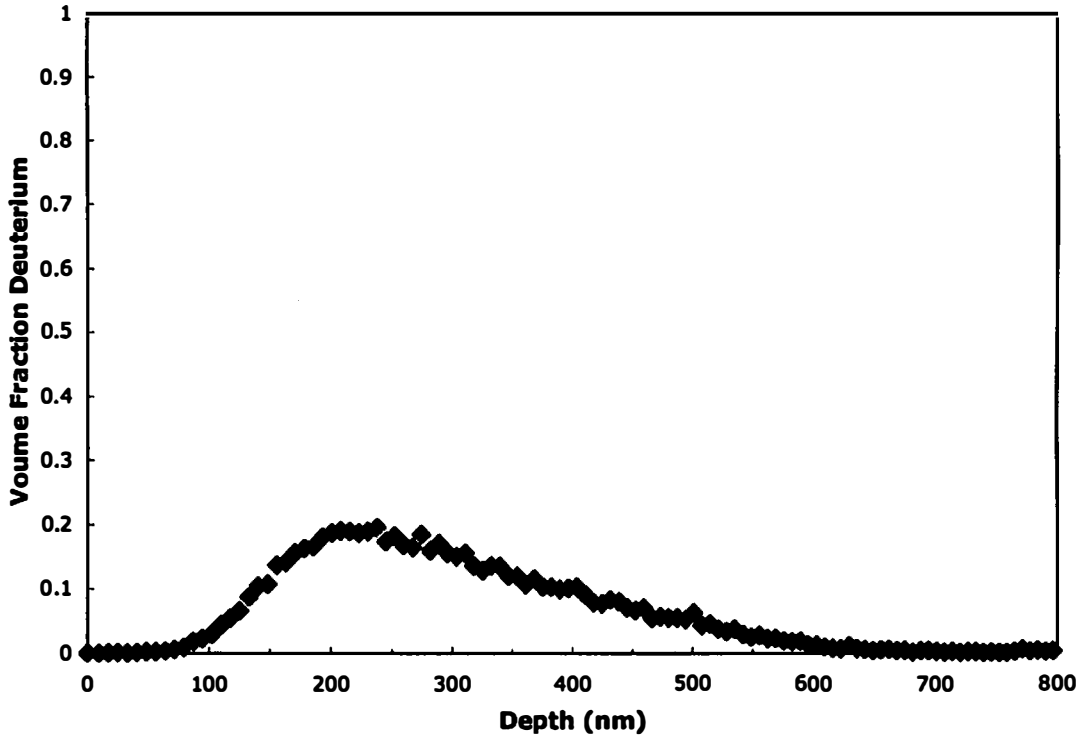

Figure 2.9 Typical output from the Convert7.for program showing volume fraction ^{2}H versus depth (nm).

A system containing dPS, dPMMA and one of three alternating copolymer compatibilizers with molecular weights of 85,000, 96,000, and 497,000 were also studied using FRES. In this experiment, FRES was used to monitor the polymer/copolymer interfacial width for each alternating copolymer system before annealing and after 12h of annealing. A representation of the samples assembled for the FRES experiments is shown in figure 4.7 and were constructed by spin coating a dPMMA film (320±4nm) on a silicon wafer followed by floating a layer of alternating copolymer (280±5nm) on top of the dPMMA. Finally, a layer of dPS (330±3nm) was floated from a glass slide onto the alternating copolymer to create a sandwich of alternating copolymer between the dPS and dPMMA and the resulting sample was then cut into smaller samples. One sample was not annealed and one sample was annealed for 12h at 150°C for each copolymer used.

For the final study, a system of dPS, dPMMA, and various block copolymers listed in table 4.2 consisting of blocks of PS and PMMA were subjected to depth profile analysis using both FRES and neutron reflectivity. In this experiment, FRES was used to study the interfacial width of the multiblock compatibilizer and each homopolymer without annealing and after 12 hours of annealing. The samples studied by the FRES experiment are illustrated in figure 4.10 and consisted of a dPMMA layer spun coat onto a Si wafer followed by floating a block copolymer film from a glass slide onto the dPMMA layer. Finally, dPS was spun coat onto a glass slide and floated onto the block copolymer creating a sandwich of block copolymer between dPS and dPMMA.

Individual samples were cut into smaller samples. One sample was not annealed and one was annealed for 12h at 150°C for each copolymer used.

2.12 Neutron Reflectivity

A brief description of neutron reflectivity and its utility in depth profiling polymer samples is found in Chapter I. Raw data from neutron experiments are reflected intensity (I) as a function of Q_z, the z component of the wave vector transfer that can also be defined as $(4\pi/\lambda)\sin\theta$. Data must be reduced to account for background and the intensity of the incident beam (I_0). The raw data obtained in the experiments was reduced using the reflred program provided by the National Institute of Standards and Technology (NIST) Center for Neutron Research (NCNR). The program allows the background spectra to be subtracted from the raw data. The resulting curve is then divided by the intensity of the incident beam over the entire range of Q for which the data was collected to yield a plot of intensity (I/I_0) vs. Q. A model of the system and the corresponding scattering length density (SLD) were created using the reflfit program provided by NCNR. A model reflectivity curve is created from the SLD and fit to the measured reflectivity data using reflfit.

Reflectivity data for the dPMMA, dPS, and blocky copolymer samples were obtained from the NG-1 reflectometer at the National Institute of Standards and Technology (NIST) National Center for Neutron Research. The wavelength of the neutrons used was 4.75Å with a wavelength spread of 0.05Å. The resulting reflectivity

data was reduced via the reflred program and the resulting curves were fit using the reflfit program to generate scattering length density profiles.

Samples were prepared in a similar fashion to those described for the FRES experiments as illustrated in figure 4.10 with the exception that the dPS and dPMMA layers were only 56±2nm thick and all the block copolymer thicknesses were 35.2±0.3nm. After construction, these samples were annealed for 12 hours at 150°C

Chapter 3

Reactive Compatibilization of a Model System with Difunctional Oligomers

3.1 System Description

The feasibility of a proposed reactive processing scheme to create blocky copolymers in-situ at the polymer/polymer interface is studied. The model system is shown schematically in figure 1.7. In this scheme, telechelic oligomers that are composed of the same monomers as the two homopolymers are added to a blend. In this figure, the homopolymers are denoted by the solid (homopolymer A) and dotted (homopolymer B) long chain molecules, while the telechelic oligomers are denoted as shorter chains with reactive end groups (stars and circles). The oligomers are designed so that the stars and circles are mutually reactive, i.e. epoxide and carboxylic acid or anhydride and amine. As these four components are added to the processing equipment it is expected that the solid-line oligomers will dissolve in the homopolymer A phase while the dotted oligomers will dissolve in the homopolymer B phase. During mixing, the stars and circles will only encounter each other at the biphasic interface and will react to form a copolymer chain with two reactive end groups. Thus, this condensation polymerization of the oligomers can continue to occur during processing and a long chain blocky copolymer will be created at the interface to act as a compatibilizer. The small size of the oligomers will allow them to diffuse to the interface more quickly than long chain molecules and may alleviate the excess time needed in the blending process for the diffusion of a long chain copolymer additive to the interface.

A model system of poly (bisphenol-A-co-epichlorohydrin) (PBAE) and poly (ethylene oxide) (PEO) was studied as a means to evaluate the feasibility of this scheme to compatibilize of two immiscible polymers with dramatically different physical properties. The system contained both homopolymers along with difunctional oligomers of each homopolymer. The PBAE oligomer was terminated with epoxy groups while the PEO was terminated with amine functionalities. These oligomers can diffuse through their prospective homopolymers and contact a corresponding oligomer from the other phase at the polymer/polymer interface. Therefore, only at the interface will the oligomers meet and have the opportunity to react and form a block copolymer compatibilizer during the mixing process.

There is a possibility that in this processing scheme, one amine group on the PEO oligomer could react with two epoxy groups on PBAE oligomers creating a branch site, thus impacting the rheological and mechanical properties of the final blend; amines are well known curing agents for epoxy resins. However, the extent of cross-linking or branching is reduced when the amine concentration differs from the optimal one amine hydrogen for each epoxy group.[95] Thus, each reactive amine group in this system could react with two epoxide groups. For the model system, the molar ratio of amine to epoxy is 1:1, rather than the optimal crosslinking ratio of amine to epoxy (1:2), thus branching or crosslinking of the growing copolymer compatibilizer should be minimized in this study. Moreover, primary amines react about twice as fast as secondary amines and would therefore be expected to be the major species attacking the epoxide rings, further suggesting that branching of the compatibilizer is minimal in this study.[96]

3.2 Initial Reactive Compatibilization Experiments

This set of experiments was completed to examine the feasibility of using the reactive processing of telechelic oligomers to create blocky copolymers in-situ during processing to act as interfacial modifiers in phase-separated blends. Initially, the investigation focused on the ability of the synthesized blocky copolymers to improve the mechanical properties of the blend as a function of the concentration of reactive oligomer. Pursuant to this, reactive oligomer pairs (1:1 weight ratio) were introduced into blends of PEO:PBAE (30:70) at 0.5, 1, 2, 5, and 10 weight %. Each sample in this experiment was mixed for 15 minutes at 150 °C before being extruded, molded into tensile bars, and mechanically tested.

The initial data were very scattered, showing very little reproducibility for identical blend compositions. The modulus of the samples varied dramatically and the ultimate strain ($\Delta L/L$) ranged from 0.32 to 1.52 for the initial samples subjected to mechanical testing. It is important to note that the tensile bars were molded over several days, but the Instron data itself was collected at the same time. Thus, the time between sample preparation and mechanical testing differed for the various samples. It is also noteworthy that during the interval between molding and testing, the samples became opaque after initially appearing clear out of the mold.

3.3 Phase Diagram

The phase diagram of the PBAE/PEO blend without any oligomer was obtained using optical microscopy and a hot stage. Blends of varying compositions were

observed over a temperature range from room temperature to 200°C. The resultant phase diagram is shown in figure 3.1 and indicates the conditions where the PEO/PBAE blend is miscible. Interestingly, the PEO and PBAE blend used in the initial experiments is miscible at the mixing conditions, i.e. 70/30 composition and 150 °C. However, when the bar was removed from the mixture and quenched to room temperature, the sample is brought below the coexistence line and phase separation may occur. This may explain the cloudiness observed in previous experiments.

To examine this more closely, a new set of experiments were designed to determine the effect of time between sample prep and mechanical testing on the samples with 10 wt% oligomer. A series of bars were mixed for 15 minutes at 150 °C, extruded, and molded to form tensile bars. Sets of bars were then subjected to tensile measurements after a specific time interval after extrusion. For each time interval, the Instron data collected were reproducible and unique. Figure 3.2 shows a typical stress-strain curve obtained from mechanical testing. The moduli reported in this dissertation are Young's moduli defined as stress divided by strain for the initial slope of the curve. The maximum elongation is the total extension of the sample at break represented by the sharp decrease on the far right hand side of the curve. Figure 3.3 shows the modulus and ultimate strain as a function of the time between sample prep and mechanical testing. This data shows that the ultimate strain decreases as a function of time, while the modulus of the blend increases with time. Thus, the scatter observed in the initial experiment is due to changes that occur in the system between sample preparation and the tensile measurements.

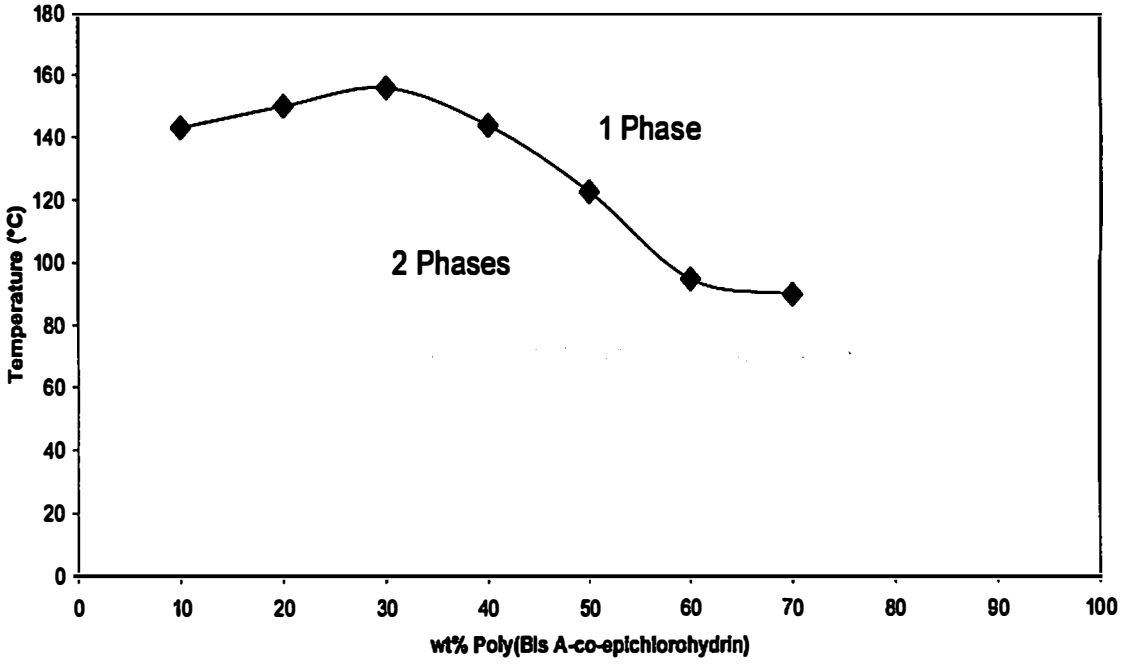

Figure 3.1 Phase diagram of PBAE/PEO blend system without oligomer. Each diamond represents the point where a phase transition from 2 to 1 phase was observed for a specific composition via optical microscopy.

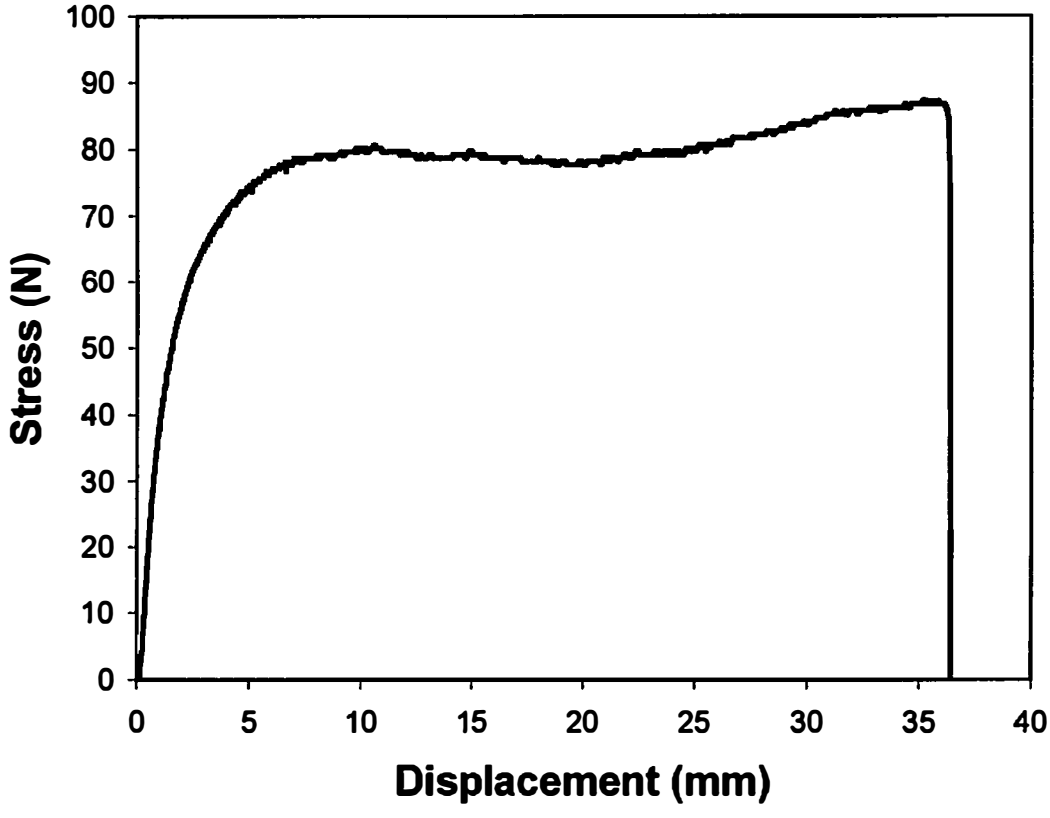

Figure 3.2 A typical curve obtained from mechanical testing. The initial slope of the curve corresponds to Young's modulus and the vertical line on the right hand side of the curve represents the maximum elongation of the sample.

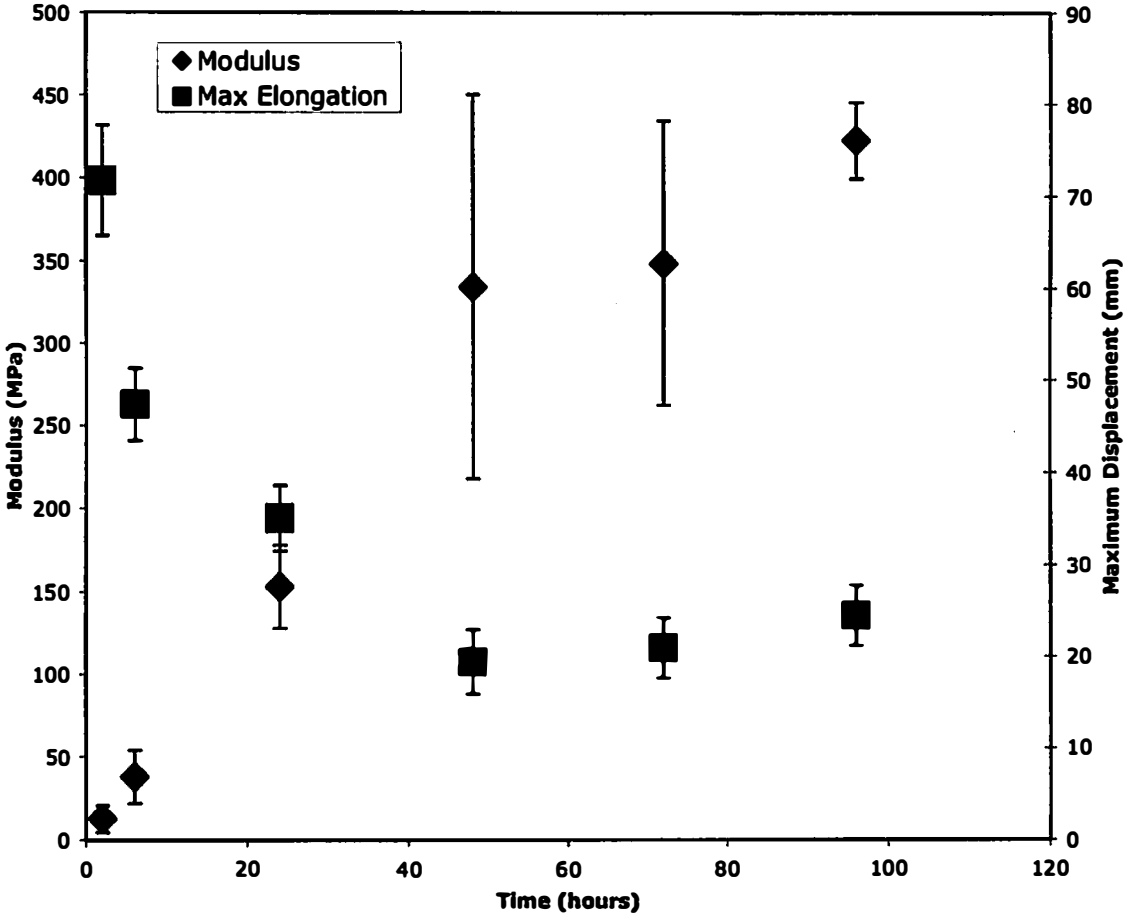

Figure 3.3 Modulus and maximum displacement as a function of time. As time from mixing increases, the modulus increases while the maximum elongation decreases.

Our interpretation of the behavior observed in figure 3.3 is that it can be explained by two possible mechanisms, both related to the presence of unreacted oligomer upon removal of the sample from the melt mixer. Any unreacted oligomer that is present can act as a plasticizer, lowering the glass transition of the sample, an effect well known in the field of reactive extrusion.[21] This decrease in the glass transition results in an increase in the mobility of the polymers at room temperature. This mobility will allow (i.) the blend to phase separate, the reactive oligomer to continue to polymerize, and additional copolymer formation at the interface or (ii.) the PEO to further crystallize. Either or both of these mechanisms can explain the observed mechanical behavior. For instance, samples tested at shorter times exhibited higher ultimate strain due to the plasticized conditions. With increased time between sample prep and mechanical testing, more oligomer reacts to form blocky copolymers, and thus less is in the system to act as a plasticizer. This manifests itself in the stress-strain behavior as a decrease in the maximum strain with time between sample prep and mechanical testing due to the loss of plasticizer. At the same time, there is an increase in the amount of blocky copolymer that is formed at the interface with time. As more copolymer forms, interfacial adhesion improves; stress is more readily transferred between phases and the modulus of the system increases. Thus, this mechanism would explain the trends in the modulus and ultimate strain observed in figure 3.3.

Alternatively, the data in figure 3.3 could be explained in terms of increased crystallinity of the PEO in the sample with time. PEO can crystallize within the polymer blend due to the presence of unreacted oligomer in the sample as it is removed

from the melt mixer. The unreacted oligomers present in the blend system act as a plasticizer and allow the PEO to crystallize over time. As the amount of crystalline PEO increases, one would expect the observed changes in the mechanical properties, i.e. that the modulus of the system increases and the ultimate strain decreases, as the modulus is expected to increase with increasing crystallinity since crystalline regions are generally stronger than amorphous regions and may act as rigid crosslinks between amorphous regions.

3.4 Optical Properties

To provide further insight into the underlying mechanisms of the mechanical behavior of the modified blends, the time evolution of the optical transparency of the blends was monitored. Figure 3.4 shows the optical transparency of three different tensile bars as a function of time after removal from the mixer. The y-axis is the transmission of He-Ne laser light through the sample, while the x-axis is time (0 to 28 hours). The scales on both x and y-axes are identical for these three curves. Curve a is the change in the transparency for the pure polymer blend, while curves b and c show the optical transmission of the samples with 5 and 10 wt% reactive oligomer, respectively. Inspection of this data shows that both the 5% and 10% reactive oligomer bars became opaque over time. This increased opaqueness could be due to the phase-separation of the homopolymers or continued crystallization of the PEO at room temperature and thus the interpretation of this data can provide additional information

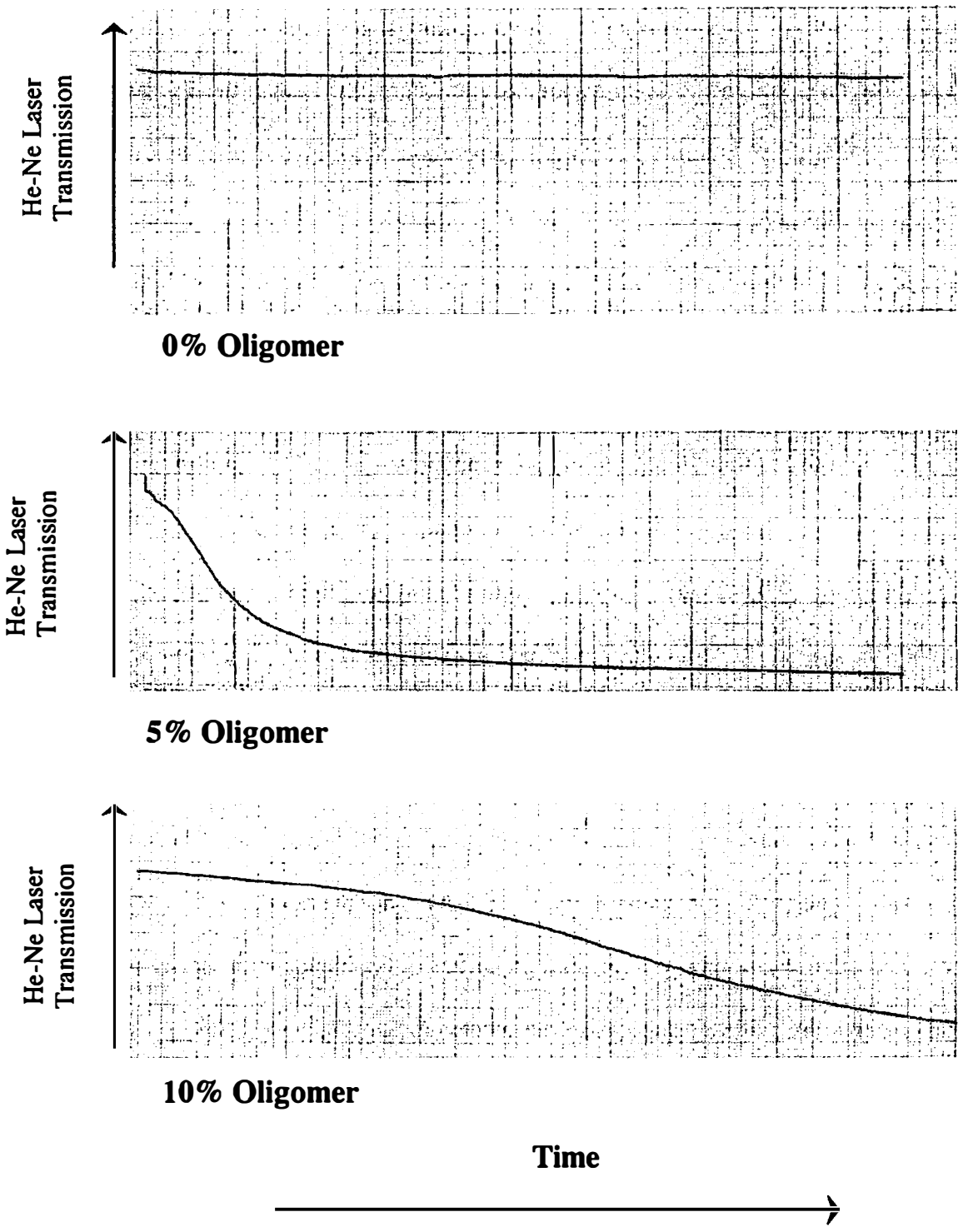

Figure 3.4 Optical transparency of several different blend samples as a function of time. The transmission of the He-Ne laser decreases with time as the samples become opaque.

regarding the relative importance of these two mechanisms in the evolution of these systems. Interestingly, the 10% bar became opaque more slowly than the 5% sample. This trend makes sense in terms of the phase separation of the blend, as it has been shown that an increase in the amount of compatibilizer in a blend will slow down the phase separation kinetics.[24-27] One would expect the increased amount of reactive oligomer present in the 10% sample to result in faster production of interfacial copolymer than for the 5% sample, and thus the 10% sample will have more compatibilizer present than in the 5% sample at any given time. This, in turn would explain the slower transition from transparent to opaque for the sample with 10% reactive oligomer. This trend, however, is counterintuitive if the crystallinity of the PEO were the primary process that was affecting the transparency. One would expect that the increased amount of oligomer would increase the mobility of the PEO and allow faster crystallization, and thus a quicker loss of transparency, for the sample with 10% reactive oligomer relative to the sample with 5% reactive oligomer. Thus, this optical data suggests that the crystallinity of the PEO is not the dominant process in determining the microscopic structure and properties of the blends with reactive oligomer providing evidence supporting the success of the proposed reactive compatibilization scheme.

3.5 Differential Scanning Calorimetry I: T_g of Blend

Differential Scanning Calorimetry was used to monitor the glass transition temperature of the blend over the various time constraints between mixing and

mechanical testing to verify the plasticizing effect of the oligomers and the midpoint T_g is reported. Figure 3.5 shows a typical DSC curve for a 70:30 PBAE:PEO blend with 10% oligomer two hours after mixing. A plot of T_g vs. time after removal from the melt mixer of a 70:30 PBAE:PEO blend with 10% oligomer is depicted in Figure 3.6. In this figure, the square on the y axis is the T_g of the blend without any oligomer, determined experimentally, which aggress with that calculated by the Fox-Flory equation. Only 1 T_g was observed during the DSC experiments for each timeframe. It can be seen in figure 3.6 that as time increases, the T_g of the blend increases as well. These data supports the explanation that the unreacted difunctional oligomer acts as a plasticizer in the early stages after mixing; this plasticizing effect lowers the Tg of the blend. At longer times, the difunctional oligomers continue to react depleting the system of low molecular weight oligomers that would lower the Tg of the blend. The consequence of these phenomena is an increase in the Tg over time.

3.6 Differential Scanning Calorimetry II: PEO Crystallinity

To differentiate between the two possible mechanisms (increased PEO crystallinity vs. continued copolymer formation and phase separation) the behavior of the blend system with 10% reactive oligomers was compared to the behavior of a PBAE:PEO blend system containing 10% unreactive oligomers. The unreactive oligomers were the same structure and molecular weight as their reactive counterparts, except the PEO was not amine terminated. Figure 3.7 shows the change in the percent

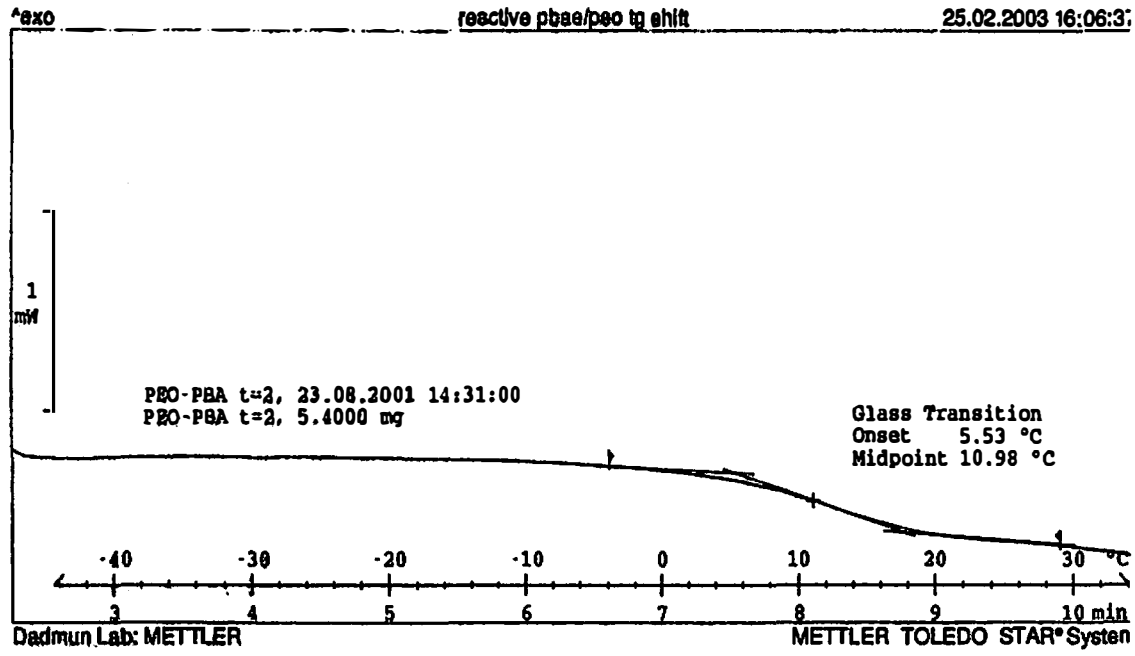

Figure 3.5 A DSC curve illustrating the T_g midpoint of a PBAE/PEO (70/30 wt%) blend with 10 percent reactive oligomer two hours after mixing.

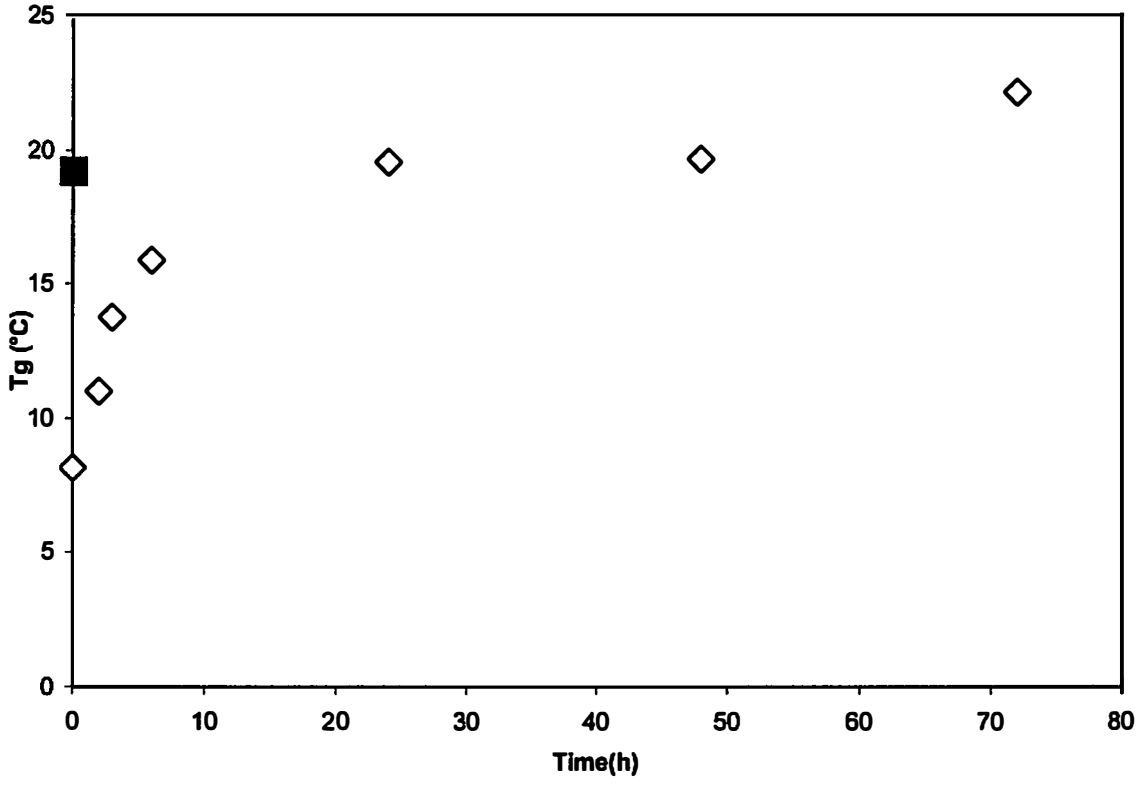

Figure 3.6 T_g of (PBAE/PEO) 70/30 blends with ten percent reactive oligomers as a function of time from mixing. The square on the x axis represents the T_g of the blend without oligomers that was obtained via DSC and the Fox-Flory equation.

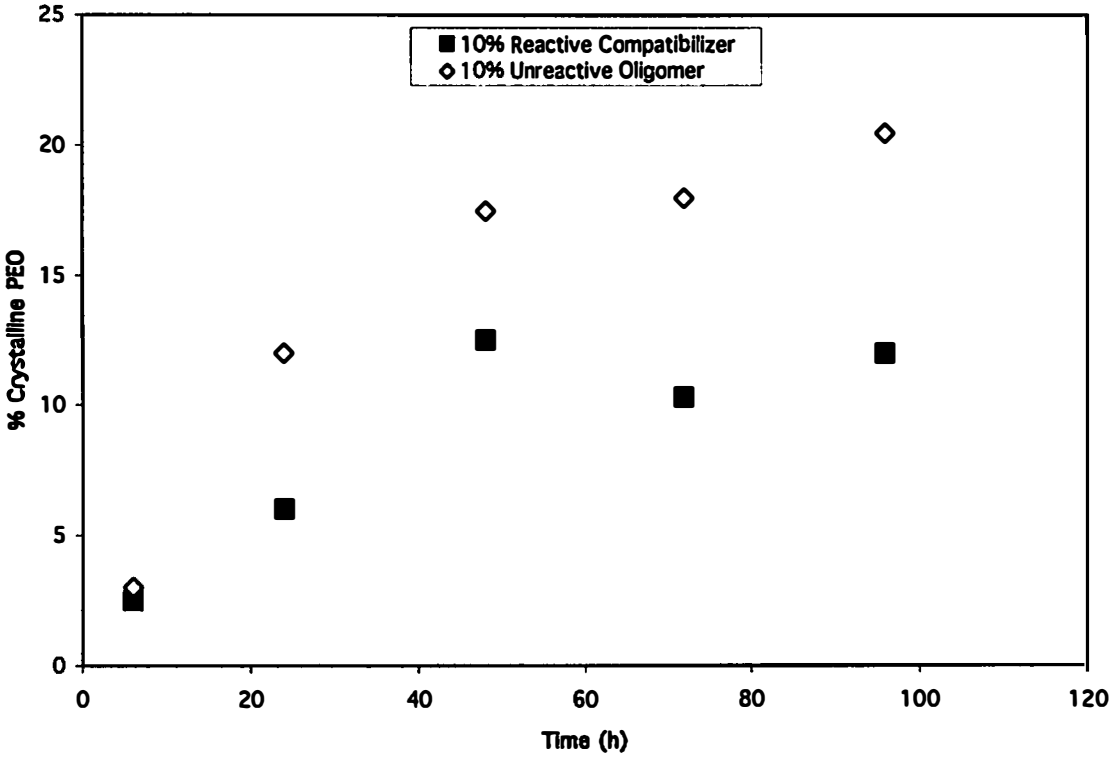

Figure 3.7 Change in percent crystallinity as a function of time for reactive (squares) and unreactive (diamonds) blend samples.

crystallinity of the two similar systems as a function of time after removal from the melt mixer as determined by differential scanning calorimetry. This data illustrates that in the system with reactive oligomers, the PEO was only 2% crystalline at 6 hours, increases with time, and levels out at 12% crystallinity within 96 hours. In comparison, blends containing unreactive oligomer, the PEO was 3% crystalline at 6 hours, increases with time at a level that is always higher than the system with reactive oligomers, and levels out at 21% crystalline by 96 hours. Thus, the samples with unreactive oligomers were unfailingly more crystalline than the sample with reactive oligomers, suggesting that an increase in the PEO crystallinity is not the only factor affecting the microscopic structure and mechanical behavior of the samples with reactive oligomers.

The crystallinity information from DSC by itself does not clarify whether crystallinity or continued reaction at the interface is responsible for the trends observed in figure 3.3, since the crystallinity of the PEO in the blend with reactive oligomers does increase with time. To differentiate the relative importance of the two mechanisms, it is necessary to correlate the crystallinity of the samples to their mechanical properties.

Thus, figure 3.8 shows the change in the modulus with time after removal from the melt mixer for the blend with reactive oligomers and the blend containing unreactive oligomers over a time span of 96 hours. This data shows that both blends exhibit similar time dependencies of the modulus. The moduli for the reactive compatibilized system are consistently higher than that of the blend with unreactive oligomers present.

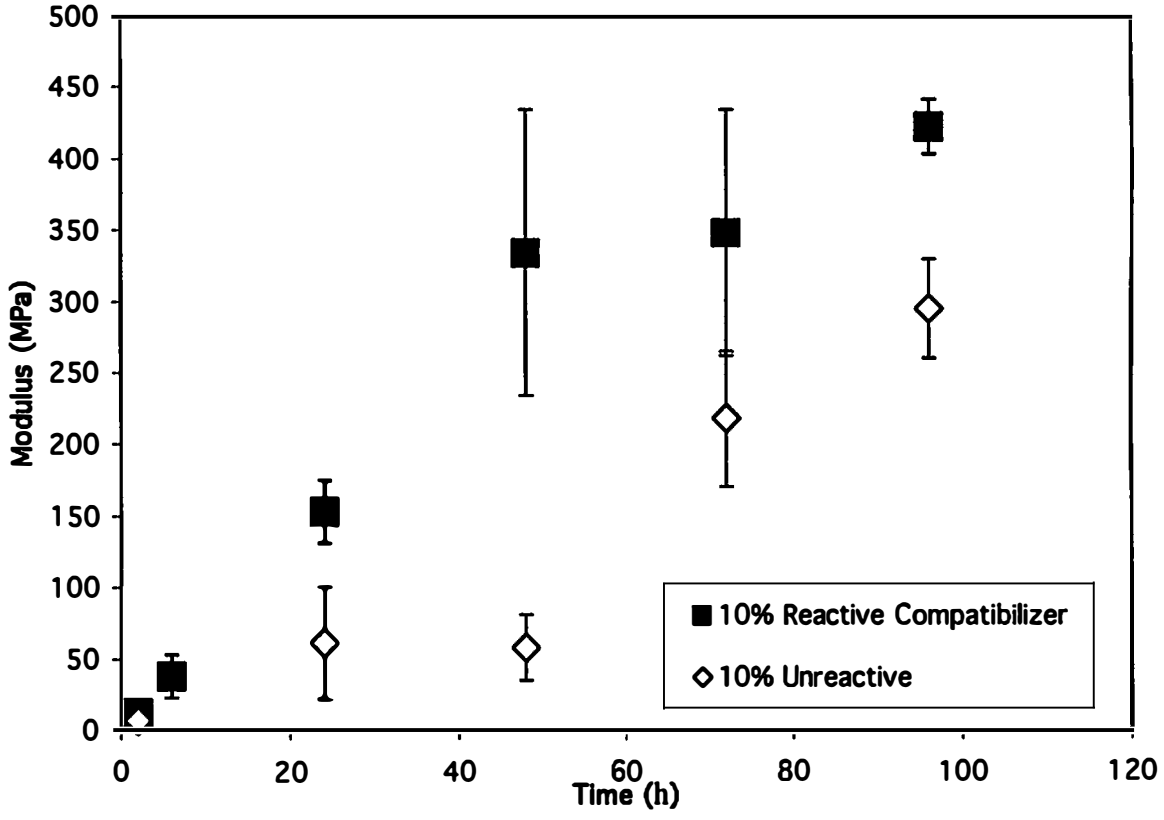

Figure 3.8 Modulus versus time for reactive and unreactive blend samples. The error bars represent one standard deviation.

The final analysis that allows a conclusion on the relative importance of the two competing mechanisms is to combine the last two figures to show the relationship between the mechanical properties of the two blends and their amount of crystallinity. Figure 3.9 shows this data for the blends with reactive and unreactive oligomers, and demonstrates that at any given crystallinity, the reactive oligomer blend sample has a higher modulus than its unreactive blend counterpart. Thus, there must be an additional contribution to the stiffness of the blends beyond merely an increase in crystallinity, and it is our interpretation that the difference between the mechanical properties of the systems with reactive and unreactive oligomers is due to the presence of blocky copolymeric compatibilizers that are formed in-situ from the reactive oligomers. The presence of the compatibilizers improves interfacial adhesion between the phase-separated samples, and the increased interfacial adhesion in the reactive blend increases it's modulus compared to that of the blend with unreactive oligomers at the same percent crystallinity. Thus, although the data indicate that crystallinity plays a role in the altering the physical properties of the reactively compatibilized blend over time, it is not solely responsible for the increase in the mechanical properties of the system.

3.7 Comparison of Miscible and Compatibilized Samples

One final test to verify the ability of oligomers to effectively compatibilize an immiscible polymer blend is to compare the properties of phase separated, miscible, and compatibilized blends. Unfortunately, this analysis can not be completed using a blend with (PBAE/PEO) (70/30 wt/wt) composition. As can be seen from Figure 3.1, the

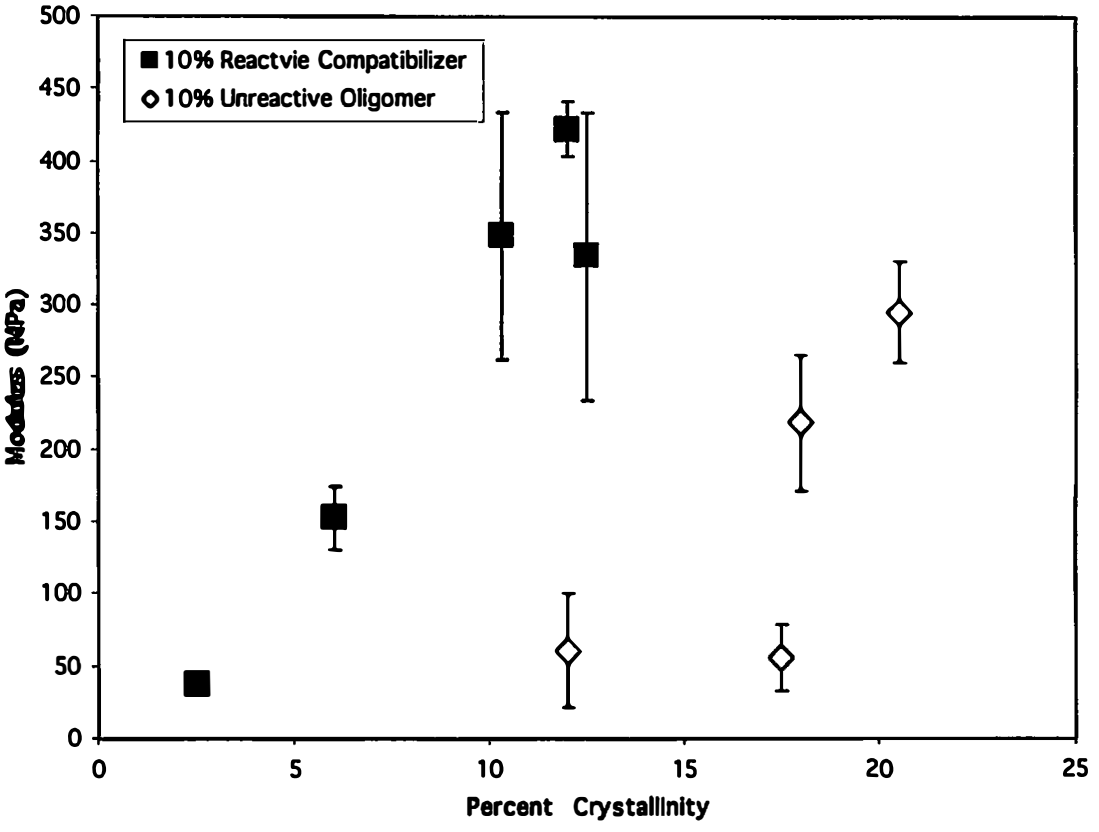

Figure 3.9 Modulus versus percentage crystallinity of the PEO for PBAE/PEO (70/30 wt%) blends with 10% reactive and unreactive oligomer. The error bars represent one standard deviation.

two-phase region for this blend composition is below 88°C. In order to blend the two homopolymers, the temperature of the mixer must be above the Tg of PBAE (88°C). Therefore, blends used in this study were composed of PBAE and PEO with a 30/70 wt/wt ratio. For this composition, the two-phase region has a ceiling of 158°C that allows blending in both the 1 and 2 phase regions.

PBAE/PEO (30/70 wt/wt) blends were thus made with no reactive oligomer and 5% reactive oligomer. Each blend was melt processed at 125°C and 135°C. The mechanical properties were then determined and the results were compared to blends that were processed in the 1 phase region at 170°C. All samples were rapidly quenched after processing and at least five samples were tested for each composition and processing temperature. Table 3.1 shows the results of mechanical testing of each sample. The moduli of the blends without reactive oligomer blended in the 2-phase region are 510 and 520 MPa. These moduli are within experimental error for the two processing temperatures. The moduli of the blends with no reactive oligomer are also 16% less than those of the miscible blend. In contrast, the moduli of the blends with 5% reactive oligomer are 598 and 647 MPa. The system blended in the miscible region of the phase diagram had a modulus of 618MPa. The modulus of the miscible blend lies between that of both reactive compatibilized blends and all three are within experimental error of each other. Thus, the reactive compatibilized blends have a modulus equal to that of the miscible blend.

In the system with no reactive oligomer, the weakest point of the blend lies at the biphasic polymer interface so when these samples are tensile tested, this interface

Table 3.1 Modulus of PEO/PBAE (70/30) blends as a function of processing Temperature and reactive oligomer. The error represents one standard deviation.

Temperature of mixing (°C)	Modulus (MPa) Not Compatibilized	Modulus (MPa) Compatibilized
125 (immiscible)	520±20	598±20
135 (immiscible)	510±20	647±20
170 (miscible)	618±20	-

provides a point for the blend system to yield to the stress. Thus, the moduli of the blends processed in the 2-phase region are lower than the blend processed in the miscible region due to the presence of this weak interface. However, when the blend contains 5% reactive oligomer, an interfacial block copolymer can be produced at this interface. The block copolymer increases interfacial adhesion and prevents droplet coalescence. When these samples are subject to tensile tests, the interface has been strengthened which correlates to a more robust material. In fact, the interface strength approaches that of the bulk materials and the moduli of the reactively processed blends approaches that of the miscible system.

3.8 Conclusions

Overall, the results of this set of experiments indicate that this reactive processing scheme is feasible, however caution must be taken. At a level of 5 wt% and 10 wt% oligomer, 15 minutes is insufficient time to allow completion of the oligomer reactions for mixing in the Atlas mini mixer and unreacted oligomer behaves as a plasticizer altering the engineering properties of the blend. Further experiments using fluorescent labeling[28] to quantify the kinetics of the blocky copolymer synthesis during processing are planned in our lab to more carefully describe the kinetics of this reactive processing scheme and allow further optimization of this procedure. It is also important to note, however, that the mixing that occurs in the melt mixer is not equivalent to that which would be expected in large scale industrial equipment, and thus one would expect

that the actual rate of copolymer production would occur more quickly in a processing device that creates more interface during operation, such as a twin screw extruder.

The data in this dissertation provides evidence that the addition of telechelic reactive oligomers to a polymer blend will provide a mechanism by which blocky copolymeric compatibilizers can be formed during processing, as demonstrated by the changes in the mechanical and optical properties of the phase separated polymer blends. The results also show, however, that the presence of unreacted smaller oligomers can act as a plasticizer in the blend and can thus detrimentally affect the mechanical properties of the blend if any remains after processing. Careful control of the mixing conditions or post processing thermal annealing is required to minimize this potentially deleterious effect. However, the data presented here suggest that this optimization is possible.

Chapter IV

Compatibilization and Depth Profiling of the Polymer/Polymer Interface

4.1 Background

The enhancement of mechanical properties is one method of determining the effectiveness of a compatibilizer, since the mechanical properties of an immiscible polymer blend can be improved by using a compatibilizer as illustrated in Chapter III. However, the improvement of mechanical properties is related to the compatibilizer migrating to the interface, improving interfacial adhesion, and preventing droplet coalescence of the individual components of the blend. Thus, monitoring the ability of a compatibilizer to migrate to an interface as well as its ability to interact with each of the homopolymers are important factors of a compatibilization scheme, and thus monitoring these processes provides a mechanism to understand a particular compatibilization process.

Once a copolymer is placed between a polymer/polymer interface, the effectiveness of the copolymer to act as a compatibilizer has been shown to be related to the width of the polymer/copolymer interfaces.[19] A sharp polymer/copolymer interface indicates one where the copolymer and polymer do not effectively entangle. Such a sharp interface is usually the weakest point in the blend and the location of mechanical failure. A broader copolymer/polymer interface indicates effective interacting between the copolymer and homopolymer through entanglement, resulting in stronger interfaces

that translate to enhanced mechanical properties. Depth profiling polymer samples is an excellent method to monitor the migration of compatibilizers to a polymer/polymer interface during the compatibilization process as well as determination of the width of the final polymer/copolymer interface at equilibrium.

In this study, the complementary techniques of FRES and neutron reflectivity were used to determine depth profiles of compatibilized polymer systems. Other methods of depth profiling exist such as SIMS and X-ray photoelectron spectroscopy (XPS). However, these methods are not as well suited to soft materials (SIMS) or do not probe deep enough into the sample to produce a useful depth profile (XPS). In the case of SIMS, the technique is invaluable for determining the depth profiles of inorganic substrates such as silicon, however when used for organic, soft materials such as polymers the technique is less effective. Primary atomic ions used in most SIMS experiments are too energetic and destroy the sample before sputtered layers can reach the detector. The high energy atomic primary ions cause chain scission and produce a high number of free radical species in the sample which can then rearrange or form a highly crosslinked structure. This phenomenon in turn causes a loss of sputtered sample and a degradation of signal at the detector. In the case of XPS, an incident beam of x-rays causes photoelectrons to be emitted which are detected and analyzed by their energy. This technique, however, is only appropriate for surface analysis since only the top 3nm of the sample yield a signal, therefore XPS can not be used to depth profile the polymer systems described in the following experiments.

In contrast, both FRES and neutron reflectivity have proven to be valuable tools for studying polymer samples. Neutron reflectivity can yield results with a depth resolution in angstroms without destroying soft materials while FRES can be used for depths up to 900nm and has a depth resolution of around 80nm for polymers. In both techniques, one part of the sample must be deuterated to provide the contrast necessary to obtain a depth profile.

4.2 Depth Profiling of a Reactive Processing System using FRES

The formation of block copolymers via reactive compatibilization and the resulting changes in mechanical properties were discussed in Chapter III. The following study continues to focus on reactive oligomers and on the proposed reactive processing scheme, particularly on the ability for reactive oligomers to migrate to the polymer/polymer biphasic interface and react. Although this technique can not determine if reaction is occurring once the oligomer reaches the interface, it does provide information on the position of the reactive oligomer over time. The addition of the Mylar stopping foil before the detector to selectively eliminate $^{4}He^{+}$ ions also slows down the ^{1}H and ^{2}H ejected from the sample which effectively decreases the sharpness of the corresponding peaks and sets the resolution of the measurements at 80nm.

In this experiment, PMMA terminated at one end with an acid functionality (PMMA-COOH), PS, and deuterated telechelic PS terminated with epoxy functionalities (dPS-diepoxy) were used to study the migration of the reactive species to the polymer biphasic interface. As the dPS-diepoxy encounters the interface, it has the

ability to react twice with PMMA-COOH and form triblock copolymers. Two sample geometries were made for this study and are illustrated in figures 4.1 and 4.2.

The first sample geometry (figure 4.1) consists of a PMMA-COOH layer that is directly spin coated onto a Si wafer. Next, a PS film was spin coated onto a glass slide and then the PS film was floated onto deionized water and placed on top of the PMMA-COOH. Finally, the dPS-diepoxy was spin coated onto a glass slide and floated on top of the PS layer to create a trilayer sample. The second sample geometry (figure 4.2) is prepared by spin coating a PMMA-COOH layer directly onto a Si wafer followed by spin coating a blend of PS and dPS-diepoxy (8.4% by weight) directly onto a glass slide and floating them onto the PMMA-COOH layer. For each sample geometry one sample was made and then cut into smaller samples that were placed in a vacuum oven at 170°C for times spanning from 2 minutes to 120 hours. In addition to the bilayer and trilayer samples, a standard sample was made consisting of a 50/50 wt/wt mixture of PS and dPS which was spin coated onto a Si wafer which was used to calibrate the ^{1}H and ^{2}H signal from FRES.

4.3 FRES Results of Reactive Processing Samples

The migration of dPS-diepoxy through PS to the PS/PMMA-COOH interface (sample geometry 1)was studied as a function of anneal time. Figure 4.3 shows the depth profiles of the sample as a function of time annealed for this sample geometry. In this figure the surface of the polymer is located at 100nm and the PMMA surface is at 600nm. The surface of the polymer sample at 100nm is due to the resolution of the

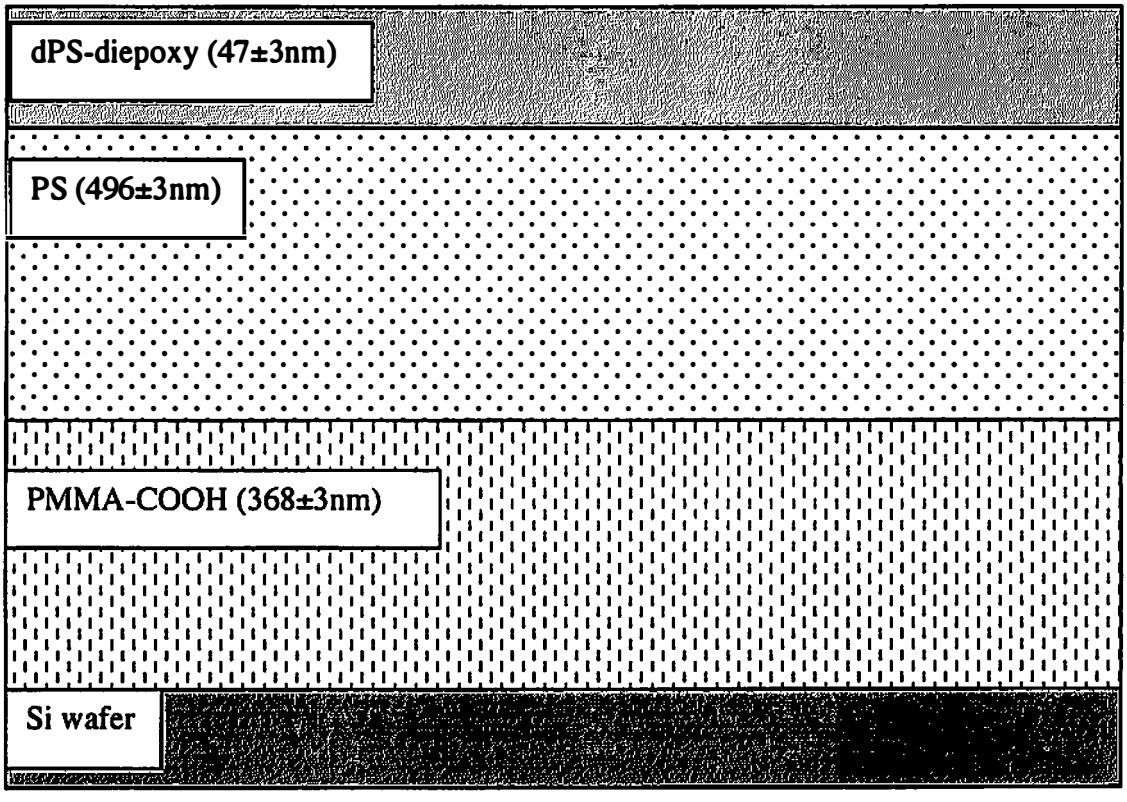

Figure 4.1 Illustration of sample geometry for trilayer sample used in FRES studies. For this geometry the dPS-diepoxy must migrate through 496 nm of PS to reach an interface where it can react with PMMA-COOH.

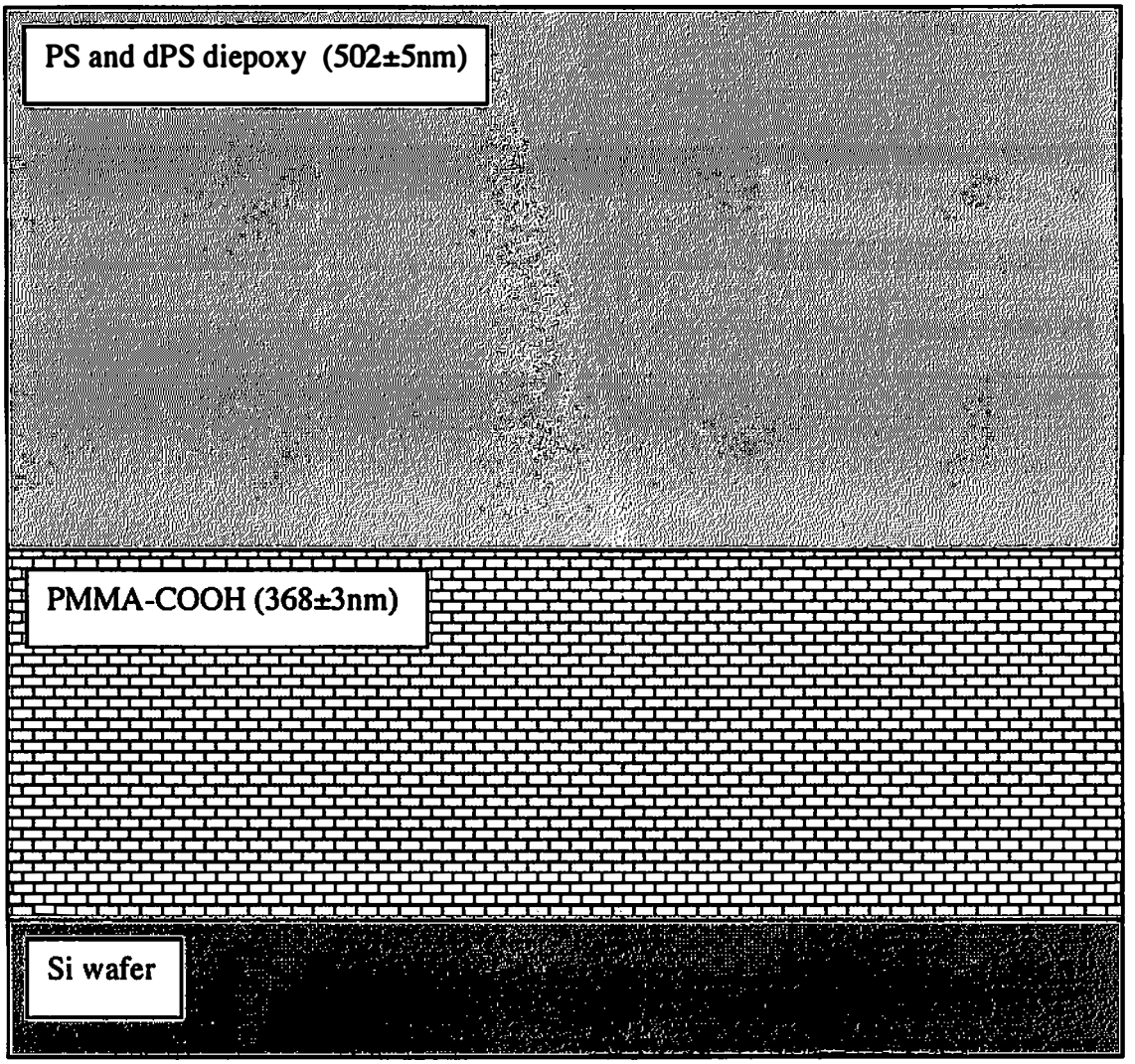

Figure 4.2 Illustration of bilayer sample used in FRES experiments. This sample contains dPS-diepoxy distributed throughout the PS.

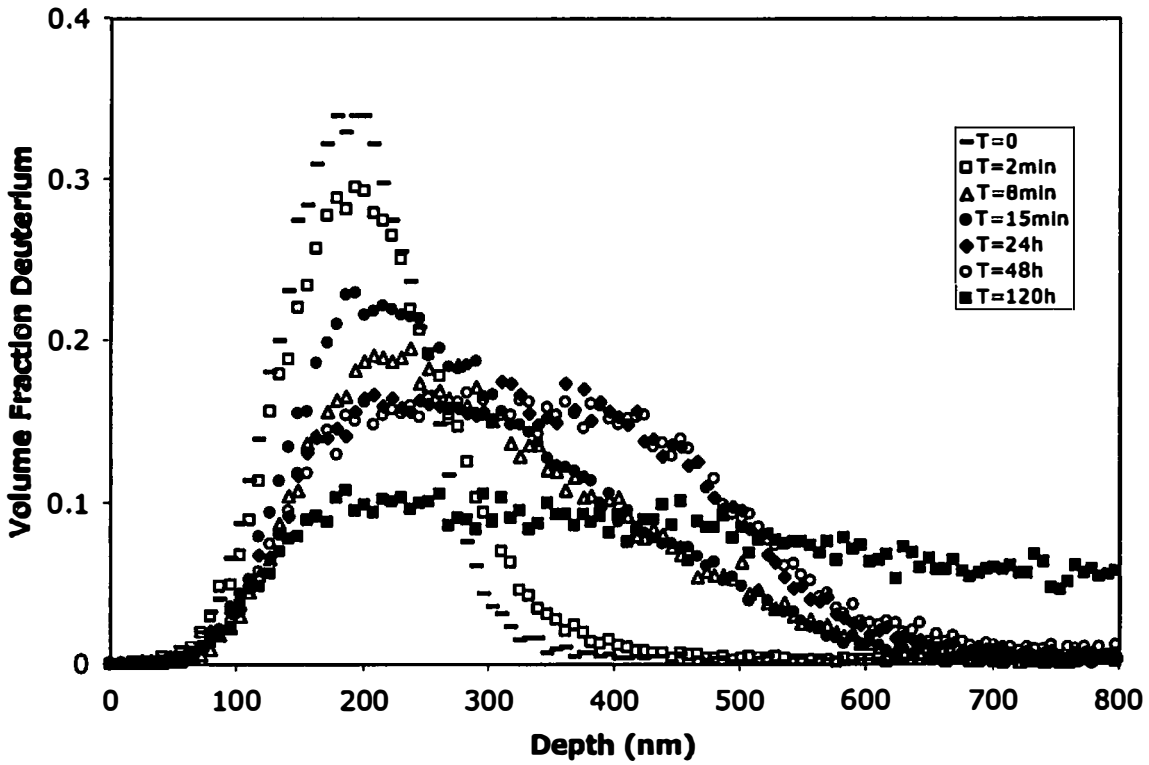

Figure 4.3 FRES ^{2}H depth profiles of the trilayer system at various annealing times. As annealing time increases deuterated material migrates through the PS to the PS/PMMA-COOH interface. The PS/PMMA-COOH interface is located at 600nm.

instrument. The peak at 100nm at time=0 is the dPS-diepoxy and the remaining curves show dissolution of this telechelic in the film as a function of time. During short time intervals, the peak spreads out to 600nm while at longer time scales the peak continues to spread beyond 600nm. When annealing at 170°C, it takes only 8 minutes for the dPS-diepoxy to migrate from the surface to the interface of the PS/PMMA-COOH as evidenced by the dPS-diepoxy signal at the PS/PMMA interface at 600nm in the 8 minute graph. Note also that the profiles indicate deuterium distributed deeper than 600nm at times greater than 48h.

Figure 4.4 shows the depth profiles as a function of annealing time for the bilayer sample geometry. The surface of the sample is at 100nm due to instrument resolution and the PMMA surface is located at 550nm. The broad peaks from 100nm to 550nm are the dPS-diepoxy distributed throughout the PS matrix. This peak remains unchanged for time scales up to 24h. At times greater than 24 hours the peak begins to spread and deuterated material is found deeper than 550nm.

4.4 Discussion of FRES Results for Reactive Processing Samples

For each system, the dPS-diepoxy is monitored as a function of annealing time. For the trilayer geometry, at t=0 hours the dPS-diepoxy is at the surface of the sample indicated by the sharp peak at 100nm. Within 8 minutes, the dPS-diepoxy has migrated to the PMMA-COOH surface at 600nm. From 8 minutes through 48 hours there is dPS-diepoxy at the PMMA-COOH surface. After 48 hours, the dPS-diepoxy migrates deeper than 600nm. For the bilayer system, dPS-diepoxy is located throughout the PS

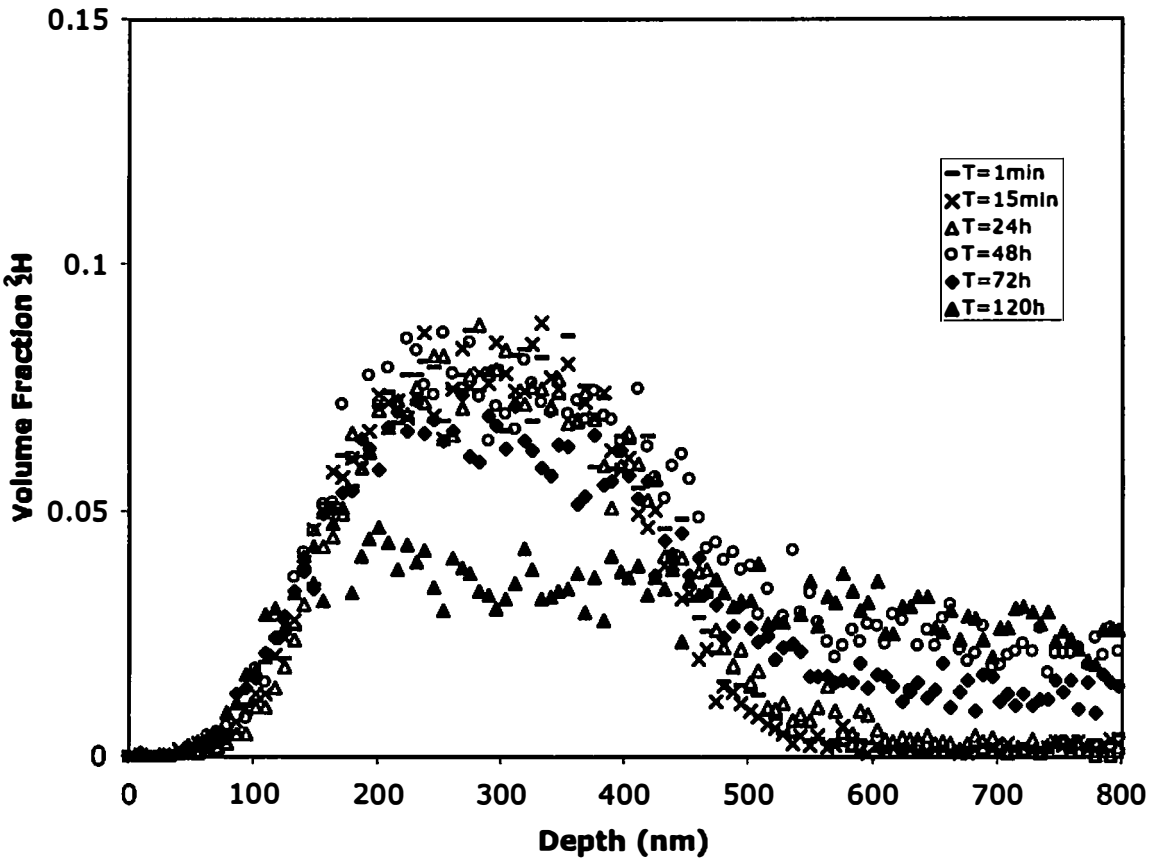

Figure 4.4 FRES ^{2}H depth profiles for the reactive processing bilayer samples as a function of time.

and at the PMMA-COOH surface at 550nm from t=0 to 24 hours. After 24 hours, the dPS-diepoxy migrates deeper than 550nm. Thus, the difunctional oligomer migrates to the PS/PMMA-COOH interface and is available to react with PMMA-COOH. The data at long time scales may indicate the formation of triblock copolymer from the reaction of one dPS-diepoxy with two PMMA-COOH, but other processes may explain the data

The presence of deuterated PS deep into the PMMA layer of both sample geometries at long times could be attributed to several possible mechanisms. First, the dPS may be miscible with the PMMA at the molecular weights and temperatures that were chosen for this experiment and over large time scales the dPS-diepoxy not only migrates to the interface, but also continues to migrate into the PMMA phase. Alternatively, the deuterated PS may react with the PMMA-COOH as expected forming a diblock or triblock copolymer that is primarily PMMA and is thus miscible with the PMMA matrix. Finally, the PS could dewet the PMMA-COOH film resulting in up to micron thick layers of PS instead of the 500nm that was originally placed on the PMMA-COOH, resulting in a signal that indicates ^2H in the top 800nm of the sample.

More specifically, dewetting of the polymer film from the PMMA-COOH surface would result in thicker domains of PS forming as the polymer tries to minimize the surface area between itself and the PMMA-COOH. This in turn would result in ^2H from the dPS-diepoxy being up to 800nm from the top of the sample surface where the ^2H must travel through more PS. Thus, the ^2H signal that is observed deeper than 600nm in both the trilayer and bilayer samples could be from PS in thicker droplets on the surface of the PMMA-COOH.

Wang et al. have used scanning force microscopy to monitor the dewetting of PS on PMMA and reported holes 30μm in diameter when a 272nm PS film dewet from a 486nm PMMA film.[97] Thus, atomic force microscopy was used to examine the surface of our sample for evidence of void formation and variations in surface topography that are indicative of dewetting. The area profile of the sample annealed for 120h was examined over a 50μm^2 area and is shown in figure 4.5. This illustrates that the surface height of the sample did not vary by more than 5nm. If dewetting were occurring it is expected that voids greater than 500nm deep with diameters up to 30μm would be detected throughout the sample as the PS tries to minimize surface area with the PMMA-COOH and form large droplets of PS on the PMMA-COOH surface area. Thus, our data indicate that dewetting is not occurring for our samples.

As mentioned above, an alternate explanation for the observed deuterium within the sample at depths greater than 600nm is that the dPS-diepoxy may be miscible with the PMMA as the dPS telechelic molecules are relatively small. However, a polymer/polymer blend will be miscible only if χ is below a critical χ (χ_c) for the system. A general method for determining the χ_c of a system is to use the Flory-Huggins theory, which provides the equation used for this calculation as

$$\chi_c=1/2(1/(N_1^{1/2})+1/(N_2^{1/2}))^2$$

In this equation χ_c is the critical χ, and N is the degree of polymerization for polymer 1 and 2 respectively. The degree of polymerization is found by dividing the molecular weight of the polymer by the molecular weight of the monomer repeat unit that makes up the polymer. In our system, the PMMA-COOH has a molecular weight

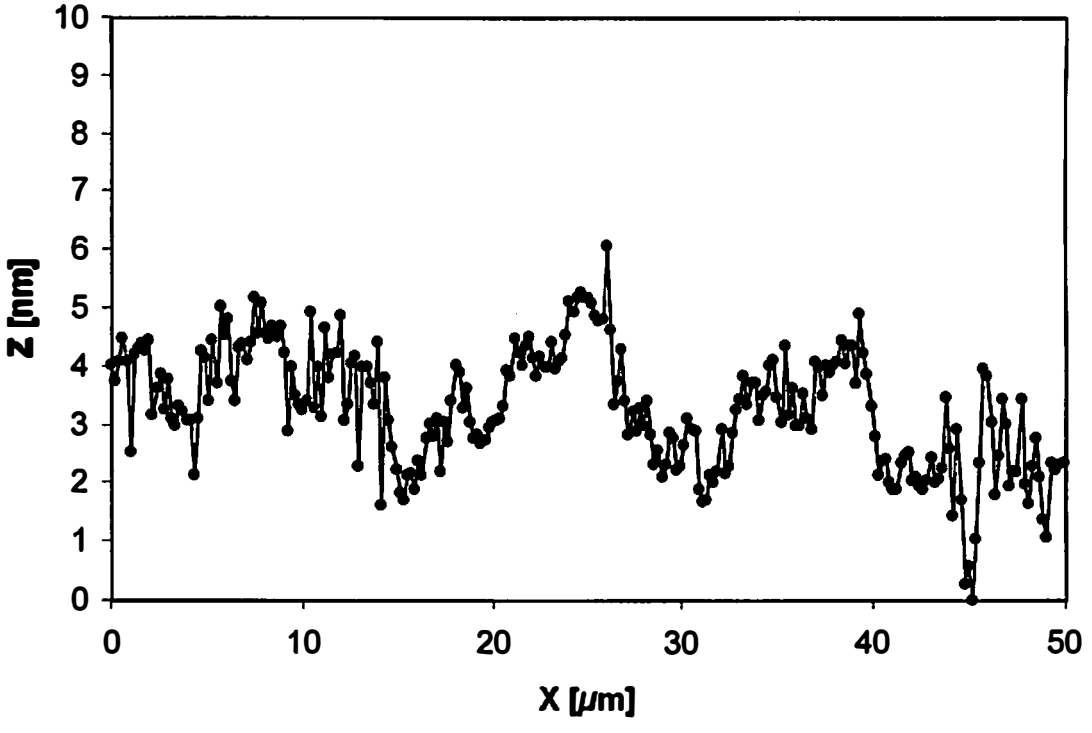

Figure 4.5 AFM surface profile for a bilayer sample annealed for 120h. The sample has a surface roughness of 5nm.

of 13,500 and the molecular weight of methyl methacrylate is 100, providing an N_1 of 135 while the dPS-diepoxy has a molecular weight of 10,600 and the monomer weight of deuterated styrene is 112 that yield an N_2 of 95. Substituting these values of N_1 and N_2 into the equation above leads to a χ_c equal to 0.018.

This calculated value of χ_c is reasonable when compared to similar systems from the literature. Sferrazza calculated χ_c for a d-PS/PMMA system in which the d-PS and PMMA molecular weights were varied [98]. For a system of d-PS with a molecular weight of 10,000 and PMMA with a molecular weight of 7600, the χ_c was calculated at 0.026. It is expected that increasing the molecular weight of the PMMA would cause the χ_c to decrease, thus a χ_c of 0.018 for our system with PMMA-COOH having a molecular weight of 13,500 appears reasonable.

The interaction parameter (χ) of the polymers in the system must be determined or estimated for comparison with χ_c in order to determine if the system being studied is miscible. To do this, the work of Russell et al. was used to obtain values of χ for a PS/PMMA system. Russell et al. studied the interaction parameter χ as a function of temperature for PS and PMMA.[99] In this study of diblock copolymers, Russell used small angle neutron scattering to determine the value of χ for a block copolymer with a PS block that was 13,000 and a PMMA block that was 15,000 at three temperatures. They reported the value of χ to be 0.0383 at 120°C, 0.0373 at 162°C, and 0.0370 at 180°C.[99]

It is reasonable to believe our system would have similar values of χ at the above temperatures due to the similarity of the molecular weights of the PS and the PMMA in the two systems. At the annealing temperature of 170°C, the samples would have a χ value of about 0.0370 that is well above the calculated χ_c of 0.018. A χ that is substantially above the calculated χ_c indicates a system is not completely miscible at the temperatures used for annealing.

In addition, Callaghan and Paul studied blends of PMMA with PS and the interaction energies associated with the blends.[100] This study concluded that the UCST for PS/PMMA blends occurred at a temperature greater than 200°C for blends containing PMMA with a molecular weight of 10,500 and PS with a molecular weight of 4,200. Blends containing PS with a molecular weight of 9,200 and PMMA with a molecular weight of 4,250 also had a UCST greater than 200°C[100]. Although the molecular weights are not exactly those of the current experiment, the processing temperature of 170°C should still be well below the upper critical temperature of the polymer blend. Both the data from Russell and Callaghan support the conclusion that our system is not completely miscible at the annealing temperature.

However, the dPS-diepoxy could be partially miscible in the PMMA-COOH at our annealing temperature of 170°C. The temperature dependence of χ for a PS/PMMA system has been determined by Russell et al.[99] as

$$\chi=(.028\pm.002)+(3.9\pm.06)/T$$

where χ is the interaction parameter and T is the temperature in Kelvin. At 170°C (443K), the χ value is 0.037. The coexistence phases in the blend can also be

determined from Flory-Huggins theory. When two phases exist in equilibrium, the chemical potential, μ, of each species must be equal. The chemical potential can be determined as the derivative of the free energy with respect to ϕ. Therefore, from Flory-Huggins theory, the derivative of the free energy of a polymer blend with respect to ϕ_1 yields

$$\partial f/\partial\phi_1=(\ln \phi_1+1)/N_1- (\ln\phi_2+1)/N_2+\chi(\phi_2-\phi_1)$$

where ϕ is the volume fraction of component 1 or 2 and N is the degree of polymerization of component 1 and 2 respectively[101]. $\partial f/\partial\phi_1$ can then be calculated as a function of blend composition for a given χ, such as figure 4.6 which is a plot of $\partial f/\partial\phi_1$ versus ϕ(PS) for χ=.037. Examination of figure 4.6 show many values of ϕ that have identical values for $\partial f/\partial\phi_1$. However, the coexistence phases can be obtained by dividing the graph into two equal area sections. For this graph, the x-axis serves as a guide to divide the function into two equal areas. The area under the crest of the curve on the left hand side is equal to the area above the trough of the curve on the right hand side. The curve crosses the x-axis at ϕ(PS) equal to 0.028 and 0.989. These values of ϕ(PS) are the coexistence compositions of the blend when χ is equal to 0.037. Thus, for our blend annealed at 170°C, no more than 2.8% of dPS-epoxy can mix with the PMMA-COOH phase. As our data show that at least twice that amount is found in the PMMA-COOH layer, mixing of the telechelic dPS-diepoxy chains and PMMA-COOH cannot explain our data.

Therefore, there must be another explanation for this observation. As the dPS-diepoxy migrates to the interface, it has the ability to react with two PMMA-COOH

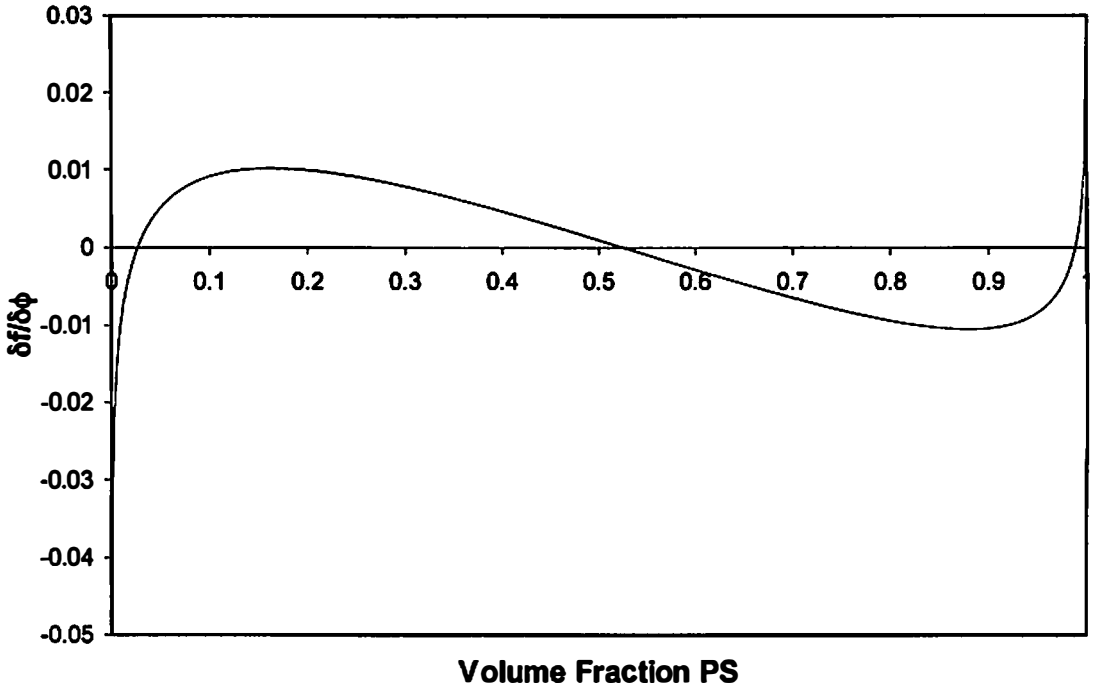

Figure 4.6 A plot of $\partial f/\partial \phi$ versus volume fraction of PS for a PS/PMMA system with a χ of 0.037. Although not symmetric, the x-axis is a good estimate of a line that bisects the curve into two equal areas. The curve crosses the axis at 0.028 and 0.989 which corresponds to the volume fraction of PS in the coexistence compositions.

which leads to an ABA triblock copolymer where the A represents PMMA-COOH and the B is the dPS-diepoxy. In addition to forming a compatibilization layer at the PMMA/PS interface, a triblock copolymer may form micelles with the minority (PS) block forming the core and the PMMA majority blocks forming a coronal shell. The ability of block copolymers to form micelles in a copolymer/homopolymer blend was studied by Huang et al.[102] They reported organized, spaced structures of copolymer micelles within a homopolymer matrix. Therefore, the resulting triblock copolymer may form micelles that migrate into the PMMA-COOH phase since the triblock is PMMA rich.

Unfortunately, FRES can not distinguish actual composition of reactive end groups and therefore can not directly measure if a reaction has occurred at the interface. However, the detection of the deuterium label well into the PMMA phase coupled with the fact that the dPS-diepoxy is not miscible in the PMMA-COOH layer supports the conclusion that the dPS-diepoxy is reacting with the PMMA-COOH. The deuterium label detected throughout the PS and PMMA-COOH phases could then represent broad interfaces between any formed copolymer and the existing homopolymers as the copolymer stretches across the PS/PMMA-COOH interface. Interaction of the copolymer with each homopolymer suggests that the copolymer formed would in fact be a good compatibilizer for the system.

In addition, neither the trilayer nor bilayer samples exhibited deuterated material deeper than 600nm (i.e. below the PS/PMMA interface) before 48 hours of annealing. It is clear that the dPS-diepoxy is present around the PS/PMMA interface in the bilayer

samples (sample geometry 2) from the beginning of the experiment. For the trilayer sample, dPS-diepoxy migrates to the PS/PMMA-COOH interface within 8 minutes at 170°C yet no deuterated material migrates into the PMMA-COOH phase until 24 hours for either system.

One interpretation of this result is that the dPS migrates quickly to the interface, but reacts slowly. This makes sense as any given polymer chain may sample the interface multiple times before encountering another chain with the appropriate available functional group to react. Since there is no mechanical mixing during the annealing in this process, this reaction could take much longer. Only after sufficiently reacting would the deuterated material be able to migrate into the PMMA-COOH layer, and 48 hours represents the minimum amount of time for this reaction to occur without mixing.

The results are supported by both the outcome of reactive compatibilization as discussed in Chapter III and previous work reported by Schulze.[60]. In Chapter II, the reaction of oligomer containing diepoxy functionalities with oligomers containing diacid endgroups at a polymer/polymer interface was found to continue even after 15 minutes of mixing. In addition, Schulze reported that reactive compatibilizer samples the interface several times before a significant amount of reaction ever occurs. Although reactive compatibilizers diffused to the polymer/polymer interface within an hour, it took nearly 24h for substantial reaction to occur.[60] It should be noted that Schulze used compatibilizers that contained amine and anhydride functionalities that are known to react much faster than the epoxy-acid reaction, which may account for the

additional time needed to react in our system. Thus, the rather slow coupling of reactive oligomers to form blocky copolymer at the interface as compared with their diffusion to the interface could be one hurdle for this reactive compatibilization process as unreacted low molecular weight compatibilizer can change the desired properties of the system via acting as a plasticizer. In addition, the increase of mixing time to the order of days would not be feasible for any large-scale production of a compatibilized polymer blend.

4.5 Alternating Copolymer as Compatibilizer for a Polymer/Polymer Interface

Previous work in our lab has studied the ability of alternating copolymers to act as a compatibilizer for polymer blend systems. Arlen et al. used alternating copolymers of PS/PMMA to compatibilize a dPS/dPMMA blend and found that as the molecular weight of the compatibilizer increased the fracture toughness of the polymer blend also improved. In addition, neutron reflectivity studies of two separate molecular weight alternating copolymers showed that the interfacial width of the polymer/copolymer interface of the larger molecular weight compatibilizer was greater than that of the lesser molecular weight copolymer.[2]

FRES experiments were conducted to further develop the relationship between interfacial width and the ability of the alternating block copolymer compatibilizer to strengthen the interface of a polymer blend. A system containing dPS, dPMMA and one of three alternating copolymer compatibilizers with molecular weights of 85,000, 96,000, and 497,000 were studied. In this experiment, FRES was used to monitor the

polymer/copolymer interfacial width for each alternating copolymer system before annealing and after 12h of annealing. A representation of the samples assembled for the FRES experiments is shown in figure 4.7 and were constructed by spin coating a dPMMA film (320±4nm) on a silicon wafer followed by floating a layer of alternating copolymer (280±5nm) on top of the dPMMA. Finally, a layer of dPS (330±3nm) was floated from a glass slide onto the alternating copolymer to create a sandwich of alternating copolymer between the dPS and dPMMA and the resulting sample was then cut into smaller samples. One sample was not annealed and one sample was annealed at 150°C for 12h.

4.6 Results of FRES on Alternating Copolymer Samples

The raw data of the FRES experiment is reported as a curve of count versus channel and then converted into volume fraction versus depth as described in Chapter II. Figure 4.8 is the resulting volume fraction versus depth for hydrogen within the sample. The x axis in this figure is not scaled for hydrogen since the convert7.for program used to reduce the data scales the x axis to the deuterium peak, thus the ^{1}H peak is centered at 1400nm. The peak associated with the hydrogenated alternating copolymer in the depth profile (figure 4.8) is fit to a hyperbolic tangent function on both the left hand side and right hand side of the curve as illustrated in figure 4.9. To quantify the width of the alt-PS and alt-PMMA interfaces, the data is fit to a function consisting of four parameters that include a shift along the x and y axis and a stretch of the function along both the y and x directions. The parameter that effectively stretches

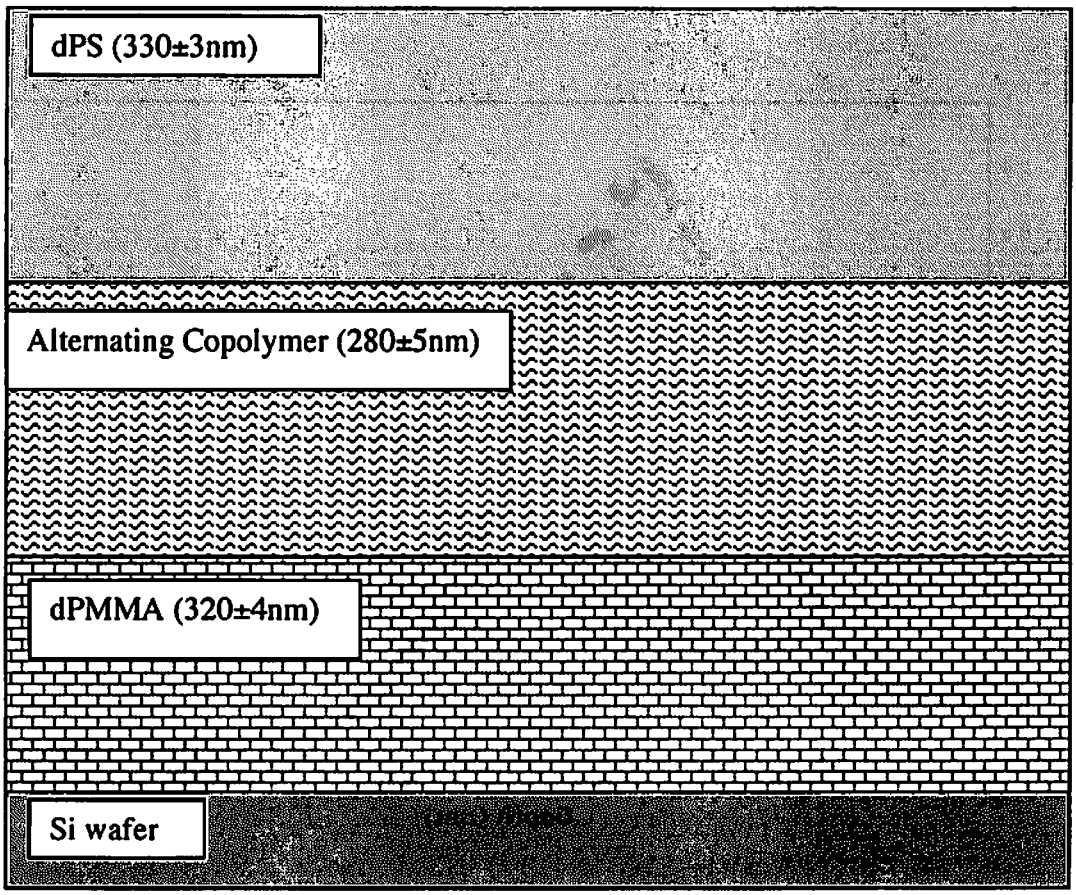

Figure 4.7 Illustration of geometry used for studying alternating copolymers between dPS and dPMMA via FRES.

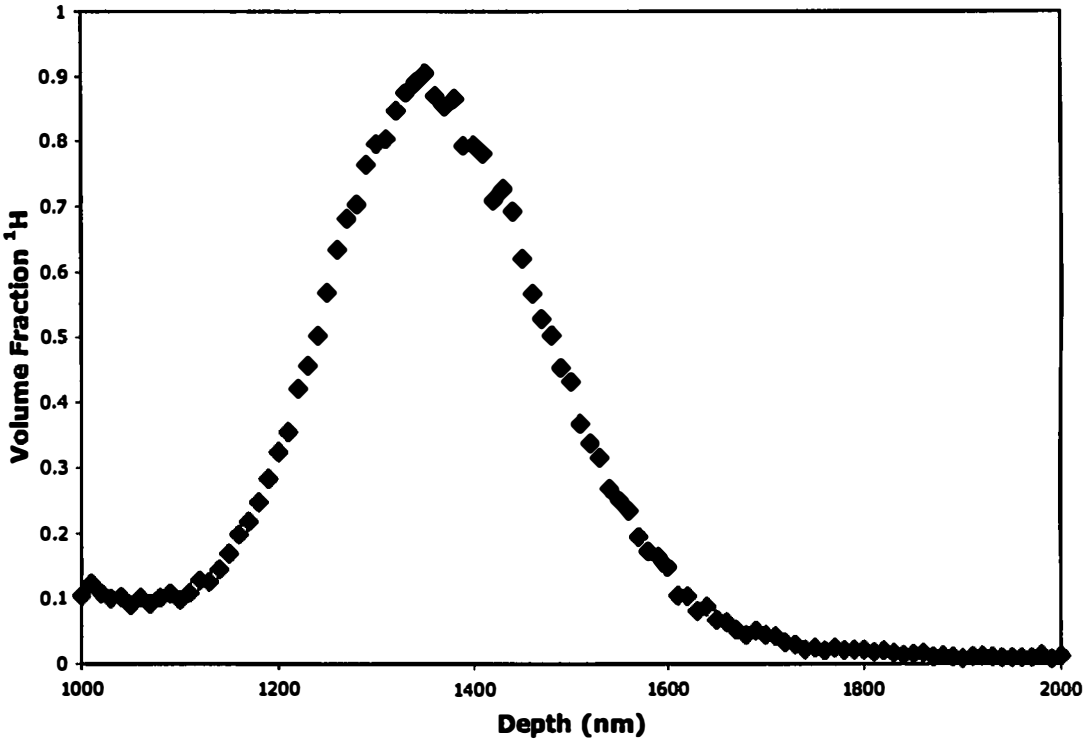

Figure 4.8 Typical data from FRES of volume fraction of ^{1}H versus depth for the alternating copolymer in the trilayer samples.

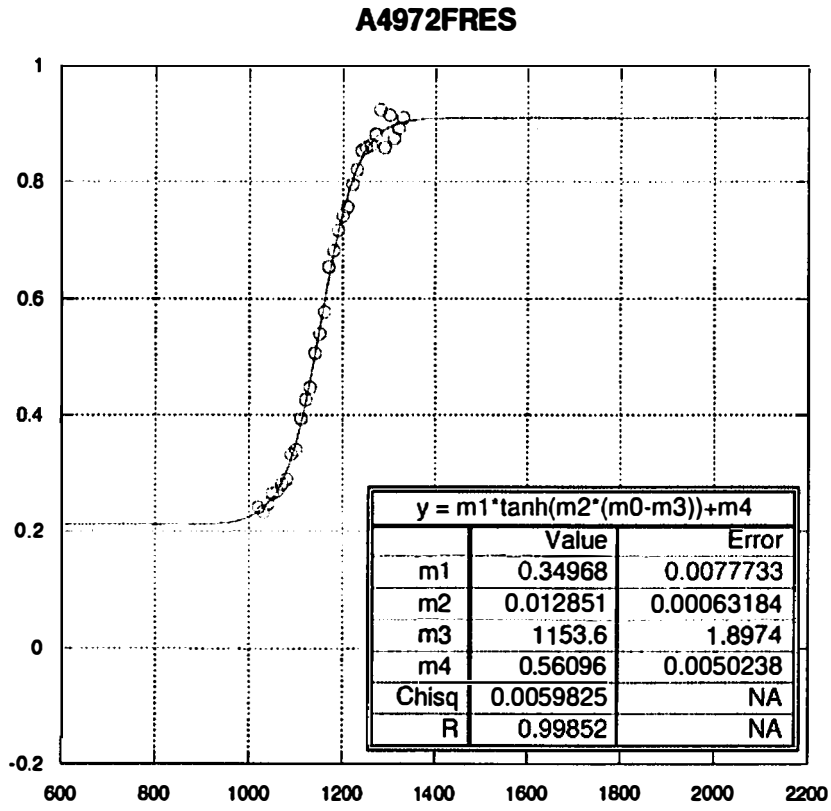

Figure 4.9 The left hand side of a hydrogen peak from FRES fit to a hyperbolic tangent function.

the function parallel with the x axis corresponds to (interfacial width)$^{-1}$. Thus, the resulting fits yield a quantification of the interfacial width between the alternating copolymer and the homopolymer corresponding to each side of the curve. Subtracting the interfacial width of the unannealed sample from the interfacial width of a given sample at an annealing time of 12 hours provides a measure of the interfacial broadening of the interfaces. The values obtained for the interfacial broadening for each alternating copolymer and the dPMMA are shown in table 4.1. The values for the interfacial broadening are 4nm for alt85 and 0nm for alt96 while the interfacial broadening jumps to nearly 33nm between the alternating copolymer and the dPMMA for alt497.

4.7 Alternating Copolymer FRES Discussion

Arlen used ADCB to determine the fracture toughness of PS/PMMA blends reinforced with alternating copolymers of various molecular weights (85,000, 96,000, and 497,000) as shown in table 4.1.[2] The study found alt497 the best compatibilizer by far with a fracture toughness of 24 J/m^2, while the data presented here indicate the alt497 clearly showed the largest interfacial broadening between the alternating copolymer and the dPMMA after annealing at 12h at 150°C. In fact, the interface broadened nearly eight fold relative to the alt96 or alt 85. This corresponds well with the ADCB study showing alt497 to be the best compatibilizer while alt85 and alt96 are among the least effective compatibilizers for the PS/PMMA blend system.

Table 4.1 Width of the copolymer/dPMMA interface determined by FRES for the alternating copolymer system along with corresponding fracture toughness when the copolymer is used as a compatibilizer for a PS/PMMA system as reported by Arlen.[2]

Copolymer	Copolymer/dPMMA Interfacial Broadening (nm)	G_c (J/m^2)
Alt-85	4	9.6 +/- 0.4
Alt-96	0	15.5 +/- 1.2
Alt-497	33	24.2 +/- 1.9

Neutron reflectivity studies were previously done on the alt497, dPS, and dPMMA system.[2] Alt497 was found to broaden the alternating copolymer and dPMMA interface by 29nm after annealing for two hours at 150°C. In comparison, the FRES indicates an interfacial broadening between the alt497 and the dPMMA of 33nm. Thus, qualitatively the FRES data shows that the larger molecular weight alternating copolymers broaden the copolymer/dPMMA interface the most.

Interestingly, only alt85 showed any interfacial broadening between the alternating copolymers and the dPS layer for the remaining FRES experiments. However, Arlen previously studied the miscibility of P (S-alt-MMA) in both dPS and dPMMA. The turbidity of solution cast films of the alternating copolymers with dPS and dPMMA was determined and the results showed that P (S-alt-MMA) was more soluble in dPMMA than in dPS.[2] In addition Dadmun showed that alternating copolymers tended to expand along the polymer/polymer biphasic interface while block copolymers stretched across the interface.[23] Entanglements of the homopolymer with an alternating copolymer can occur since the alternating copolymer is stretched along the interface that allows for compatibilization even at low interfacial widths. Thus, it is not surprising that the FRES data shows an interfacial broadening between the alternating copolymer and the dPMMA and little to no interfacial broadening between the P (S-alt-MMA) and the dPS.

4.8 Blocky Copolymers as Compatibilizers

Previous chapters and discussions have focused on the creation of blocky copolymers at a polymer/polymer interface via in-situ reactive compatibilization. The formation of blocky copolymers was chosen since blocky type copolymers have been shown to act as an effective compatibilizer for polymer blends. Eastwood et al. have reported the fracture toughness of PS/PMMA blends when compatibilized with multiblock copolymers consisting of both PMMA and PS. [1] The study focused on the ability of the copolymer to compatibilize the blend system as a function of both block size and number of blocks composing the copolymer. However, only mechanical fracture toughness was investigated and no depth profiling studies pertaining to how the compatibilizer interacts at the interface of the PS/PMMA blend were undertaken.

For this study, a system of dPS, dPMMA, and various block copolymers listed in table 4.2 consisting of blocks of PS and PMMA were subjected to depth profile analysis using both FRES and neutron reflectivity. In this experiment, FRES was used to study the interfacial width of the multiblock compatibilizer and each homopolymer without annealing and after 12 hours of annealing. The samples studied by the FRES experiment are illustrated in figure 4.10 and consisted of a dPMMA layer spun coat onto a Si wafer followed by floating a block copolymer film from a glass slide onto the dPMMA layer. Finally, dPS was spun coat onto a glass slide and floated onto the block copolymer creating a sandwich of block copolymer between dPS and dPMMA. The sample was thin cut into smaller samples. One sample was not annealed and one was annealed at 150°C for 12 hours.

Table 4.2 Block copolymers used for FRES depth profiling experiments.

Abbreviated Name	Copolymer Description
SMS-21	Triblock copolymer with 21,000 molecular weight blocks
MSMSM-21	Pentablock copolymer with 21,000 molecular weight blocks
SMSMSMS-21	Heptablock copolymer with 21,000 molecular weight blocks
MSM-30	Triblock copolymer with 30,000 molecular weight blocks
SMSMS-30	Pentablock copolymer with 30,000 molecular weight blocks
SMS-50	Triblock copolymer with 50,000 molecular weight blocks

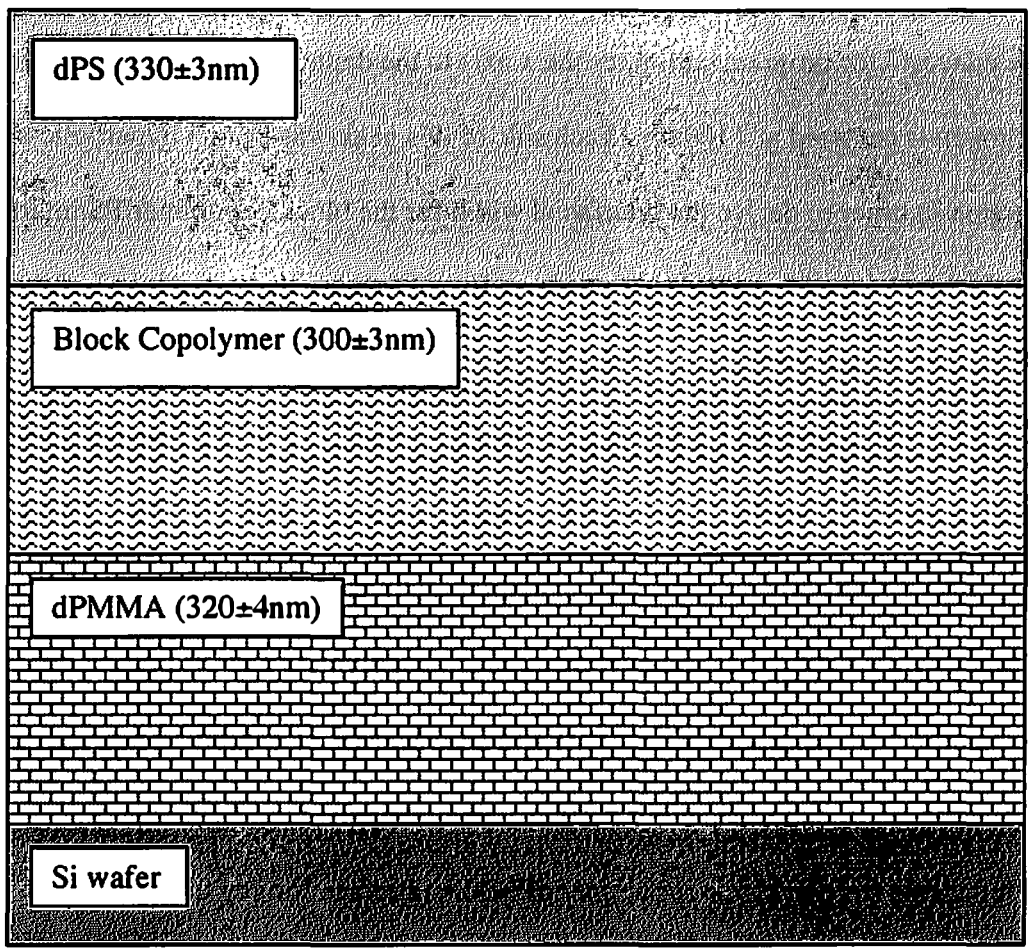

Figure 4.10 Geometry of samples used for block copolymer depth profile studies using FRES.

4.9 FRES Results of Block Copolymer

FRES data were analyzed as described in Chapter II resulting in a volume fraction versus depth for hydrogen corresponding to the block copolymer (figure 4.11) The convert7.for program calibrates the x axis to the deuterium peaks and therefore the hydrogen is centered at 1300nm. Each side of this peak was fit to a hyperbolic tangent function in order to derive the interfacial width for the block copolymer/PS interface and the block copolymer/PMMA interface. By subtracting the initial interfacial width determined at time zero from the interfacial width determined after 12 hours of annealing, the interfacial broadening can be determined. Table 4.3 lists the interfacial broadening of the interfaces between the blocky copolymer and the dPS. Two block copolymers, SMS-50 and SMSMS-30, exhibit relatively large interfacial broadening, ($\geq$20nm) while the SMS-21 and MSM-30 block copolymers exhibit little to no broadening ($<$2nm). Both MSMSM-21 and SMSMSMS-21 exhibit a relatively small amount of interfacial broadening(5-10nm). Interestingly, the FRES experiments show no broadening of the block copolymer dPMMA interface for any of the block copolymer studied.

4.10 Discussion of FRES Data for Block Copolymers

The fracture toughness reported by Eastwood for a system containing PMMA, PS and an interfacial modifier is shown in table 4.3.[1] Two block copolymers, SMSMS-30 and SMS-50, are clearly the two compatibilizers that led to the greatest

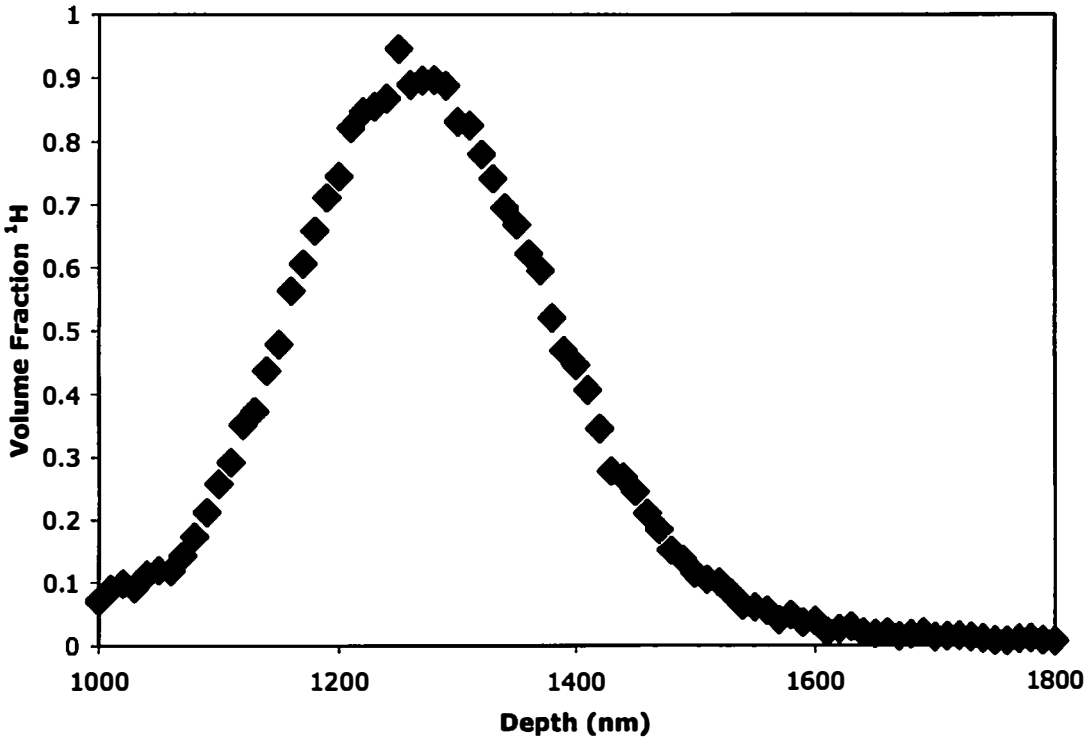

Figure 4.11 A typical FRES curve illustrating volume fraction ^{1}H versus depth for a multiblock copolymer in a trilayer sample.

Table 4.3 Interfacial broadening determined by FRES for several block copolymer samples along with fracture toughness of PS/PMMA samples compatibilized with the same copolymer as reported by Eastwood.[1]

Block Copolymer	Interfacial Broadening (nm)	G_c (J/m^2)
SMS-21	1	20
MSMSM-21	10	25
SMSMSMS-21	7	35
MSM-30	0	30
SMSMS-30	20	60
SMS-50	15	50

fracture toughness for the PS/PMMA system. Systems containing SMSMS-30 have a G_c of 60J/m^2 and systems with SMS-50 have a G_c of 50J/m^2. Both systems are at least 40% higher in fracture toughness than the next best compatibilized system. The general FRES trends indicate that the improved interfacial width may be related to their compatibilization ability.

Similarly, both MSMSM-21 and SMSMSMS-21 broaden the interface of the block copolymer/PS by 6-10nm. In turn, these block copolymers in a PS/PMMA system have a fracture toughness of 25 and 35J/m^2 and are listed among the mid range of block copolymer compatibilizers for a PS/PMMA system studied. In addition SMS-21 only broadens the interface by 1nm and merely has a G_c of 20J/m^2 which is the lowest of all the copolymers studied for the PS/PMMA system. One copolymer, MSM-30, seems out of order when comparing the interfacial broadening with the Gc reported by Eastwood. Although Eastwood reports the G_c of the PS/PMMA system compatibilized with MSM-30 as 30 J/m^2, the interfacial broadening of this same system was near 0nm that is the lowest interfacial broadening while having one of the top three improvements in fracture toughness. The results suggest that a good compatibilizer will interact with the homopolymers and broaden the interface between the compatibilizer and the homopolymer, and that FRES provides a qualitative correlation to fracture toughness.

4.11 Neutron Reflectivity Results for Block and Random Copolymers

In addition to FRES, neutron reflectivity was used to quantify the interfacial broadening of the block copolymer compatibilizers as well as one random copolymer with dPS and dPMMA. Samples were prepared in a similar fashion to those described for the FRES experiments as illustrated in figure 4.10 with the exception that the dPS and dPMMA layers were only 56±2nm thick and all the block copolymer thicknesses were 35.2±0.3nm. After construction, these samples were annealed for 12 hours at 150°C before reflectivity curves like those illustrated in figure 4.12 were obtained at NIST at the National Center for Neutron Research. The reflectivity curve is a plot of reflectivity versus Q_z and were generated from raw data via the reflred program obtained from NIST which subtracts background from the raw data and normalizes the scans to the incident neutron beam as described in chapter 2. Finally, scattering length density profiles were modeled to the reduced reflectivity curves using the reflfit program also obtained from NIST. A reflectivity curve that has been fit and the corresponding scattering length density profile are shown in figures 4.13 and 4.14 respectively. The scattering profile in figure 4.14 is a plot of Nb versus depth (Å) where N is the number of scattering sites and b is the scattering length.

The scattering length density profiles provides a means to determine the thickness of each of the layers corresponding to dPS, block copolymer, and dPMMA as well as the width of the dPS/copolymer and dPMMA/copolymer interfaces. The interfacial width can be described by a hyperbolic tangent function. The full width at

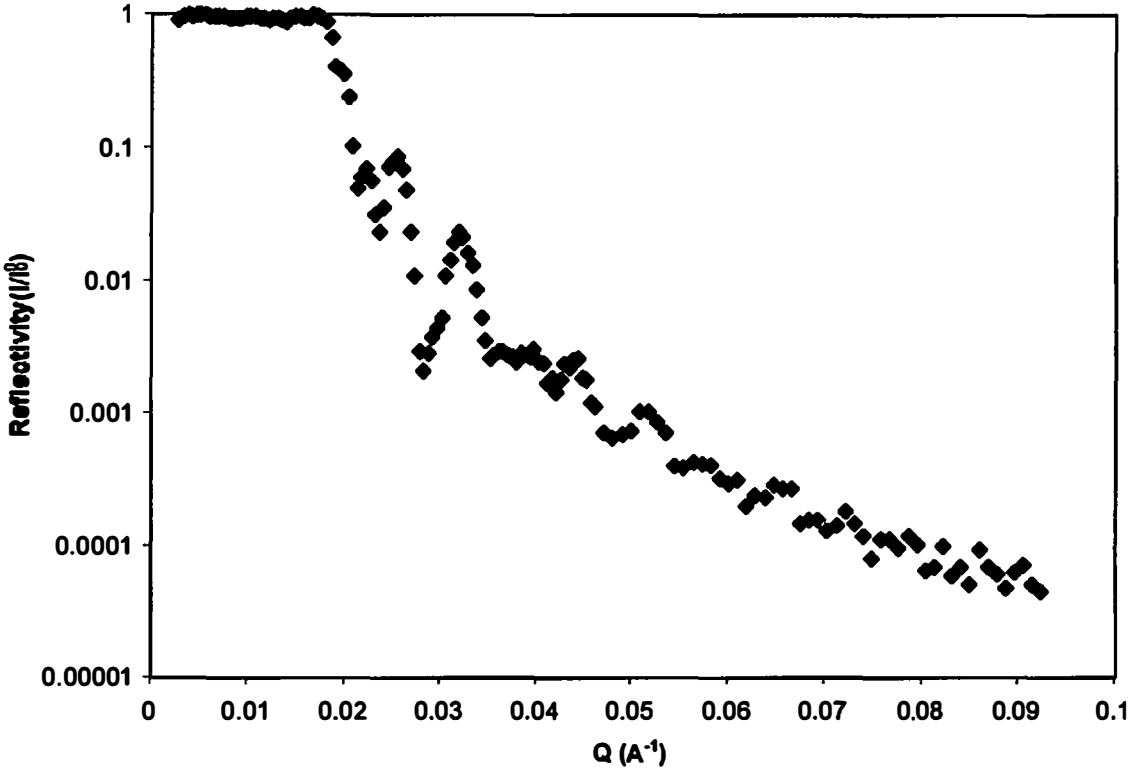

Figure 4.12 Example of a reflectivity curve obtained at NIST.

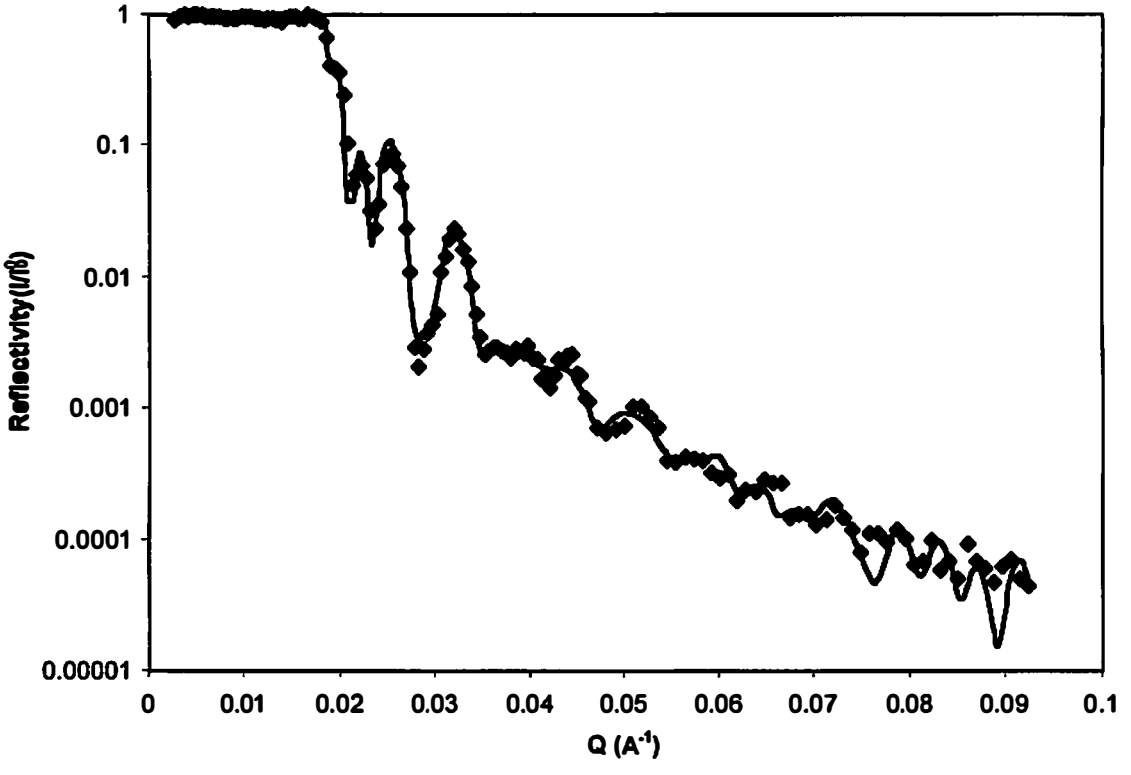

Figure 4.13 Example of a fit to a neutron scattering curve for a random copolymer.

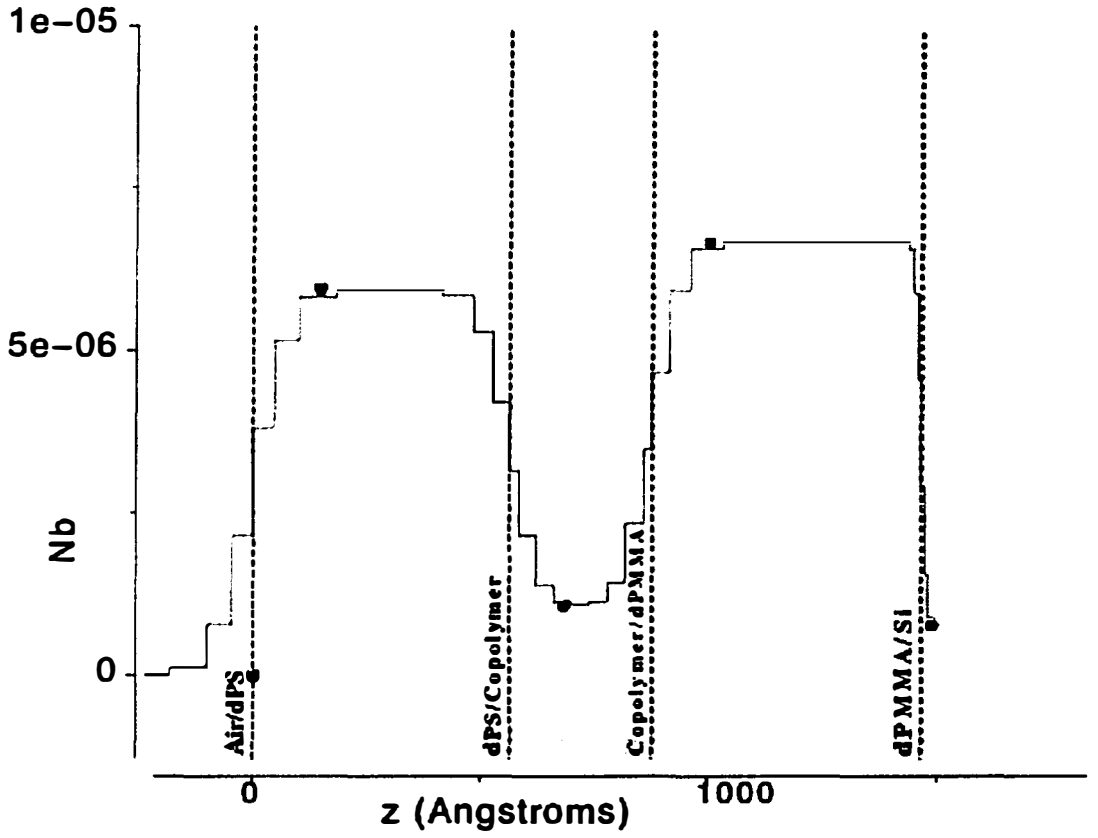

Figure 4.14 Scattering profile of a system containing a random copolymer corresponding to fit neutron reflectivity curve illustrated in figure 4.13. The y axis is Nb where N is the number of scattering sites and b is the scattering length.

half maximum (FWHM) of this function is the interfacial width. Table 4.4 lists the copolymer thickness and the interfacial width between the copolymer and each homopolymer after annealing for the five samples studied. It can be seen from table 4.4 that the copolymer SMSMS-30 layer broadened from 350Å to 520Å, a difference of 170Å and the width between the copolymer and the dPS and dPMMA was 242Å and 384Å respectively. The copolymer SMS-50 also grew in thickness from 350Å to 483Å with an interfacial width with dPS of 98Å and an interfacial width with dPMMA of 244Å. The remaining three copolymers did not broaden as a layer and had minimal interfacial width (≤151Å) with dPS or dPMMA.

4.12 Discussion of Neutron Reflectivity Data of Block Copolymers

Entanglements of the copolymer with each homopolymer in the blend are effective interactions for strengthening a polymer/polymer interface. A copolymer/homopolymer interface with many entanglements becomes broader as the two polymers interact. ' A copolymer with few entanglements with a homopolymer will have a small interfacial width. Thus, an interface with a smaller interfacial width (fewer entanglements) will likely be the source of mechanical failure. Although the data obtained from the neutron reflectivity show that the copolymers thickness and interfacial width with dPMMA grew in the following order: SMSMS-30>SMS-50>>diblock>SMSMSMS-21>random, the smaller interfacial width between the copolymer and dPS is presumed to be the site of failure.

Thus, the dPS/copolymer interfacial width obtained from neutron reflectivity was compared to the fracture toughness data obtained by Eastwood and listed in table 4.4. [1] It can be seen that the fracture toughness of the different copolymers corresponds well to the minimal interfacial width of the system. Eastwood found that SMSMS-30 imparted a fracture toughness of 22 J/m^2 to the blend system when the copolymer layer was 50nm thick and the same copolymer grows to a thickness of 520Å with a copolymer/dPS width of 242Å. Both SMSMSMS-21 and the diblock copolymer have a minimal interfacial width with styrene of 141 and 149Å respectively and it follows that both polymers would have the next highest fracture toughness in this series. The sequence is rounded out by the random copolymer with a minimal interfacial width of 121Å and a fracture toughness of 14.8J/m^2 and SMS-50 with a fracture toughness of 14 J/m^2 and a minimal interfacial width of 98Å.

Qualitatively, this data shows that as the minimal interfacial width increases, the fracture toughness of the sample also increases. Previous studies have reported means to quantify the relationship between fracture toughness and minimal interfacial width. Brown reported a model of craze fracture at a crack tip[103] where G_c is defined as:

$$G_c=G_c^*/\ln\{[1-(1.2\sigma_c/\sigma_f)^2]^{-1}\}$$

where G_c^* is a constant and σ_c is the craze widening stress defined by

$$\sigma_c=f_{mono}\rho_{mer}w_{min}^*/2$$

and σ_f is the fibril failure stress defined as

$$\sigma_f=f_{mono}\rho_{mer}w_{min}/2$$

Table 4.4 Thickness and interfacial width for various block copolymers studied with neutron reflectivity in a PS/PMMA system along with fracture toughness results reported by Eastwood for the same system.[1]

Copolymer	Thickness (Å)	Width with dPS (Å)	Width with dPMMA (Å)	G_c (J/m^2)
SMSMS-30	520	242	384	22.4
SMS-50	483	98	244	14.1
Diblock	331	149	151	15.9
SMSMSMS-21	328	141	144	16.8
Random	315	121	122	14.8

In both instances, f_{mono} is the static friction coefficient per monomer, ρ_{mer} is the number density of repeat units, and w_{min}^* is the narrowest interface where crazing is observed.Substituting for s_f and s_c in Brown's definition of G_c yields the following relationship:

$$G_c=G_c^*/\ln\{[1-(1.2w_{min}^*/w_{min})^2]^{-1}\}$$

where G_c^* and w_{min}^* are constants and w_{min} is the minimal interfacial width of the system. In addition, Benkoski et al. reported that the fracture toughness of a polymer system scales with interfacial width according to the following relationship:

$$w_{(min)}^2 \sim G_c$$

where $w_{(min)}$ is the minimal interfacial width of a copolymer/homopolymer interface and G_c is the fracture toughness of the system.[41]

Figure 4.15 shows the square of the interfacial width as a function of the fracture toughness for the same sample with a dotted line representing a linear fit to the data. It can be seen that our data show fracture toughness scale as the minimal interfacial width squared. Brown's theory relating fracture toughness to interfacial width is only true for systems that fail by crazing and fibril fracture at the interface ($G_c>10J/m^2$). For systems with lower G_c, failure is presumed to occur through chain pullout due to the lack of sufficient entanglements.[63] Since the data presented follows Brown's theory, failure in our system may occur through crazing and fibril fracture even for the compatibilizers that have the weakest fracture toughness.

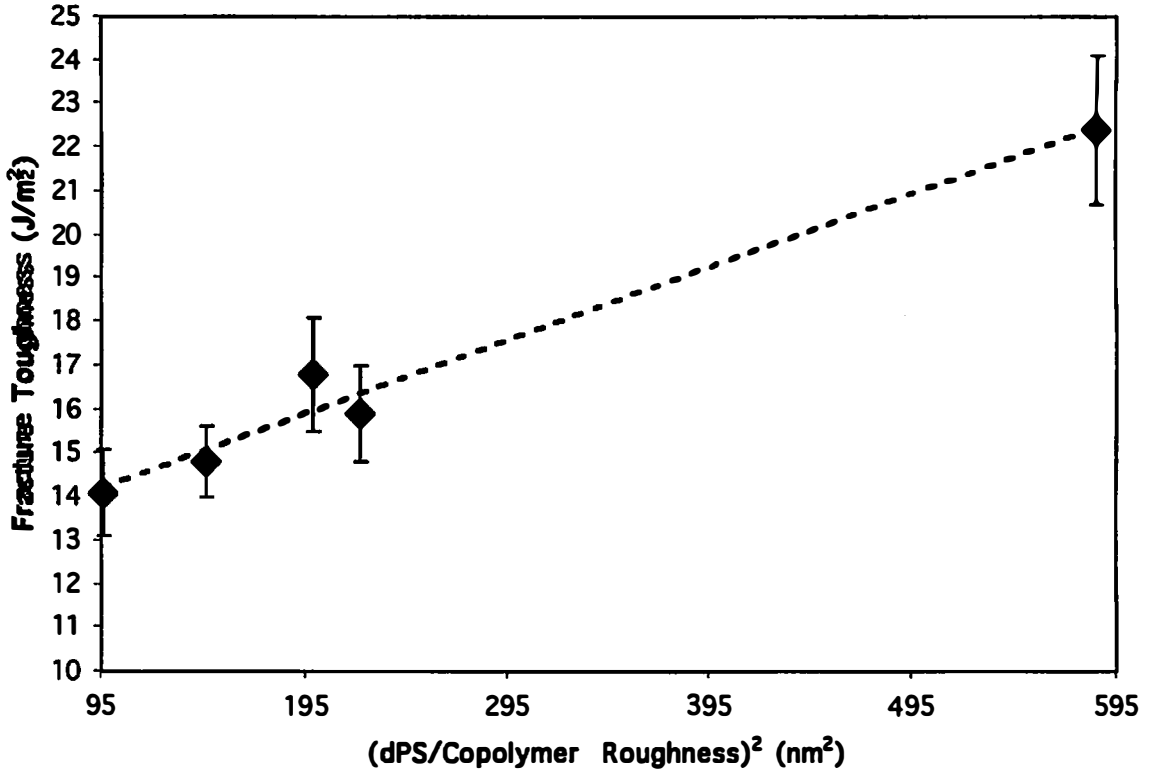

Figure 4.15 Fracture toughness versus interfacial width squared for a series of copolymers. The dotted line is a linear fit to the data.

Schnell and Creton have also studied the relationship between fracture toughness and the interfacial width.[63,104] Their studies used polymers that were eight times larger than the entanglement molecular weight. In addition, the systems studied were homopolymer/homopolymer interfaces. They found that once the interfacial width reaches 12nm fracture toughness no longer varies with interfacial width and reaches a plateau. Our research differs in that our system contains copolymer compatibilizers at the interface. For the compatibilizers studied, fracture toughness continues to increase even after the interfacial width exceeds 12nm. The increase in our system fracture toughness with interfacial width after 12nm may be due to increased entanglements between the homopolymer/copolymer. These entanglements create stronger interfaces than the homopolymer/homopolymer interfaces studied by Schnell and Creton and yield higher fracture toughness values with increased interfacial width (>12nm).

4.13 Conclusions

Depth profiling is a useful technique when studying the compatibilization of a polymer blend system. The migration of a reactive compatibilizer to the polymer/polymer interface as well as a study of the interfaces of the compatibilizer and each homopolymer was investigated using both FRES and neutron reflectivity. FRES proved to be a good qualitative method for determining compatibilizer position as well as interfacial width. When studying reactive compatibilization, both the trilayer and

bilayer sample geometries showed deuterated PS reactive oligomer migrating into the PMMA bottom layer. This is interesting since the dPS and PMMA should not be miscible for the molecular weights and annealing temperatures used in this study but can be explained in terms of the formation of triblock copolymers. If the dPS-diepoxy reacts with two PMMA-COOH, a triblock copolymer consisting of twice the amount of PMMA compared to PS will be formed. This triblock copolymer could then migrate into the PMMA-COOH layer resulting in the deuterium label being found deeper than the PS/PMMA-COOH interface.

FRES was also useful in qualitatively describing the interfacial width between alternating, block, and random copolymers with dPS and dPMMA. The interfacial width described by FRES was compared with fracture toughness data reported by Arlen and Eastwood. Although no quantitative conclusions can be drawn due to the limited resolution of FRES, a qualitative trend showing an increased fracture toughness associated with an increase in the interfacial width was observed.

In addition to FRES depth profiles, neutron reflectivity was used to study both block and random copolymers at a dPS/dPMMA interface. Neutron reflectivity allowed the quantitative analysis of the interface including thickness of the polymer or copolymer layer and the interfaces between the copolymer and each homopolymer. This data could then be directly compared to fracture toughness data reported by Eastwood and the results show that fracture toughness scales as the square of the minimal interfacial width. For all of the polymers studied with neutron reflectivity, the minimal interfacial width was consistently between the copolymer and the PS. Neutron

reflectivity proved to be the best method to monitor the copolymer/polymer interfaces and thickness, however this technique could only be used sparingly due to the cost and time constraints involved with using a neutron source.

4.14 Dissertation Conclusions

The compatibilization of polymer blends has been examined using a reactive processing scheme to create block copolymers at a polymer/polymer biphasic interface. A model system consisting of PBAE, PEO, diamine terminated PEO oligomers, and diepoxy terminated PBAE oligomers was studied. This system allowed a comparison between miscible samples blended at 170°C, and immiscible uncompatibilized and compatibilized samples blended at 125°C and 135°C. It was determined that the addition of 5%wt reactive oligomer in the PBAE/PEO (30/70 wt%) blend increased the modulus of the immiscible samples to that of the miscible samples.

Further DSC experiments also showed that the T_g of the blend was reduced due to the presence of unreacted oligomers in the sample. The reduction of the T_g may allow PEO to continue to crystallize at room temperature. Therefore, additional studies of the PEO/PBAE system were necessary to determine if the increase in modulus was due to an increase in the percent crystallinity of the PEO or from compatibilization. PBAE/PEO (70/30 wt%) samples were blended that contained nonreactive oligomers (10 wt%) or reactive oligomers (10 wt%). The percent crystallinity for both the nonreactive and reactive oligomer samples increased over time, but the crystallinity in the nonreactive samples was consistently higher. The modulus of both the nonreactive

and reactive samples increased with time after mixing and the reactive samples modulus were consistently larger. The modulus of the nonreactive and reactive samples were compared as a function of percent crystallinity of the blend. The reactive compatibilized samples had a larger modulus than the nonreactive samples at any given percent crystallinity.

Thus, these results indicate that crystallization and compatibilization both have a role in the increased modulus of the modified PBAE/PEO blends. However, crystallization can not account for the increase in modulus of the reactive compatibilized blends over the nonreactive blends. The data suggests that reactive compatibilization is responsible for the additional increase in the modulus of the reactive compatibilized blends. Thus, reactive compatibilization of the PBAE/PEO system is feasible.

FRES was also used to continue the study of reactive compatibilization of polymer blends. For this study thin layers of PS, PMMA-COOH, and dPS-diepoxy were used as a model system. Samples were created using a spin coating and floating techniques as described in Chapter 2. FRES results showed that the dPS-diepoxy diffused through 500nm of PS to the PS/PMMA biphasic interface within 8 minutes. After 24h, deuterated material (dPS-diepoxy) began diffusing into the PMMA-COOH layer. Miscibility of the dPS-diepoxy and PMMA-COOH was ruled out through an analysis of χ while dewetting of the PS from the PMMA-COOH layer was invalidated using AFM. Thus, these results are interpreted to indicate that the dPS-diepoxy reacts with the PMMA-COOH and can then form micelles which are distributed throughout

the PMMA-COOH. Thus, the data suggest that reaction of the dPS-diepoxy and PMMA-COOH occurs within 24h without mixing.

Compatibilization of a dPS/dPMMA polymer blend system using alternating copolymers with molecular weights of 85,000 (alt85), 96,000 (alt96), and 497,000 (alt497) was also studied using FRES. Samples were created using a spin coating and floating techniques as described in Chapter 2. The technique provides a qualitative method for comparing the interfacial broadening of the copolymer with each homopolymer. The results showed that the largest molecular weight copolymer (alt497) broadened the copolymer/dPMMA interface more than alt85 or alt96. This data is consistent with data from Arlen that determined PS/PMMA samples compatibilized with alt497 have a higher fracture toughness than PS/PMMA samples compatibilized with alt85 or alt96.

Compatibilization of a dPS/dPMMA polymer blend system using blocky copolymers with different block molecular weights and overall molecular weights as described in table 4.2 was examined using FRES and neutron reflectivity. FRES results suggest a correlation between the interfacial broadening of the block copolymer/dPS interface and the fracture toughness previously reported by Eastwood. Neutron reflectivity data confirmed this analysis and quantified the relationship. The neutron reflectivity data show that the block copolymer/dPS interface has the thinnest interfacial width and should be the site of failure. In addition the fracture toughness of the system reported by Eastwood scales as the minimal interfacial width (block copolymer/dPS) squared.

All results suggest the feasibility of compatibilization of a polymer blend system through copolymers and reactive compatibilization. Our data suggest that sufficient reaction time is critical for the oligomers to react at the interface and become compatibilizers. In addition, both the alternating and blocky copolymer data suggest that the molecular weight of the compatibilizer is an important factor for blend compatibilization in the reactive compatibilization process. For the reactive compatibilization scheme considered as well as the block copolymer compatibilizers it is also necessary for the individual block segments to be above the entanglement molecular weight to be the most efficient compatibilizers.

4.15 Future Work

Continued work is necessary to promote further understanding in the field of polymer blend compatibilization. Neutron reflectivity proved to be the best technique to study the migration of compatibilizer to the interface due to its superior resolution and sensitivity to hydrogen and deuterium. Therefore neutron reflectivity studies of the PS/PMMA-COOH blend system compatibilized with dPS-diepoxy as described in figures 4.1 and 4.2 would support the data obtained from FRES. In addition, the molecular weight of the dPS-diepoxy could be varied to study the effect of the molecular weight of the dPS block of the compatibilizer formed at the interface. This system could also be subjected to various mechanical tests such as dynamic mechanical analysis to relate physical properties to the interfacial widths obtained via neutron scattering. The next step would be to create a PS/PMMA system with deuterated

reactive telechelic oligomers in each phase. The formation and buildup of a deuterated layer between the PS and PMMA as well as the interfacial width of this deuterated layer with each homopolymer could be monitored as a function of time by neutron reflectivity. PS/PMMA blend with reactive telechelic oligomer in each phase could also be studied using ADCB. The fracture toughness of the system could be studied as a function of anneal time and as a function of the molecular weight of each oligomer. These results could then be compared to data obtained for the same system via neutron reflectivity.

List of References

(1) Eastwood, E.; Dadmun, M. *Macromolecules* 2002, *35*, 5069-5077.
(2) Arlen, M. J. In *Chemistry*; The University of Tennessee: Knoxville, 2003; p 177.
(3) Odian, G. *Principle of Polymerization*, 3 ed.; John Wiley & Sons, Inc.: New York, 1991.
(4) Paul, D.; Bucknall, C. B., Eds. *Polymer Blends Volume 2: Performance*; John Wiley and Sons: New York, 2000; Vol. 2.
(5) *www.enme.edu/ice_lab/extruder/node1.html* 2004.
(6) Anastasidadis, S.; Gancarz, I.; Koberstein, J. *Macromolecules* 1989, *22*, 1449-1453.
(7) Brown, H. R. *Macromolecules* 1989, *22*, 2859-2860.
(8) Charoensirisomboon, P.; Chiba, T.; Torikai, K.; Saito, H.; Ougizawa, T.; Inoue, T.; Weber, M. *Polymer* 1999, *40*, 6965-6975.
(9) Teyssie, P.; Fayt, R.; Jerome, R. *Makromol. Chem., Macromol. Symp.* 1988, *16*, 41-56.
(10) Billmeyer, F., Jr. *Textbook of Polymer Science*, 3 ed.; John Wiley & Sons: New York, 1984.
(11) Allcock, H.; Lampe, F. *Contemporary Polymer Science*, 2 ed.; Prentice-Hall, Inc.: Englewood Cliffs, 1990.
(12) Painter, P.; Coleman, M. *Fundamentals of Polymer Science An Introductory Text*; Technomic Publishing Co. Inc.: Lancaster, 1994.
(13) Koning, C.; VanDuin, M.; Pagnoulle, C.; Jerome, R. *Prog. Polym. Sci.* 1998, *23*, 707-757.
(14) Ajji, A.; Utracki, L. A. *Polym. Eng. Sci.* 1996, *36*, 1574-1585.
(15) Pugh, C.; Percec, V. *Macromolecules* 1986, *19*, 65-71.
(16) Pearce, E.; Kwei, T.; Min, B. *J. Macromol. Sci., Chem.* 1984, *A21*, 1181-1216.
(17) Creton, C.; Kramer, E.; Hui, C.-Y.; Brown, H. *Macromolecules* 1992, *25*, 3075-3088.
(18) Jones, R. *Current Opinion in Solid State & Materials Science* 1997, *2*, 673-677.
(19) Kulasekere, R.; Kaiser, H.; Ankner, J.; Russell, T. P.; Brown, H. R.; Hawker, C. J.; Mayes, A. M. *Macromolecules* 1996, *29*, 5493-5496.
(20) Dai, K.; Kramer, E.; Shull, K. *Macromolecules* 1992, *25*, 220-225.
(21) Balazs, A.; DeMeuse, M. *Macromolecules* 1989, *22*, 4260-4267.
(22) Rigby, D.; Lin, J.; Roe, R. J. *Macromolecules* 1985, *18*, 2269-2273.
(23) Dadmun, M. *Macromolecules* 1996, *29*, 3868-3874.
(24) Datta, S.; Lohse, D. *Polymeric Compatibilizers: Uses and Benefits in Polymer Blends*; Hanser/Gardner Publications, Inc.: Cincinnati, 1996.
(25) Coran, A. Y.; Patel, R. *Rubber Chem. Technol.* 1983, *56*, 1045-1060.
(26) Dalai, S.; Wenxiu, C. *J. Appl. Polym. Sci.* 2002, *86*, 3420-3424.
(27) Lai, M.; Yang, Y.; Liu, J. *J. Appl. Polym. Sci.* 2002, *83*, 2906-2914.
(28) Moly, K.; Oommen, Z.; Bhagawan, S.; Groeninckx, G.; Thomas, S. *J. Appl. Polym. Sci.* 2002, *86*, 3210-3225.

(29) Sanchez, M.; Ferrer, G.; Cabanilles, C.; J.M., D.; Prada, M.; Ribelles, J. *Polymer* 2001, *42*, 10071-10075.
(30) Radmard, B.; Dadmun, M. *Polymer* 2001, *42*, 1591-1600.
(31) Viswanathan, S.; Dadmun, M. *Macromolecules* 2002, *35*, 5049-5060.
(32) Hashimoto, T.; Izumitani, T. *Macromolecules* 1993, *26*, 3631-3638.
(33) Izumitani, T.; Hashimoto, T. *Macromolecules* 1994, *27*, 1744-1750.
(34) Park, D.-W.; Roe, R.-J. *Macromolecules* 1991, *24*, 5324-5329.
(35) Shull, K.; Kramer, E. *Macromolecules* 1990, *23*, 4769-4779.
(36) Shull, K.; Kramer, E.; Hadziioannou, G.; Tang, W. *Macromolecules* 1990, *23*, 4780-4787.
(37) Vilgis, T.; Noolandi, J. *Macromolecules* 1990, *23*, 2941-2947.
(38) Adedeji, A.; Lyu, S.; Macosko, C. *Macromolecules* 2001, *34*, 8663-8668.
(39) Lyu, S.; Jones, T.; Bates, F.; Macosko, C. *Macromolecules* 2002, *35*, 7845-7855.
(40) Dadmun, M.; Waldow, D. *Physical Review E* 1999, *60*, 4545-4550.
(41) Benkoski, J.; Fredrickson, E.; Kramer, E. *J. Polym. Sci., Part B: Polym. Phys.* 2001, *39*, 2363-2377.
(42) Creton, C.; Kramer, E.; Hadziioannou, G. *Macromolecules* 1991, *24*, 18461853.
(43) Feng, Y.; Weiss, R.; Karim, A.; Han, C.; Ankner, J.; Kaiser, H.; Peiffer, D. *Macromolecules* 1996, *29*, 3918-3924.
(44) Noolandi, J.; Hong, K. *Macromolecules* 1984, *17*, 1531-1537.
(45) Roe, R.-J.; Kuo, C.-M. *Macromolecules* 1990, *23*, 4635-4640.
(46) Sabouri-Ghomi, M.; Ispolatov, S.; Grant, M. *Physical Review E* 1999, *60*, 4460-4464.
(47) Maric, M.; Macosko, C. *J. Polym. Sci., Part B: Polym. Phys.* 2002, *40*, 346-357.
(48) Levitt, L.; Macosko, C. *Macromolecules* 1999, *32*, 6270-6277.
(49) Brown, B. In *Reactive Extrusion: Principles and Practice*; Xanthos, M., Ed.; Hanser Publishers: New York, 1992; p 75.
(50) Lu, Q.-W.; Hoye, T.; Macosko, C. *J. Polym. Sci., Part A: Polym. Chem.* 2002, *40*, 2310-2328.
(51) Schulze, J.; Moon, B.; Lodge, T.; Macosko, C. *Macromolecules* 2001, *34*, 200-205.
(52) Yin, Z.; Koulic, C.; Jeon, H.; Pagnoulle, C.; Macosko, C.; Jerome, R. *Macromolecules* 2002, *35*, 8917-8919.
(53) Maurits, N. M.; Sevink, G. J. A.; Zvelindovsky, A. V.; Fraaije, J. G. E. M. *Macromolecules* 1999, *32*, 7674-7681.
(54) O'Shaughnessy, B.; Sawhney, U. *Macromolecules* 1996, *29*, 7230-7239.
(55) Yeung, C.; Herrmann, K. *Macromolecules* 2002, *ASAP*, ASAP.
(56) Cartier, H.; Hu, G.-H. *Polymer* 2001, *42*, 8807-8816.
(57) Charoensirisomboon, P.; Chiba, T.; Solomko, S.; Inoue, T.; Weber, M. *Polymer* 1999, *40*, 6803-6810.
(58) Orr, C. In *Department of Chemical Engineering and Materials Science*; University of Minnesota: Minneapolis, 1997.
(59) Char, K.; Yang, Y. *Macromolecular Theory and Simulation* 2001, *10*, 565-572.

(60) Schulze, J.; Cernohous, J.; Hirao, A.; Lodge, T.; Macosko, C. *Macromolecules* 2000, *33*, 1191-1198.
(61) Composto, R.; Walters, R.; Genzer, J. *Materials Science & Engineering, R: Reports* 2002, *R38*, 107-180.
(62) Grull, H.; Schreyer, A.; Berk, N.; Majkrzak, C.; Han, C. *Europhys. Lett.* 2000, *50*, 107-112.
(63) Schnell, R.; Stamm, M.; Creton, C. *Macromolecules* 1999, *32*, 3420-3425.
(64) Hayashi, M.; Grull, H.; Esker, A.; Weber, M.; Sung, L.; Satija, S.; Han, C.; Hashimoto, T. *Macromolecules* 2000, *33*, 6485-6494.
(65) Gupta, R.; Lavery, K.; Francis, T.; Webster, J.; Smith, G.; Russell, T. P.; Watkins, J. *Macromolecules* 2003, *ASAP-WEB*, WEB.
(66) Lynn, G.; Dadmun, M.; Wu, W.-L.; Lin, E.; Wallace, W. *Liq. Cryst.* 2002, *29*, 551-557.
(67) Penfold, J. *Current Opinion in Colloid and Interface Science* 2002, *7*, 139-147.
(68) Penfold, J.; Thomas, R. K. *J. Phys.: Condens. Matter* 1990, *2*, 1369-1412.
(69) Chen, J.; Gardella, J. *Macromolecules* 1999, *32*, 7380-7388.
(70) Mehl, J.; Hercules, D. *Macromolecules* 2001, *34*, 1845-1854.
(71) Wien, K. *Nucl. Instrum. Methods Phys. Res., Sect. B* 1997, *131*, 38-54.
(72) Yokoyama, H.; Kramer, E.; Rafailovich, M.; Sokolov, J.; Schwarz, S. *Macromolecules* 1998, *31*, 8826-8830.
(73) Fuoco, E.; Gillen, G.; Wijesundara, M.; Wallace, W.; Hanley, L. *J. Phys. Chem.* 2001, *105*, 3950-3956.
(74) Gillen, G.; Roberson, S. *Rapid Commun. Mass Spectrom.* 1998, *12*, 1303-1312.
(75) Huang, J.; Ju, M.; Hung, C.; Luoh, W.; Chang, F. *J. Appl. Polym. Sci.* 2003, *87*, 967-975.
(76) Na, Y.; He, Y.; Shuai, X.; Kikkawa, Y.; Doi, Y.; Inoue, Y. *Biomacromolecules* 2002, *3*, 1179-1186.
(77) Phinyocheep, P.; Axtell, F. H.; Laosee, T. *J. Appl. Polym. Sci.* 2002, *86*, 148-159.
(78) Pracella, M.; Rolla, L.; Chionna, D.; Galeski, A. *Macromolecular Chemistry and Physics* 2002, *10/11*, 1473-1485.
(79) Tang, L.; Tam, K.; Yue, C.; Hu, X.; Lam, Y.; Li, L. *J. Appl. Polym. Sci.* 2002, *85*, 209-217.
(80) Wu, C.; Liao, H. *J. Appl. Polym. Sci.* 2002, *86*, 1792-1798.
(81) Abd-El-Messieh, S. L.; Eid, M. A. M.; Hussein, A. I. *J. Appl. Polym. Sci.* 2002, *86*, 540-552.
(82) Bertin, S.; Robin, J. *Eur. Polym. J.* 2002, *38*, 2255-2264.
(83) Liu, X.; Boldizar, A.; Rigdahl, M.; Bertilsson, H. *J. Appl. Polym. Sci.* 2002, *86*, 2435-2448.
(84) Pawlak, A.; Morawiec, J.; Pazzagli, F.; Pracellla, M.; Galeski, A. *J. Appl. Polym. Sci.* 2002, *86*, 1473-1485.
(85) Sailaja, R. R. N.; Chanda, M. *J. Appl. Polym. Sci.* 2002, *86*, 3126-3134.
(86) Zhang, X.; Huang, H.; Zhang, Y. *J. Appl. Polym. Sci.* 2002, *85*, 2862-2866.
(87) Zheng, X.; Zhang, J.; Jiasong, H. *J. Appl. Polym. Sci.* 2003, *87*, 1452-1461.

(88) Orr, C. A.; Cernohous, J. J.; Guegan, P.; Hirao, A.; Jeon, H.; Macosko, C. *Polymer* 2001, *42*, 8171-8178.
(89) Hadjichristidis, N.; Iatrou, H.; Pispas, S.; Pitsikalis, M. *J. Polym. Sci., Part A: Polym. Chem.* 2000, *38*, 3211-3234.
(90) Eastwood, E. In *Chemistry*; The University of Tennessee, Knoxville: Knoxville, 2002; p 198.
(91) Eastwood, E.; Dadmun, M. *Macromolecules* 2001, *34*, 740-747.
(92) Brandrup, J.; Immergut, E.; Grulke, E., Eds. *Polymer Handbook*; John Wiley & Sons, Inc.: New York, 1999.
(93) Denis, F. A.; Hanarp, P.; Sutherland, D. S.; Dufrene, Y. F. *Nano Letters* 2002, *2*, 1419-1425.
(94) Schreckenbach, A. *Polymer* 1997, *38*, 3069-3083.
(95) Skeist, I.; Somerville, G. R. *Epoxy Resins*; Reinhold Publishing Corporation: New York, 1962.
(96) Lee, H.; Neville, K. *Handbook of Epoxy Resins*; McGraw-Hill: New York, 1967.
(97) Wang, C.; Krausch, G.; Geoghegan, M. *Langmuir* 2001, *17*, 6269-6274.
(98) Sferrazza, M.; Xiao, C.; Jones, R. *J. Phys.: Condens. Matter* 2001, *13*, 10269-10277.
(99) Russell, T. P.; Hjelm, r.; Seeger, P. *Macromolecules* 1990, *23*, 890-893.
(100) Callaghan, T.; Paul, D. *Macromolecules* 1993, *26*, 2439-2450.
(101) Benmouna, F.; Daoudi, A.; Roussel, F.; Leclercq, L.; Buisine, J.; Coqueret, X.; Benmouna, M.; Ewen, B.; Maschke, U. *Macromolecules* 2000, *33*, 960-967.
(102) Huang, Y.-Y.; Chen, H.-L.; Hashimoto, T. *Macromolecules* 2003, *36*, 764-770.
(103) Brown, H. R. *Macromolecules* 2001, *34*, 3720-3724.
(104) Creton, C. *Contact Angle, Wettability and Adhesion* 2002, *2*, 1-12.

Vita

Charles O'Brien was born in the town of Norton, VA. He spent four years at The College of William and Mary where he received a B.S. in Chemistry in 1996. That same year he began graduate school in polymer science at the University of Akron. He transferred to The University of Tennessee, Knoxville to pursue a PhD in Chemistry in 1998.